

---

[All ETDs from UAB](#)

[UAB Theses & Dissertations](#)

---

2016

## Elementary Photoreceptor Signaling in Human Vision

Kady Scarlett Bruce  
*University of Alabama at Birmingham*

Follow this and additional works at: <https://digitalcommons.library.uab.edu/etd-collection>

---

### Recommended Citation

Bruce, Kady Scarlett, "Elementary Photoreceptor Signaling in Human Vision" (2016). *All ETDs from UAB*. 1276.

<https://digitalcommons.library.uab.edu/etd-collection/1276>

This content has been accepted for inclusion by an authorized administrator of the UAB Digital Commons, and is provided as a free open access item. All inquiries regarding this item or the UAB Digital Commons should be directed to the [UAB Libraries Office of Scholarly Communication](#).

ELEMENTARY PHOTORECEPTOR  
SIGNALING IN HUMAN VISION

by

KADY SCARLETT BRUCE

LAWRENCE C. SINCICH, COMMITTEE CHAIR  
CHRISTINE A. CURCIO  
PAUL D. GAMLIN  
TIMOTHY W. KRAFT  
YUHUA ZHANG

A DISSERTATION

Submitted to the graduate faculty of The University of Alabama at Birmingham,  
in partial fulfillment of the requirements for the degree of  
Doctor of Philosophy

BIRMINGHAM, ALABAMA

2016

Copyright by  
Kady Scarlett Bruce  
2016

# ELEMENTARY PHOTORECEPTOR SIGNALING IN HUMAN VISION

KADY S. BRUCE

VISION SCIENCE GRADUATE PROGRAM

## ABSTRACT

To perceive a spot of light at photopic threshold, a minimum number of photons must be absorbed by cone photoreceptors. While many factors affecting psychophysical threshold have been studied, few have been examined at the single-cone level. Here we reveal how variation in synaptic weighting and signal integration among cones in the human retina occurs *in vivo*. Using an adaptive optics scanning laser ophthalmoscope (AOSLO) equipped with stimulation capabilities, we targeted cone-sized stimuli to single cones. Perceptual increment thresholds were measured from individual cones and cone pairs in 7 subjects using a Bayesian-based staircase method of threshold estimation. In 42 of 99 cone pairs, thresholds differed between cones ( $p < 0.05$ ), and differences in threshold as small as 14% were detectable. To determine if the observed variability was real, we examined several factors that could lead to threshold differences. We found that thresholds were consistent over multiple days, that cone reflectivity in AOSLO images was unrelated to threshold ( $n = 494$  tests;  $p = 0.19$ ), and that stimulus delivery errors were not a cause (average error = 0.2 arcmin;  $R^2 = 8 \times 10^{-5}$ ).

To investigate how cone signals combine, individual cones in pairs were stimulated simultaneously and analyzed with respect to their signal summation. All pairs exhibited summation, with 17/99 pairs manifesting linear summation, and 42/99 integrating signals according to a two-detector model. The nature of signal integration was not correlated with eccentricity, but was related to inter-cone distance (most linear

pairs were located within 1.5 cone spacings of one another), suggesting bipolar cells as the site of cone signal summation.

Using longitudinal imaging, we found that some cones were persistently poorly reflective. To test if these were functional, 10 dark cones from 5 subjects were targeted for threshold testing. All 10 dark cones had thresholds comparable with those from normally reflective cones measured concurrently ( $p = 0.49$ ), indicating that low cone reflectivity is not a reliable indicator of cone sensitivity in normal retinas. These results should be considered in the clinical setting, where microperimetry and AOSLO imaging are used to assess visual function in patients with retinal disease.

Keywords: psychophysics, retina, optical imaging, summation, threshold, photoreceptors

## ACKNOWLEDGEMENTS

My advisor, mentor, and friend—Lawrence Sincich.

My partner, Alex.

My family, specifically for never setting a limit on my aspirations.

My colleagues: William Tuten, Wolf Harmening, Bradley Langston, and Daniel Turner.

My committee members.

# TABLE OF CONTENTS

	Page
ABSTRACT.....	iii
ACKNOWLEDGEMENTS.....	v
LIST OF FIGURES .....	ix
LIST OF ABBREVIATIONS.....	xi
CHAPTER	
1. INTRODUCTION .....	1
Functional anatomy of the primate retina .....	3
Photoreceptor function.....	4
Horizontal and bipolar cell function and connectivity.....	8
Amacrine and ganglion cell function and connectivity .....	13
The S cone pathway.....	16
Receptive fields.....	17
Summation .....	19
Single spot stimuli.....	20
Grating stimuli .....	23
Multi-spot stimuli.....	25
Temporal summation .....	28
Spatial considerations with stimuli .....	29
Fixational eye movements .....	29
Chromatic dispersion .....	31
Vascular interference .....	34
Characterization of delivered stimuli.....	35
Psychophysical testing and variability.....	38
Comprehensive bibliography.....	42
2. CONE SIGNAL SUMMATION AND THRESHOLD VARIABILITY IN THE HUMAN RETINA.....	60
Abstract .....	61
Introduction.....	62
Methods.....	64
AOSLO imaging.....	65
Microstimulation with AOSLO .....	66
Psychophysical procedures .....	68

Inter-cone distance experiments .....	70
Cone weighting and summation calculations .....	70
Cone reflectance quantification .....	72
Results.....	73
Threshold variability for microstimuli delivered to single cones .....	73
Two-cone signal summation.....	77
Discussion.....	80
References.....	87
Figures.....	97
3. NORMAL PERCEPTUAL SENSITIVITY ARISING FROM WEAKLY REFLECTIVE CONE PHOTORECEPTORS.....	108
Abstract .....	109
Introduction.....	110
Methods.....	112
Retinal imaging.....	112
Single cone microstimulation with AOSLO .....	113
Psychophysical experiments .....	114
Identification of retinal vessels .....	116
Reflectance quantification and longitudinal imaging .....	117
Results.....	118
Imaging characteristics of poorly reflective cones .....	118
Psychophysical testing of poorly reflective cones .....	120
Discussion.....	122
Acknowledgements.....	127
References.....	128
Figures.....	134
Appendix.....	139
APPENDIX A: UNIVERSITY OF ALABAMA AT BIRMINGHAM INTERNAL REVIEW BOARD APPROVALS AND PERMISSIONS .....	142



APPENDIX B: UNIVERSITY OF ALABAMA AT BIRMINGHAM INFORMED  
CONSENT DOCUMENT FOR HUMAN SUBJECTS .....173

## LIST OF FIGURES

<i>Figures</i>	<i>Page</i>
INTRODUCTION	
1 Anatomy of the retina. ....	4
2 Intensity-response function of a cone photoreceptor .....	6
3 Intensity-response functions of cones on different intensity backgrounds .....	7
4 Intensity-response function of an ON bipolar cell .....	11
5 Variations in single spot stimuli used to probe spatial summation.....	21
6 Summation in single ganglion cells of the frog retina .....	22
7 Variations in grating stimuli used to probe spatial summation.....	24
8 Multispot stimuli configurations used to probe spatial summation.....	26
9 Retinal motion in fixating subjects ranges over many cones.....	30
10 Longitudinal and transverse chromatic dispersion in multiwavelength retinal imaging .....	33
11 Calculated light distribution of delivered stimulus with and without AOSLO correction .....	36

## TWO-CONE SUMMATION IN THE HUMAN RETINA

1 Retinal areas targeted for microstimulation are chosen to avoid vasculature.....	97
2 Example cone pairs with similar and different thresholds.....	98
3 Individual cones exhibit variation in perceptual threshold.....	99
4 Cone thresholds are consistent over time.....	100
5 Cone reflectance is unrelated to threshold.....	101

6	Threshold differences do not arise from systematic errors in stimulus delivery .....	102
7	Cone pairs can exhibit two styles of signal summation.....	103
8	Style of cone signal summation does not vary with eccentricity.....	104
9	Summation style depends on distance between cones.....	105
10	Linear summation occurs with closely spaced cones .....	106
11	Cone signal pathway determines style of summation.....	107

NORMAL PERCEPTUAL SENSITIVITY ARISING FROM WEAKLY REFLECTIVE  
CONE PHOTORECEPTORS

1	Relationship between poorly reflective cones and retinal vasculature .....	134
2	Identifying dark cones for longitudinal imaging and functional testing.....	135
3	Poor cone reflectivity can be persistent or intermittent .....	136
4	Microstimulation increment thresholds show no difference in light sensitivity between dark and normally reflective cones.....	137
5	Comparison of single-cone reflectance and threshold.....	138
A1	Highlighting variability among normally reflective cone pairs.....	139
A2	Distribution of raw threshold measurements .....	140
A3	Persistently dark cone remains dark over time .....	141

## LIST OF ABBREVIATIONS

AO: adaptive optics

AOM: acousto-optic modulator

AOSLO: adaptive optics scanning laser ophthalmoscope

a.u.: arbitrary units

cGMP: cyclic guanosine monophosphate

GABA: gamma-Aminobutyric acid

IPL: inner plexiform layer

IR: infrared

L: long-wavelength

LCA: longitudinal chromatic aberration

LED: light-emitting diode

LGN: lateral geniculate nucleus

MEMS: micro-electromechanical systems

M: middle-wavelength

PSF: point spread function

S: short-wavelength

SD: standard deviation

TCA: transverse chromatic aberration

UAB: University of Alabama at Birmingham

UCB: University of California Berkeley

## INTRODUCTION

In the absence of knowing how it functions at a cellular level, the eye was often considered a wondrous organ. In the early 19<sup>th</sup> century, for instance, the eye was used as an exemplar in theology to argue for nothing less than the existence of a divine creator. William Paley, a clergyman, used the idea that complex natural organs must be made by such a creator, in the same way that a complex mechanical device, like a watch or telescope, must be made by a skilled designer. His rhetoric rings of the pulpit:

Were there no example in the world, of contrivance, except that of the *eye*, it would alone be sufficient to support the conclusion which we draw from it, as to the necessity of an intelligent Creator. It could never be got rid of; because it could not be accounted for by any other supposition...Its coats and humours, constructed, as the lenses of a telescope are constructed, for the refraction of rays to a point, which forms the proper action of the organ...these provisions compose altogether an apparatus, a system of parts, a preparation of means, so manifest in their design, so exquisite in their contrivance, so successful in their issue, so precious, and so infinitely beneficial in their use, as, in my opinion, to bear down all doubt that can be raised upon the subject. (Paley 1809, p. 75-76).

Fifty years later, Charles Darwin recognized the challenge that the eye offered in his scientific argument for natural selection, although he necessarily hedged toward it being conceivable that the eye can arise from evolutionary processes. In *On the Origin of Species*, he wrote:

To suppose that the eye, with all its inimitable contrivances for adjusting the focus to different distances, for admitting different amounts of light, and for the correction of spherical and chromatic aberration, could have been formed by natural selection, seems, I freely confess, absurd in the highest degree. Yet reason tells me, that if numerous gradations from a perfect and complex eye to one very imperfect and simple, each grade being useful to its possessor, can be shown to exist; if further, the eye does vary ever so slightly, and the variations be inherited, which is certainly the

case; and if any variation or modification in the organ be ever useful to an animal under changing conditions of life, then the difficulty of believing that a perfect and complex eye could be formed by natural selection, though insuperable by our imagination, can hardly be considered real (Darwin 1859, p. 186-187).

The reverence with which these authors regarded the harmony of the anatomy and function of the eye is a feeling that I hope is also expressed in this dissertation. Since those days, science has revealed many details of how the retina works, cell by cell, but our knowledge about how the eye subserves vision is still incomplete.

The world around us is wildly diverse—full of sights, smells, sounds, tastes, and textures. This circus of potential stimuli, infinitely large, is both detected and processed by our sensory systems. As you sip a piping hot cup of fresh coffee, you all at once smell, taste, feel, hear, and see; nothing exists in isolation. Even in the laboratory, few opportunities arise to directly examine the harmony of perception. This is particularly true at the cellular level. The human retina is comprised of millions of light-sensing cells, each of which contribute some miniscule portion to how we see the world. We are interested in one class of these photoreceptors, called cones, which are involved in daylight vision. The response of just one of these cone photoreceptors is sufficient to drive a downstream neuron in the retina to respond with an action potential. However, the firing of one such action potential does not necessarily yield perception. Can a single cone photoreceptor drive perception? This question was not reasonably approachable until recently. Using a newly developed retinal microstimulator, which is equipped with adaptive optics retinal imaging, real-time video stabilization, and multiwavelength stimulus delivery channels, we are able to reliably and repeatedly deliver stimuli to a single cone photoreceptor in the living eye.

The primary goal of this dissertation is to use cone-targeted stimulation to reveal how cone photoreceptors integrate their signals. While the activity of a single cone may be sufficient to drive perception, it is the synchronous stimulation of multiple cones within the retinal mosaic that affords our unique, highly developed sense of sight. As light enters the eye from the outside world, these cone cells generate signals that are then combined and interpreted downstream, leading to perception. Yet how these signals integrate has not been directly examined at the most basic level — within cone pairs. Here, I describe the framework for the summation of cone signals arising from pairs of cones in the human retina.

### Functional anatomy of the primate retina

In the retina, biologically useful information is extracted from incoming fluctuations in light as signals are propagated through the retina, optic tract, and into the brain. How does the visual system determine what parts of the light signal are salient? The answer to that question is different for each part of the visual pathway, and also depends on what the animal itself is doing at any given moment. For the retina itself, where the first step in vision takes place, the most salient information is variations in light intensity. By comparing changes in light intensity, be they spatial, temporal, or spatiotemporal, the retina can record and transmit changes in the images that are cast upon it by the lens. This identification of differences in light intensity, or contrast, is a major function of the retina, and it is unsurprising, therefore, that the retinal circuitry is

anatomically “wired” to extract contrast from the light patterns present in the outside world (Figure 1). In this section I will briefly review the anatomy and physiology of the cellular elements in the retina that ultimately provide the brain with signals about relative light intensity.

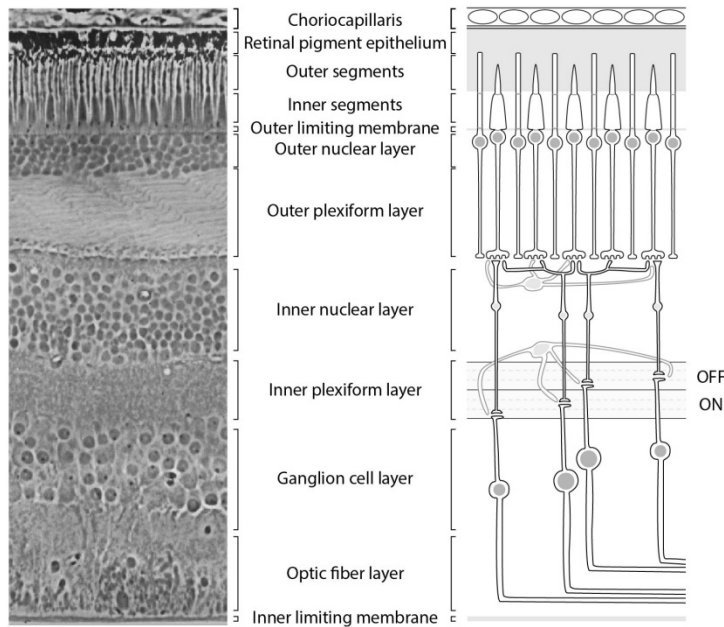


**Figure 1. Anatomy of the retina.** (Left) A section of human retina imaged using phase contrast microscopy (1.25 mm from fovea; reproduced with permission from Boycott *et al.* 1969). (Right) A schematized version of retinal circuitry, emphasizing the cone pathways that are primary participants in our experiments.

### *Photoreceptor function*

The first and perhaps most critical step in vision is the transduction of light energy, carried by photons, into chemical signals. This photon capture is accomplished by photopigments, found within the outer segments of photoreceptors. One type of photoreceptor, termed “rods” for the long, cylindrical appearance of their outer segments, contains a photopigment called rhodopsin. Rods are extremely sensitive to light, and have been shown to respond to single photons at both psychophysical and single-cell levels (Hecht *et al.* 1942; Baylor *et al.* 1984). Rods, therefore, are ideal for transducing visual signals in low light. A second type of photoreceptor, called “cones” for the conical



appearance of their outer segments, each contain one of three closely related photopigments. The cones are classified by the specific type of photopigment, or opsin, they express. The opsins are discriminated by the wavelength of light that each photopigment maximally absorbs: long-wavelength (L) cones (~560 nm), middle-wavelength (M) cones (~530 nm), and short-wavelength (S) cones (~430 nm) (Dartnall *et al.* 1983; Baylor *et al.* 1987; Schnapf *et al.* 1987).

In either type of photoreceptor, rods or cones, photons entering the eye are absorbed by photopigments, located in the outer segments of the photoreceptors. Upon absorption, phototransduction ensues, through which the incoming light signal is converted into a chemical signal (reviewed in Burns *et al.* 2005). First, the incoming photon is absorbed by 11-*cis*-retinal. The absorbed energy causes isomerization of the retinal to the *trans* form, which activates the opsin where the retinal is bound. This process initiates an amplifying catalytic cascade involving the G-protein transducin and phosphodiesterase, ultimately lowering the concentration of cyclic guanosine monophosphate (cGMP). This cascade culminates in the closing of membrane-bound cGMP-gated cation channels, which reduces the influx of Na<sup>+</sup> and Ca<sup>+2</sup>, thus hyperpolarizing the membrane voltage. As the membrane hyperpolarizes, cyclic nucleotide-gated channels begin to close, Ca<sup>+2</sup> entry is blocked, but continues to be extruded by the Na<sup>+</sup>-K<sup>+</sup>-Ca<sup>+2</sup> exchanger, causing a drop in intracellular Ca<sup>+2</sup>. Because Ca<sup>+2</sup> is necessary for vesicle transfusion at the photoreceptor pedicle, the decrease in intracellular calcium causes a decrease in the release of the excitatory neurotransmitter glutamate. This graded variation in neurotransmitter release, whereby an increasing the amount of light would proportionally decrease the release of glutamate, represents the

basic photoreceptor response to an increase in light (von Gersdorff *et al.* 1994; Rieke *et al.* 1996).

Of central importance to this thesis is how cones respond to very brief flashes of light. Overall, cones are less sensitive to light than rods, needing on the order of 50 photons to be absorbed—i.e. ~50 photoisomerizations—before exhibiting a measurable response in complete darkness (Schnapf *et al.* 1990; Koenig *et al.* 2011). In the presence of a dark background, the intensity-response function rises exponentially and then gradually approaches a maximum value, indicative of a saturating function (Figure 2). Depending on the recording conditions, the intensity-response curve follows either a Michaelis-Menten relation

$$r/r_m = i/(i + i_{half})$$

or an exponential saturating function

$$r/r_m = 1 - e^{(-ki)}$$

or sometimes a combined version of the two, where  $r$  is the peak response amplitude,  $r_m$  the maximum response,  $i$  the photon density of the stimulus,  $i_{half}$  the half-saturation density, and  $k$  is a constant (Baylor *et al.* 1987; Schnapf *et al.* 1990; Schneeweis *et al.* 1999). Empirical data show that the operating range of cones is at least 3 orders of

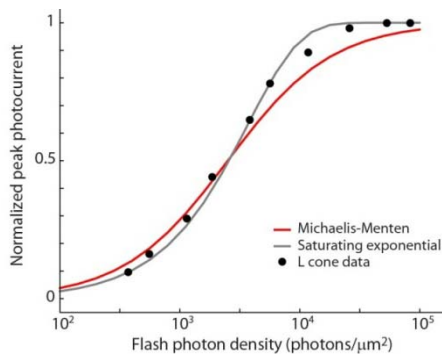


**Figure 2. Intensity-response function of a cone photoreceptor.** Example intensity-response function of a cone photoreceptor in the macaque monkey in response to 10 msec flashes of light delivered in the dark (black circles; adapted from Baylor *et al.* 1987). Data are superimposed on two theoretical intensity response relationships: the Michaelis-Menton relation (red) and an exponential saturating function (gray).

magnitude in light intensity, with a half-saturating value of  $\sim 700$  photons/ $\mu\text{m}^2$  in humans (Schnapf *et al.* 1987, also see Baylor 1987 for review).

The shape of the intensity-response function changes very little in the presence of different background light intensities, as cones adapt to such ambient light after a short period of time (Figure 3; *in vivo*: Valeton *et al.* 1983; *in vitro*: Schnapf *et al.* 1990). The effect of this shift in the response function means that the cones can follow increments as

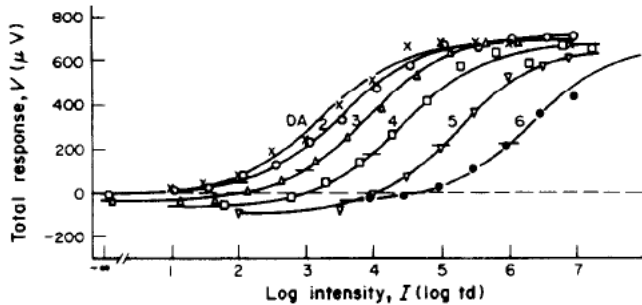


**Figure 3. Intensity-response functions of cones on different intensity backgrounds.** Family of intensity-response curves recorded across the outer segment layer *in vivo* in response to the presence of steps of incremental and decremental steps of light against a range of steady background illuminations. The small horizontal line in each curve represents the background response level. Responses above these lines are increment responses, below are decrement responses. Note that the shape of the curve is essentially constant over 5 log units of background intensity (reproduced with permission from Valeton *et al.* 1983).

well as decrements in light intensity, with the response moving up or down from the half-saturation point, accordingly. Within a 1 log unit range of light intensities from this point, the intensity-response function is effectively linear. One main hypothesis examined in *Chapter 2* is whether brief stimuli of threshold intensity appear to combine linearly, as might be predicted by small shifts along the intensity-response function near the half-saturation value.

An additional factor that impacts the intensity-response function of cones is the coupling of L and M cones to one another via electrical gap junctions (Hornstein *et al.* 2004). This cone to cone coupling may be beneficial in luminance detection tasks by

averaging out noise over a population of cones with correlated inputs, thereby increasing the signal-to-noise ratio (Lamb *et al.* 1976; Tessier-Lavigne *et al.* 1988; DeVries *et al.* 2002). Using an electrical model of the cone network, it was predicted that the signal-to-noise ratio in macaque cones will improve by ~35% for luminance stimuli equal to or larger than the area of coupled cones (Hornstein *et al.* 2004). The magnitude of this effect, however, is also dependent on several other factors such as optical blurring, cone signal convergence, neural noise, and synaptic filtering. Still, cone to cone coupling may produce an effect in the context of the experiments outlined in this dissertation.

### *Horizontal and bipolar cell function and connectivity*

The first synapse conveying photopic visual information within the retina occurs at the pedicle of the cone photoreceptors, where elaborate synapses are formed with horizontal cells and bipolar cells. From this point on, I will solely be reviewing pathways related to the cone photoreceptors, as the background illumination we employed is rod-saturating (discussed in *Chapter 2*). Additionally, I will focus on pathways and cells related to L and M cones, as the S cone (discussed later) has been shown to be 2.6 log units less sensitive to the wavelength of our 543 nm stimulus. Each L or M cone photoreceptor in the primate retina synapses onto at least eight different types of cone bipolar cells, and at least one horizontal cell Boycott *et al.* 1991.

Horizontal cells are inhibitory interneurons that receive glutamatergic input from photoreceptors and provide inhibitory feedback to both photoreceptors and bipolar cells using gamma-aminobutyric acid (GABA) (Stell 1965). There are two types of horizontal

cells in primates, called H1 and H2 ((Boycott *et al.* 1969; Kolb *et al.* 1994); but see Ahnelt *et al.* 1994 for a potential third type). Each horizontal cell has dendritic arbors that scale in size, and number of synaptic contacts, with eccentricity; in the fovea, H1 cells contact ~7 cones, while H2 cells contact ~11-14 cones each (Boycott *et al.* 1987; Wassle *et al.* 1989; Ahnelt *et al.* 1994; Ahnelt *et al.* 1994). Both types of cells are thought to anatomically contact all types of cones; however H1 cells synapse onto primarily L and M cones, with only a few S cone contacts, while H2 cells synapse onto all cone pedicles within reach, including S cones (Boycott *et al.* 1987; Ahnelt *et al.* 1994; Ahnelt *et al.* 1994; Dacey *et al.* 1996). When cone-isolating stimuli were used to probe the functional strength of each cone type onto H1 and H2 cells, it was demonstrated that H1 cells primarily respond when their L and M cones were stimulated, while S cones drove H2 cells as effectively as L and M cones (Dacey *et al.* 1996).

As a cone hyperpolarizes in response to light and decreases its release of glutamate, the postsynaptic horizontal cell hyperpolarizes in kind (Dacheux *et al.* 1990; Dacey *et al.* 1996). The intensity-response function of the horizontal cell is proportional to the amount of input it receives, exhibiting a linear response to light intensity changes over 3 orders of magnitude (see Dacheux *et al.* 1990, Figure 5a). As the horizontal cell hyperpolarizes, it provides inhibitory feedback onto photoreceptors via a non-synaptic pH-dependent mechanism that acts directly on the cone's calcium current, shifting the activation range (Verweij *et al.* 1996; Verweij *et al.* 2003; Crook *et al.* 2011). Because of this inhibitory feedback from horizontal cells to cones, any stimulated cone will cause a small depolarization among all of the cones that each horizontal cell is connected to. This reduces the stimulated cone's response to light, especially for prolonged stimuli

(reviewed in Thoreson *et al.* 2012). This inhibitory feedback on cone responses was first demonstrated in turtle retina, where a single cone's response decreased as a light stimulus was increased in size to drive neighboring cones (Baylor *et al.* 1971). Through the injection of current directly into a synaptically connected horizontal cell, horizontal cells were identified as mediating this reduction in cone activity. So, in effect, horizontal cells inhibit a single cone's response to light when other, nearby cones are also receiving light signal. For light falling on a single cone, this inhibition may not be of such importance, as neighboring, unilluminated cones would only slightly depolarize. However, if stimuli were to fall on multiple cones synapsing onto the same horizontal cell, the resulting inhibitory feedback could influence any downstream response. This inhibitory action of horizontal cells is one mechanism that could contribute to non-linear summation of cone signals, as we will see in *Chapter 2*.

The third retinal cell class present at the first visual synapse is the bipolar cell, which, like cones and horizontal cells, also exhibit graded polarization in response to light (Werblin *et al.* 1969). As discussed previously, the cone response to light causes a decrease in glutamate release at the cone pedicle. In addition to the horizontal cell, this change in neurotransmitter release is also registered by two kinds of bipolar cells with opposite reactions to glutamate. The first type of bipolar cell has ionotropic glutamate receptors, which lead to membrane potential changes that have the same sign as the photoreceptor's polarization state. Because this type of cell hyperpolarizes in response to an increase in luminance, thus decreasing its own neurotransmitter release, it is called an OFF cone bipolar cell (reviewed in (Euler *et al.* 2014), (Wan *et al.* 2011)). OFF bipolar cells make a distinct type of synapse with the cone, called a flat synapse (Kolb 1970;

Kolb 1979; Mariani 1981). The second type of bipolar cell has the opposite response, hyperpolarizing in response to increased glutamate and depolarizing to decreased glutamate, due to a sign-reversing metabotropic glutamate receptor. These cells are called ON bipolar cells, as they increase neurotransmitter release in response to increasing illumination. The ON bipolar cell forms invaginating synaptic contacts with cones, encased within the cone pedicle (Kolb 1970; Kolb 1979; Mariani 1981). The presence of ON and OFF bipolar cells establishes the distinct ON and OFF pathways from the photoreceptors to the brain, responsible for signaling increases and decreases in light

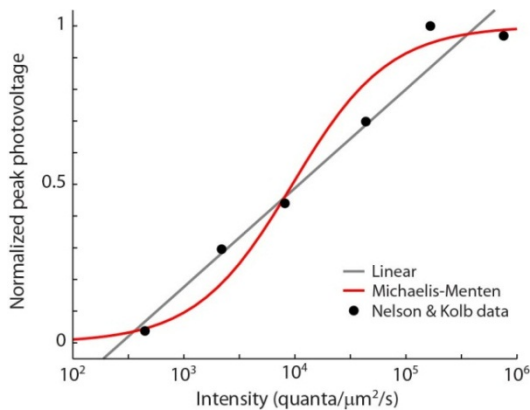


**Figure 4. Intensity-response function of an ON bipolar cell.** Original data taken from an intact cat eyecup preparation (black circles; adapted from Nelson *et al.* 1983, Figure 21b, red traces). Data are plotted against the two best-fitting intensity-response relationships: the Michaelis-Menten relation (red) and linear function (gray). The range of intensities used in this experiment may not have been wide enough to fully characterize the cell's behavior; these fits are provided as a reference, since they did not appear in the original paper.

intensity (Werblin *et al.* 1969; Boycott *et al.* 1991). Like cones, bipolar cells can exhibit a range of 1 log unit of light intensity over which their responses appear linear (Figure 4).

The ON and OFF pathways contain several types of bipolar cells, each linked to two major systems of retinal ganglion cells. The first of these systems is called the midget system, named in reference to the small spread of dendritic arbors of the ganglion cells in this class (Polyak *et al.* 1949; Boycott *et al.* 1969; Kolb *et al.* 1991; Calkins *et al.* 1994; Kolb *et al.* 2003). Midget bipolar cells generally receive input from either L or M cones, and can be ON or OFF. The midget system is unique because, in the central retina, each midget bipolar cell makes dendritic contact with just one cone pedicle, and axonal contact

with just one ganglion cell (Kolb *et al.* 1991; Dacey 1993; Calkins *et al.* 1994; Jusuf *et al.* 2006). The second major system of retinal ganglion cells is called the parasol system, which are served by diffuse bipolar cells. Both cell types have larger dendritic arbors (thus their names), and diffuse bipolar cells contact ~6 cones each regardless of eccentricity (Polyak *et al.* 1949; Boycott *et al.* 1969; Boycott *et al.* 1991; Grunert *et al.* 1994). Like the midget system, diffuse bipolar cells can be either ON or OFF, and their dendrites contact any cone in their vicinity. This makes the diffuse bipolar cells less wavelength specific than the midget bipolar cells in the central retina. Within the ON and OFF subtypes, there are three ON diffuse bipolar cells, and three OFF (Boycott *et al.* 1991). The subtypes are anatomically characterized by the level at which they terminate within the inner plexiform layer (IPL), with the three ON bipolar cells stratifying in sublayers 4-6 of the IPL, and the three OFF bipolar cells in sublayers 1-3 (primate bipolar cells are reviewed in Dacey 1999). This arrangement means that the diffuse bipolar cells could represent up to six parallel streams of information being transmitted from the cones to the ganglion cells. The inner plexiform layer may represent an additional step (beyond ON versus OFF) in functional divergence of information. In other words, even though the diffuse bipolar cells may be communicating the same cone signaling information, they connect to functionally distinct retinal ganglion cells which each ramify in a specific layer of the IPL. While it is unknown exactly what is functionally different about the subtypes of ON and OFF diffuse bipolar cells, amacrine and ganglion cells are known to have distinct properties based on the anatomical location of their dendrites within the IPL.



## *Amacrine and ganglion cell function and connectivity*

Amacrine cells represent the second type of lateral interaction present in the retina. Unlike horizontal cells, amacrine cells are not known to be exclusively inhibitory. In fact, these cells have been demonstrated to contain a variety of neurotransmitters, and the precise mechanisms these cells use to provide feedback within the retinal circuitry is incompletely understood (reviewed in Grimes 2012, Dacey 1999). Like horizontal cells, many amacrine cells contain the inhibitory neurotransmitter GABA. However, some also contain the inhibitory neurotransmitter glycine. The dominance of GABA and glycine in the amacrine cells implies that they function similarly to horizontal cells—providing local inhibitory feedback onto bipolar cells. At the bipolar-amacrine synapse in the IPL, more than 90% of the synapses are inhibitory using GABA (Koontz *et al.* 1990). Amacrine cells are thought to have direct inhibitory effects on ganglion cells as well, though less is known about their postsynaptic processes.

While previously discussed cell types have been largely characterized by their function, amacrine cells are mainly distinguished on the basis of their form (reviewed in Kolb 1997). At present, there are over 30 different types of known amacrine cells types classified on the basis of their anatomy. These cells vary greatly in size, ranging from <100  $\mu\text{m}$  to >1,000  $\mu\text{m}$  (Kolb *et al.* 1981; Dacey 1990; MacNeil *et al.* 1998; MacNeil *et al.* 1999). These size differences allow for estimation of the distance over which amacrine cells can mediate interactions among cells. Furthermore, amacrine cells either stratify in a single layer of the IPL, or they can bistratify into multiple layers. This raises the possibility of interactions occurring between IPL layers, as well as within layers. The

diversity of neurochemical properties found within amacrine cells, as well as their varied morphology and stratifications, suggests that many functions can be found in this cell type. One way to narrow in on the role that amacrine cells play in the vertical cone pathway is to look ahead to ganglion cells, and analyze how signals change as they are transmitted from ON cone bipolar cells to ON ganglion cells.

The last stage of retinal circuitry is represented by the ganglion cell. Ganglion cells receive signals from bipolar and amacrine cells, and transmit those signals from the eye to the brain. Most ganglion cells in the primate can be classified into either midget (~90%) or parasol cells (~5%) (reviewed in Dacey 1994). The remaining numbers include a diverse population of ganglion cells that are each relatively rare, often exhibiting specialized functions still awaiting elucidation. In and around the fovea, midget ganglion cells only contact one bipolar cell each, meaning that each midget ganglion cell in this area is receiving direct signals from only one cone (Kolb *et al.* 1991; reviewed in Dacey 1999). Like their bipolar cell counterparts, midget ganglion cells can be either ON cells, stratifying in the inner IPL, or OFF cells, stratifying in the outer IPL. The second major type of ganglion cell, parasol cells, receives input mainly from diffuse bipolar cells. Parasol cells are named in reference to their extensive dendritic branching, which looks like an umbrella being held over the cell body. As with the midget ganglion cells, parasol cells also come in the ON and OFF varieties, stratifying in distinct layers of the IPL (Famiglietti *et al.* 1977; Wassle *et al.* 1981; Rodieck 1998). Every class of ganglion cell independently tiles the retina, decreasing in spatial density with distance from the fovea.

While the retinal ganglion cell types can be distinguished by their anatomy and stratifications, they also vary in their patterns of excitation. Parasol ganglion cells have transient response properties to a change in stimulus intensity. Midget ganglion cells, in contrast, show a more sustained response to a stepped stimulus, although this typically leads with a higher transient phase of firing at onset (Gouras 1968; De Monasterio *et al.* 1975; Schiller *et al.* 1977; de Monasterio 1978; de Monasterio 1978). For brief stimuli, the transient responses of both cell types can be remarkably similar. This is likely due to the direct transfer of graded potentials from photoreceptor to bipolar cell to ganglion cell on light onset, a transfer of signal that can occur before modulatory influences can kick in. The differences in sustained responses between parasol and midget ganglion cells is theorized to come from amacrine cells, which have more numerous synaptic inputs onto parasol ganglion cells (Jacoby *et al.* 1996) compared to midget ganglion cells (Kolb *et al.* 1991).

Another important physiological distinction is that parasol ganglion cells are able to fire action potentials at much lower stimulus contrasts than midget ganglion cells (Benardete *et al.* 1992; Lee *et al.* 1994), provided that the stimuli are optimized for receptive field size. This suggests that parasol cells pool the signals from many cones to increase their luminance sensitivity. However, it remains unknown if the synaptic weighting of each cone onto the downstream ganglion cell varies by cell type. Thus, on a cone-by-cone basis, it remains to be determined if sensitivity for the smallest luminance increment is transmitted by only the parasol ganglion cell system. One aim of this dissertation is to assess this question.

## *The S cone pathway*

Within the three types of cones, the S cones are unique in many ways. S cones are common to all vertebrates, and consistently represent 6-10% of the total cone population (Marc 1982; Hofer *et al.* 2005). In humans, they are sparsely scattered throughout the retina, but are not present at all within the foveal center (Williams *et al.* 1981; Curcio *et al.* 1991; Roorda *et al.* 1999). Functionally, visual signals arising from S cones have lower temporal and spatial resolution than the other two cone systems (Stockman *et al.* 1991; Humanski *et al.* 1992). Anatomically, S cones have many morphological and connectivity features that differentiate them from their L and M counterparts. First, S cones are distinguishable from L and M cones based on their morphological features (Ahnelt *et al.* 1987; Szel *et al.* 1988; Curcio *et al.* 1991; Ahnelt *et al.* 1994; Ahnelt *et al.* 1994; Kolb *et al.* 1997). Specifically, S cones have a longer inner segment and a narrower circumference at the outer limiting membrane (Kolb *et al.* 1997). They also contain an opsin that differs in its genetic structure from that of the L or M cone opsins, allowing for S cone specific immunostaining (Nathans *et al.* 1986; Szel *et al.* 1988).

S cones contribute to a pathway that is functionally and anatomically separate from L and M cones. Specific bipolar cells have synaptic input only from multiple S cones, and terminate in the ON sublayer 5 of the IPL (Kouyama *et al.* 1992). Postsynaptic to the S cone bipolar cell, there is also a distinct bistratified ganglion cell type within the S cone circuitry. This retinal ganglion cell stratifies in both the ON and OFF layers of the IPL, suggesting a bipartite cone input (Dacey 1993; Dacey *et al.* 1994). In the ON sublaminae, the retinal ganglion cell connects only to S cone bipolar cells (Mariani 1984;

Kouyama *et al.* 1992; Wassle *et al.* 1994), but in the OFF layers it receives excitation from bipolar cells connected to both L and M cones (Boycott *et al.* 1991). So, together with the S cone bipolar cell, these ganglion cells form the basis of a distinct pathway that carries S cone signals from the retina to the brain.

S cones have also recently been shown to provide some input to both midget and parasol ganglion cells. OFF midget cells frequently receive functional input from at least one S cone, while ON midget and ON and OFF parasol cells do so much less frequently. On average, S cones provided input to OFF midget cells ~60% of the time, ON midget cells ~16%, ON parasol ~12%, and OFF parasol ~5% (Field *et al.* 2010, their Figure 4d). Thus, while it is possible for any retinal ganglion cell class to be driven by an S cone, this data from the peripheral retina suggests that they most often synapse onto OFF midget ganglion cells specifically. In light of our cone-targeting microstimulation experiments, we will need to consider the occasional encounter with an S cone, and how that might impact summation.

### *Receptive fields*

Once light signal reaches the photoreceptors, the signals created must be combined in some way in order to be useful. The retinal circuits we have reviewed constrain how these signals are combined and propagated to each neuron along the visual pathway. A picture of how cone signals are combined begins with the idea of a receptive field, a concept first envisioned by Sherrington to describe a patch of skin in a dog which, when stimulated, would elicit a scratch reflex. Defined by Sherrington, a receptive field is

“The whole area of skin from whose points the scratch-reflex can be elicited may be conveniently termed the receptive field of that reflex” (Sherrington 1906, p. 27). Framing this concept in the visual system, a receptive field is a volume of visual space in which the presence of light will alter the firing rate of a particular neuron. However, given the projection of visual space onto the retina by the eye’s optics, a receptive field can also be defined retinotopically, with a patch of retina corresponding in location and extent to the receptive field in visual space. If we consider the receptive field of a photoreceptor, it is no more than the optical light-gathering capability of its inner/outer segments—an area only a few microns wide on the retina. As multiple photoreceptor inputs converge onto downstream neurons, the size of receptive fields for bipolar cells or ganglion cells becomes correspondingly larger.

Traditionally, receptive fields can be “mapped” by recording a single neuron’s response to a spot of light flashed ON or OFF at different locations in the visual field. The receptive fields of mammalian retinal ganglion cells were first mapped this way in the cat by Kuffler (1953). He found that specific locations on the retina elicited an ON response to light, as a cell increased its firing when a light stimulus was presented. He additionally noted that neighboring locations caused an OFF response, where the firing of the retinal ganglion cell decreased in response to light. There was a clear spatial organization of these responses: a center region dominated by either an ON or OFF response, and a surrounding region dominated by the opposite response. Depending on neuron type, these concentric receptive fields can be ON center + OFF surround, or OFF center + ON surround. These retinal ganglion cells exhibited a maximum response when

the center region alone was stimulated (regardless of polarity), and this center response could be inhibited by simultaneous stimulation in the surround.

It is worth noting here that this antagonistic effect between center and surround is not mediated by any interaction between the ON and OFF pathways just reviewed. In the center region, the discharge pattern of an ON retinal ganglion cell is directly related to the inputs of the ON bipolar cells. The surround inhibition is channeled directly through the ON bipolar cells, without the participation of any OFF bipolar cells, primarily via a non-GABAergic pathway involving horizontal cells (McMahon *et al.* 2004). This idea was confirmed empirically using a pharmacological agent, 2-amino-4-phosphonobutyric acid, to selectively block only the activity of ON bipolar cells (Shiells *et al.* 1981; Slaughter *et al.* 1981; Shiells *et al.* 1990). Under these conditions, the center and surround responses of ON centered cells were blocked, while the responses of OFF centered cells were unchanged (Schiller 1982; Horton *et al.* 1984; Schiller 1984). These results indicate that ON and OFF pathways are functionally separate in the retina, with the separation maintained (to some extent) at the next step in the visual pathway, the lateral geniculate nucleus (LGN) (Schiller 1992).

### Summation

Up until now, we have mainly been discussing the visual system as individual cells operating within a retinal circuit. Now we will step away from this cellular based approach, and move into looking at the visual system as just that, a system. While each

individual cell plays a crucial role in the relaying and transforming of visual signals along the pathway, it is the pooling or some other combination of these signals at each successive step in the system that leads to any percept more complicated than simply light detection. This idea of signal summation has been explored at some length by many investigators, both electrophysiologically and psychophysically. Stimuli may be summed either temporally, where multiple stimuli delivered in rapid succession evoke a greater response than a single stimulus, or spatially, where increasing the retinal area subtended by a stimulus would produce a greater response. Spatial summation was first described psychophysically by Riccò's Law (Riccò 1877). This law seeks to establish the relationship among stimulus area ( $A$ ), stimulus intensity ( $I$ ), and a constant threshold value ( $C$ ). Riccò's Law, applicable for small spot stimuli, holds when reciprocal changes in stimulus area or stimulus intensity leave threshold unaffected ( $A \times I = C$ ). The experiments described in this dissertation utilize small-spot stimuli that are  $\sim 45$  arcsec ( $\sim 3.6 \mu\text{m}$ ) in size, and would be considered well within the regime where Riccò's Law holds. In the upcoming sections, we will briefly review the literature on the subject of spatial and temporal summation, and examine how different types of stimuli impact the study of visual signal summation.

### *Single spot stimuli*

The first types of stimuli we will explore are single spots of various diameters. In psychophysics, and in early electrophysiological experiments, the size and location of the circular stimulus plays an important role in the interpretation of potential summation. An



ON center, OFF surround receptive field structure, for example, would have an optimal response if an increment filled the center (Figure 5, *center*). Studying summation requires a stimulus to elicit integration of signals from multiple receptors. When a stimulus is smaller than the field center (Figure 5, *left*), the question becomes: Does the response scale with the percentage of the field center that is stimulated? If the response does scale this way, it follows Riccò's Law and is considered linear. If the circular stimulus is increased in size beyond the field center, the OFF surround may begin to suppress or lessen the response (Figure 5, *right*). In the literature, this suppressive response is referred to as "nonlinear", because the linear relation is no longer being followed.

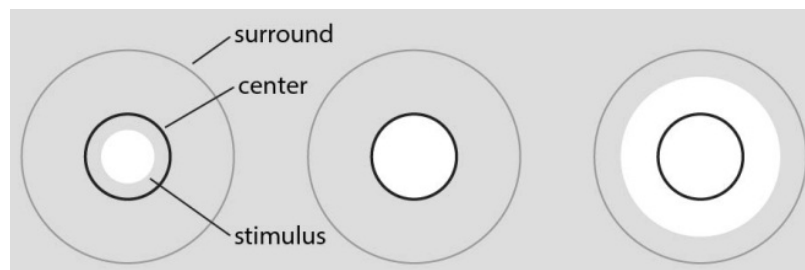


**Figure 5. Variations in single spot stimuli used to probe spatial summation.** Stimuli may be smaller in diameter than the field center, eliciting a submaximal ON response (*left*). A stimulus the same size as the field center will evoke a maximal ON response (*middle*). Stimuli larger than the center will stimulate the center and surround, activating some inhibition and producing a submaximal response from the cell (*right*).

This type of experiment is exemplified in an early paper on spatial summation done in the frog retina (Barlow 1953). Here, circular spot stimuli of increasing diameters were centered on the receptive field, while electrical responses were recorded from ganglion cells. In Figure 6, summation for two different cells is represented graphically as the size of the stimulus increases. Starting with very small spots, each cell becomes more sensitive to light, meaning that the inclusion of additional receptors adds to the response. Less incident light is necessary to produce a threshold response. Looking at the

ON-OFF cell, summation was approximately linear until the radius of the stimulus reached a critical size (in this case,  $\sim 0.25$  mm, Figure 6). At this point, the cell becomes less sensitive, and linearity fails. Similar findings of linear summation were found using other methods, including psychophysics, in a variety of species (Barlow 1957; Fankhauser *et al.* 1960; Wiesel 1960; Wiersma 1966; Cleland *et al.* 1968; Easter 1968; Freund *et al.* 1969; Naka *et al.* 1970; Arnett 1972). It should be noted that these designations, linear and nonlinear summation, are not always used to refer to the same effect as the one just described, and this issue will be discussed in detail for each instance of variation in the terms' usage.

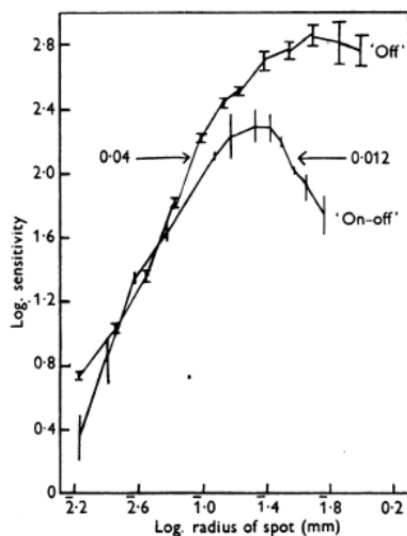


**Figure 6. Summation in single ganglion cells of the frog retina.** Arrows indicate the sensitivity corresponding to a stimulus of intensity equal to the background. Spot radius on the abscissa is not clear and may be mislabeled; text states where the spot size departs from linearity (reproduced with permission from Barlow 1953).

In experiments of this kind, then, the stimuli being used were increased in size to become sufficiently large to stimulate both the excitatory center and the inhibitory surround of the retinal ganglion cell being recorded from, resulting in less effective signal summation downstream. Similar experiments have been conducted psychophysically, with the idea that, at threshold, the perceptual response is dictated by a single ganglion cell. The area where the light signals are summed linearly across the receptive field center—as we have mentioned—is Riccò's area. This has been measured in both scotopic

(Wald 1938; Barlow 1958; Baumgardt *et al.* 1961; Hallett *et al.* 1962; Scheffrin *et al.* 1998) and photopic conditions (Graham 1939; Brindley 1954; Barlow 1958; Glezer 1965; Wilson 1970; Dannheim *et al.* 1971; Scholtes *et al.* 1977; Johnson *et al.* 1978; Lie 1980; Inui *et al.* 1981; Johnson 1986). The photopic studies, most relevant to this dissertation, employed varied experimental conditions, including variations in stimulus duration, retinal eccentricity, background intensity, and spectral composition of the stimulus. The variation in these parameters may likely have influenced the neural mechanisms mediating spatial summation, and therefore, the size of Riccò's area. However, in experiments where stimulus duration and background intensities were held constant over multiple retinal eccentricities, Riccò's area was shown to increase in size steadily with eccentricity, and was considered to roughly scale with retinal ganglion cell dendritic fields (Wilson 1970; Dannheim *et al.* 1971; Lie 1980; Inui *et al.* 1981; Johnson 1986; Spillmann *et al.* 1987; Volbrecht *et al.* 2000). Though the experiments of this dissertation are done over a relatively small range of eccentricities ( $\sim 1-4^\circ$ ), we are interested in finding out if Riccò's Law would hold true in its most simple form—combining signals from cone pairs.

### *Grating stimuli*

A second type of stimulus commonly used to characterize spatial summation is a sinusoidal grating, where stimulus contrast is modulated between 0 and 1 in the pattern of a sine wave with adjustable spatial frequencies (Figure 7). Experiments of this kind, exemplified by Enroth-Cugell *et al.* (1966), center the sinusoidal grating on the receptive

field center. The spatial phase of the stimulus allows for characterization of receptive field. In cat retinal ganglion cells, they found two distinct response patterns to phase shifts of  $90^\circ$ . The first exhibited linear summation based on the exact location of the stimulus on the receptive field center; these were called X cells. The second response pattern, found in another type of ganglion cell called Y cells, exhibited a transient response to changes in the stimulus and was insensitive to stimulus position. The cells responded at stimulus onset and offset, violating linear summation. So while X cells integrate the signals from different parts of their receptive field, proportional to the local retinal illumination, Y cells transiently respond to any change in light distribution over their field centers (Enroth-Cugell *et al.* 1966). This distinction between the two cell types was found to be independent of background luminance levels, even extending into the scotopic range (Linsenmeier *et al.* 1979). Furthermore, the distinct response properties of X and Y cells were later found to be conserved within the respective X and Y cells of the feline lateral geniculate nucleus (Shapley *et al.* 1975). In cat, therefore, these characteristic response patterns in the two distinct cell types were found to be conserved from retina to visual cortex.

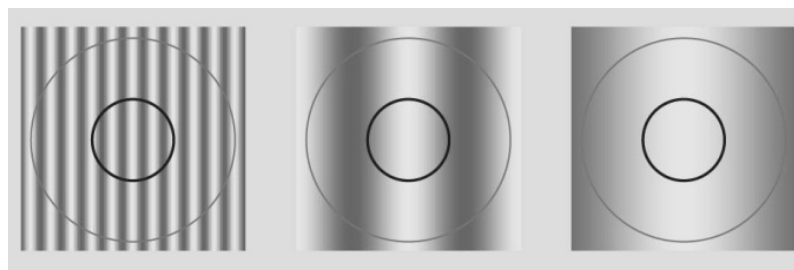


**Figure 7. Variations in grating stimuli used to probe spatial summation.** High frequency stimuli present equal amounts of light increments and decrements, and if summation was linear, would yield no response (*left*). If the frequency of the grating matches the size of the field center, a maximal response will occur (*center*). Low frequency stimuli may stimulate center and surround, evoking surround inhibition and a submaximal response (*right*).

Although the linearity seen with grating stimuli is prevalent in macaque LGN, it turns out that the homology with the cat X-Y system is imperfect. X-like linearity is found in all parvocellular neurons, but is also present in 75% of magnocellular neurons (Kaplan *et al.* 1982). The remaining magnocellular neurons have Y-like nonlinear responses, forming a third functional group. So, while summation probed with gratings can be used as a distinguishing characteristic between X and Y cells of the cat, the primate visual system does not share this distinction. The important point here is that the great majority of the cells in the primate retina and LGN seem to exhibit linear summation, specifically when grating stimuli are used (Li *et al.* 2014).

### *Multi-spot stimuli*

The experiments that most closely mirror the research described in this dissertation use small spot stimuli that encompass two separate and distinct retinal areas (Figure 8). In some studies they are referred to as “two spot experiments” (Barlow 1953; Easter 1968), and other times they are called “multi-spot experiments” (Cleland *et al.* 1968). These experiments obtain a measured threshold for a single small spot stimulus, a neighboring small spot stimulus, and both stimuli simultaneously. This experimental paradigm is the same that will be used for the experiments described in *Chapter 2*, and has previously yielded three main types of summation. First, some findings report summation which exceeds linearity. In Easter (1968), two equally sensitive receptors (within 0.1 log unit) were selected within the field centers of single goldfish ganglion cells. When the relative sensitivities of the single receptors were compared to the

measured sensitivity in the two-spot condition, it was found that summation was more efficient when two areas were illuminated simultaneously. In other words, these cells deviated from Riccò's Law, and summed their signals in a supralinear fashion, increasing downstream efficacy.

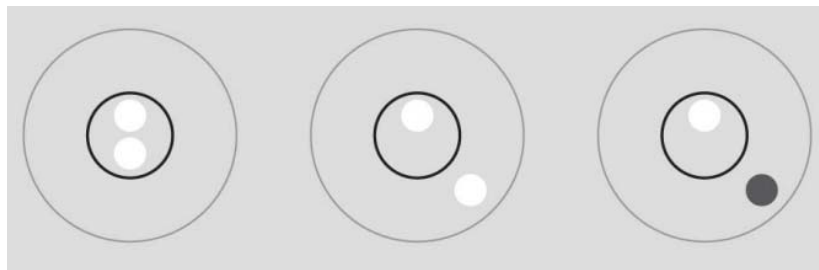


**Figure 8. Multispot stimuli configurations used to probe spatial summation.** Two stimuli presented in the field center will elicit a summing ON response (*left*). If one increment stimulus is presented in the field center, and one is in the surround, inhibition will lead to a submaximal will occur (*center*). An increment stimulus presented to the field center, combined with a decrement stimulus delivered to the surround, will combine produce an ON response greater than if the center alone was stimulated (*right*).

The second outcome that multi-spot experiments have yielded is summation that is less efficient than linearity. Stone *et al.* (1968), for example, found in cat that doubling the stimulus by presenting a second, equiluminant spot increased ganglion cell firing by a factor of  $\sim 1.5$ . Interestingly, when they doubled the stimulus by doubling the spot intensity (using the equation  $A \times I = C$ ), the ganglion cell increased its firing by a factor of only  $\sim 1.3$  (Stone *et al.* 1968). An outcome such as this one suggests the presence of an inhibitory mechanism presynaptic to the ganglion cell being recorded. In single-cell recordings using multi-spot stimuli, both stimuli must be placed within the bounds of the field center in order to observe complete summation within the ON pathway. Upon direct examination, this particular type of nonlinearity was confirmed to be related to surround inhibition by positioning one spot in the excitatory center and one spot in the inhibitory surround (Stone *et al.* 1968).

Finally, the third outcome reported in experiments using two-spot stimuli is linear summation. Two-spot experiments afford the most precise measurement of Riccò's Area, particularly in the case where each spot is cone-sized. This is one of the main goals of this dissertation: to use cone targeted microstimulation to essentially determine the minimum possible area where cone signals will abide by Riccò's Law and sum their signals linearly. This outcome has been reported previously in experiments where the stimuli are not cone-sized, but both spots fall into discrete areas of the receptive field center (i.e. Cleland *et al.* 1968).

It is important to note that these instances of summation are occurring within the retina, regardless of the type of signal integration. By recording from single optic nerve fibers, or single ganglion cells, there can be no doubt that the measured activity represents signals arising from a distinct and discrete area of the retina. In the experiments of this dissertation, results are obtained psychophysically, and so a single cell type cannot be definitively shown to mediate cone signal summation. However, it has been extensively shown that cone signals integrate their signals within the retina; something found even when single cones are targeted for microstimulation *in vitro* (Li *et al.* 2014). Some of the experiments presented in *Chapter 2* are designed to better understand which retinal cell type is primarily mediating summation measured psychophysically.

### *Temporal summation*

The early psychophysical work of Bloch (1885) showed that for stimuli of brief duration, visual thresholds were determined by the number of quanta in the stimulus—a product of the stimulus intensity and duration ( $L \times time = constant$ , where  $L$  is threshold luminance). The effects of each quantum are summed by the visual system and lead to threshold detection, an interaction called temporal summation (Bloch 1885; Graham 1937; Barlow 1958). Such temporal summation has been shown to be linear psychophysically, up to a certain duration which depends on other stimulus conditions. For photopic background illuminances, single flashes lasting less than 100 msec follow Bloch's Law (Roufs 1973), as do briefer dual flashes occurring within ~50 msec of one another (Blackwell 1963). This compares well with direct physiological measurements of cones. Cone responses to 10 msec stimuli last ~100 msec (Baylor *et al.* 1987; Schnapf *et al.* 1987). Should two dim (i.e. far from saturating) flashes of light be delivered within the 100 msec, they have the opportunity to sum along the intensity response function of the cone, assuming that neither flash alone generates a response approaching saturation. Responses in bipolar cells are likely to reflect the photoreceptor's response for stimuli delivered closely in time (Ichinose *et al.* 2014). If we consider the case of multiple stimuli delivered to multiple cones in near-simultaneous fashion, we also have to assume that the graded responses in bipolar cells will sum as if being driven by a single cone. The furthest apart in time that our stimuli were delivered was ~2 msec, making it probable that temporal summation is occurring in a downstream retinal neuron that is synaptically connected to the stimulated cones. This would allow the downstream neuron to



potentially sum the cone signals as one, effectively mitigating any concern that a lack of temporal summation could lead to nonlinear summation.

### Spatial considerations with stimuli

Experiments of the kind described in this dissertation have many practical constraints. Primarily, in order to interpret any results regarding spatial summation, it is imperative to understand and account for several variables affecting stimulus delivery. Fixational eye movements by the subject, intrinsic ocular chromatic dispersion, vascular interference, and optical spread of the stimulus itself could all contribute to an unintended spatial distribution of light. In this section I review how these factors impact the study of spatial summation and address how they are controlled for in our experiments.

#### *Fixational eye movements*

The human eye is constantly in motion, with movements usually classified into categories such as microsaccades, tremor, and drift (reviewed in Rolfs 2009). These movements are present even when a subject is actively fixating on a target. With traditional stimuli (typically subtending  $0.25^\circ$  or more), small eye movements can largely be ignored during the course of visual testing. On a microscopic scale, however, small eye movements during active fixation become substantial. A retinal movement of even a few microns would cause a cone-sized stimulus to be smeared over many cones,

effectively ameliorating the spatial discreteness of the stimulus. In a subject with good fixation, for example, fixational eye motion had a mean shift of 0.36 arcmin every 30 msec (Figure 9A). If these shifts all went in the same direction, which often occurs for brief episodes, this cumulative eye movement would move a stimulus from one cone to a neighboring cone within ~100 msec (Sincich 2016).

Eye movements such as the ones presented here could be overcome in two ways. First, stimuli targeted to the same cone could be delivered very rapidly, to mitigate most

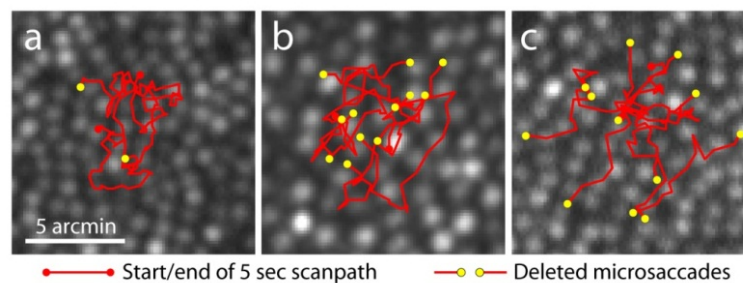


**Figure 9. Retinal motion in fixating subjects ranges over many cones.** Each panel shows the cone mosaic and the reconstructed motion path from a 5 sec stabilized adaptive optics scanning laser ophthalmoscope (AOSLO) movie recorded during active fixation at 30 Hz. Scanpaths (red) have had microsaccades deleted (yellow endpoints). Some subjects, as in (A), exhibit small frame-by-frame eye motion and rare microsaccades, while other subjects can have larger drifts and more saccades (B). Subjects can also manifest persistent drift along one axis, such as diagonal (C), with each drift canceled by a compensating microsaccade. As long as eye motion remains less than about one-third of the frame width ( $5\times$  larger than these cropped images), video stabilization can track the position of cones targeted for stimulation.

eye motion (excluding microsaccades). This would necessitate stimulus trials being delivered less than 10 msec apart, which, given the slow photocurrent response of cones, would result in temporal summation, and the successive stimuli would appear as a single stimulus (Schnapf *et al.* 1990; Cao *et al.* 2014). Within the context of our spatial summation experiments, this effectively negates the utility of this method. The second way to overcome fixational eye motion is to use an eye tracking method, which has been employed for all the experiments in this dissertation. A video-based method was recently

developed for use in adaptive optics-based systems, and is detailed further in *Chapter 2: Methods* (Arathorn *et al.* 2007; Yang *et al.* 2010).

### *Chromatic dispersion*

The lens and cornea of the normal human eye have high-order optical aberrations, which, unlike the lower-order aberrations of defocus and astigmatism, cannot be compensated for by standard corrective lenses (Liang *et al.* 1997; Hofer *et al.* 2001). Adaptive optics ophthalmoscopy has allowed these high-order aberrations to be mostly overcome, enabling the imaging of both rod and cone photoreceptors *in vivo* (Dubra *et al.* 2011). When imaging with just one wavelength, chromatic aberration is usually of little concern. However, when the imaging and stimulus wavelengths differ, chromatic dispersion must be accounted for. Essentially, as multiwavelength light is delivered to the corneal surface, the lens and other ocular media will focus each wavelength differentially. This phenomenon causes two distinct forms of optical chromatic aberrations: longitudinal and transverse.

Longitudinal chromatic aberration (LCA) occurs because a lens will focus different wavelengths of light at different axial depths. Because an 840 nm imaging beam is used to visualize the photoreceptors, LCA would cause the 543 nm stimulus beam to be at different depth of focus. It has been demonstrated that LCA in the human eye is relatively consistent among individuals (Thibos *et al.* 1990; Atchison *et al.* 2005). In the case of our imaging and stimulation wavelengths, for example, the focal difference is one diopter. Because the relationship between wavelength and focal depth can be estimated

(Equation 5a in Atchison *et al.* 2005), LCA can generally be compensated for by the static positioning of optics within the ophthalmoscope. Proper alignment brings all wavelengths into roughly equal focus on the retina (see Figure 1c from Harmening *et al.* 2012).

Following the fixed compensation of LCA, the second chromatic effect, transverse chromatic aberration (TCA) must still be accounted for. This correction is more challenging than LCA, because it depends on the position of the imaging beam relative to both the pupil and the achromatic axis of the eye (Simonet *et al.* 1990; Thibos *et al.* 1990; Harmening *et al.* 2012). This means that for each experiment, pupil position and direction of gaze must be taken into account when correcting for TCA. Once the LCA has been corrected, TCA would cause the foci for each wavelength to be shifted relative to the optical axis of the eye (Figure 10A). Along this axis, TCA is zero by definition. While aligning all of the imaging beams to the achromatic axis would effectively eliminate TCA, finding the axis in each individual is difficult in practice. The position of the achromatic axis relative to the pupil varies person by person, so TCA correction by co-aligning all wavelengths would have to be done empirically for each subject (Rynders *et al.* 1995; Marcos *et al.* 2001; Harmening *et al.* 2012).

Instead of trying to find the achromatic axis of each subject and aligning the beams to it for each subject, a novel method of correcting TCA has been developed (Harmening *et al.* 2012). In this method, TCA and beam misalignment offsets are measured in the adaptive optics scanning laser ophthalmoscope (AOSLO) images directly. This method is possible because, independent of beam paths and the placement of the imaging detectors, TCA offsets are actually displayed on the retina, and therefore

they are preserved as spatial information within the resultant AOSLO images. When compared to a standard chromatic eye model, TCA offsets measured from retinal images fit well (Figure 10B). Since TCA is dependent on pupil position and gaze, it can be demonstrated during small gaze shifts on a frame-by-frame basis within a recorded video (Figure 10C). In this particular example, the stimulation wavelength (543 nm) was offset by about two cone diameters from the imaging wavelength (840 nm). Without this TCA correction, multiwavelength delivery of light onto single cones with high spatial fidelity would be impossible.

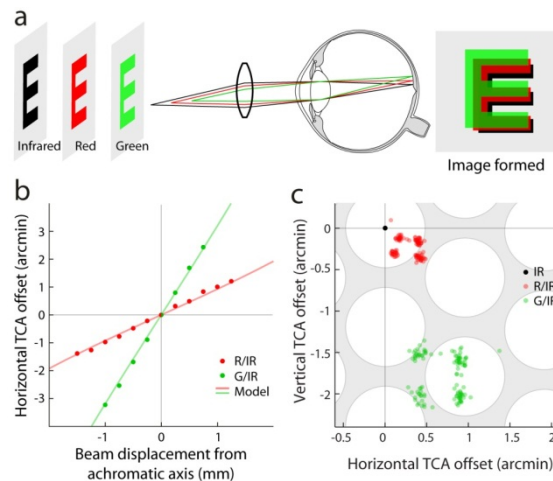


**Figure 10. Longitudinal and transverse chromatic dispersion in multiwavelength retinal imaging.** (A) Schematic of how longitudinal dispersion is corrected in an AOSLO, by setting different focal distances for each wavelength channel (represented by the separated “E”s). The focal distances were computed according to (Atchison *et al.* 2005). This leaves transverse image offsets on the retina (superimposed “E”s) that must be measured and compensated. (B) Transverse chromatic offset measurements made from retinal imaging during horizontal pupil displacements (dots, means of 20 measurements) are compared to offsets computed from a standard chromatic eye model (lines) (Thibos *et al.* 1992). Pupil displacements of 0.25 mm produce offsets in the green channel that are more than twice the size of typical foveal cones ( $\sim 0.4$  arcmin). (C) Frame-by-frame measurements of transverse offsets (relative to an infrared channel, IR, at zero) during sequential fixation on four corners of a  $1^\circ$  square. Background circles represent  $5 \mu\text{m}$  diameter cones. Adapted from Sincich 2016.

### *Vascular interference*

Retinal blood vessels and capillaries lying in front of the photoreceptors could, in principle, interfere with stimulation light being delivered to the cones or disrupt the light reflecting from the cones. Anatomically, these vascular networks can cover more than half of the retinal surface, except at the foveal avascular zone (Snodderly *et al.* 1992). Because the photoreceptors are located behind the retinal vessels, one way the vessels can interfere with imaging and stimulation light is simply by casting shadows. This has been demonstrated to directly contribute to raising threshold by at least a factor of 2 using vessel-targeted microperimetry (Tuten *et al.* 2012).

While shadowing is one form of interference arising from retinal vessels, light path distortion can also cause light being targeted for delivery to a single cone to be spatially displaced. Light path distortion arises from both the clear cylindrical vessel walls, and from the blood cells passing through the narrow vessel lumen (Sincich 2016). While shadowing may affect large swathes of cones within the retinal image, light path distortions are more likely to operate at the level of individual cones. For example, it has been noted by several groups that the reflectivity of single cones is transiently altered when a leukocyte passes over them (Nishiwaki *et al.* 1996; Tam *et al.* 2011; Uji *et al.* 2012; Sincich 2016). The irregular shape of leukocytes, and their passage through narrow capillaries, makes their light path distortion unpredictable, and the resulting changes in cone reflectivity can be variable. The most notable change when incoming light is distorted, or when the retina is being shadowed, is that cones appear darker (see *Chapter 3: Figure 1C*). These temporal changes in reflectivity have been used to identify the

location of the vessels themselves, allowing the vasculature to be mapped in locations of interest (Martin *et al.* 2005; Martin *et al.* 2009; Tam *et al.* 2010; Bruce *et al.* 2015). When cone reflectivity is compared to the overlying vasculature map, it is revealed that many of the darkest cones lie underneath the vessel lumens. However, some of the darker cones also lie where the wall of the blood vessel, which cannot be visualized in the vasculature maps, may be diverting light away from the imaging detection path (see *Chapter 3: Figure 1D*). Given this information, vasculature interference could influence psychophysical testing of individual cones, especially when threshold measurements are of interest. However, any interference effects can largely be mitigated by using a vasculature map, compiled at the retinal location being tested, to position any cone-targeted stimuli to areas free of overlying retinal vessels.

#### *Characterization of delivered stimuli*

Here I will touch on the geometry of the stimulus itself, as it can be delivered to the retina using an AOSLO microscope. As with any optical device, the size of any stimuli delivered in using this system will be limited by diffraction. While the retinal images obtained through the use of an AOSLO are comprised of pixels, individual pixels do not actually represent the light intensity profile of the beam landing on the retina. Because an AOSLO is a confocal system for imaging, out of focus and scattered light is blocked during image formation. When the light stimulus is delivered to the retina, the “unwanted” light is still present in the stimulus itself. To get a true idea of the spatial

distribution of the stimulus, therefore, the point spread function (PSF) of the optical system needs to be considered.

Within the typical imaging field used in our psychophysical experiments ( $1.28^\circ$ , equaling  $0.725 \mu\text{m}/\text{deg}$ ), each cone is  $\sim 7$ - $11$  pixels in diameter, depending on retinal eccentricity (Figure 11). In order to confine a stimulus within the visible margins of a single cone (“cone-sized”), the stimulus defined in image pixels must be smaller than the cone within the retinal image (Figure 11A, E). Once defined in image pixels, an estimate of the actual stimulus geometry can be made by convolving the PSF of the optical system with the stimulus, defined in pixels. In a diffraction-limited system, the incident beam aperture ( $5.75 \text{ mm}$  used for the calculations in Figure 11) yields a PSF with Airy disc diameter of  $24 \text{ arcsec}$ , with a stimulation wavelength of  $543 \text{ nm}$  (Mahajan 2011).

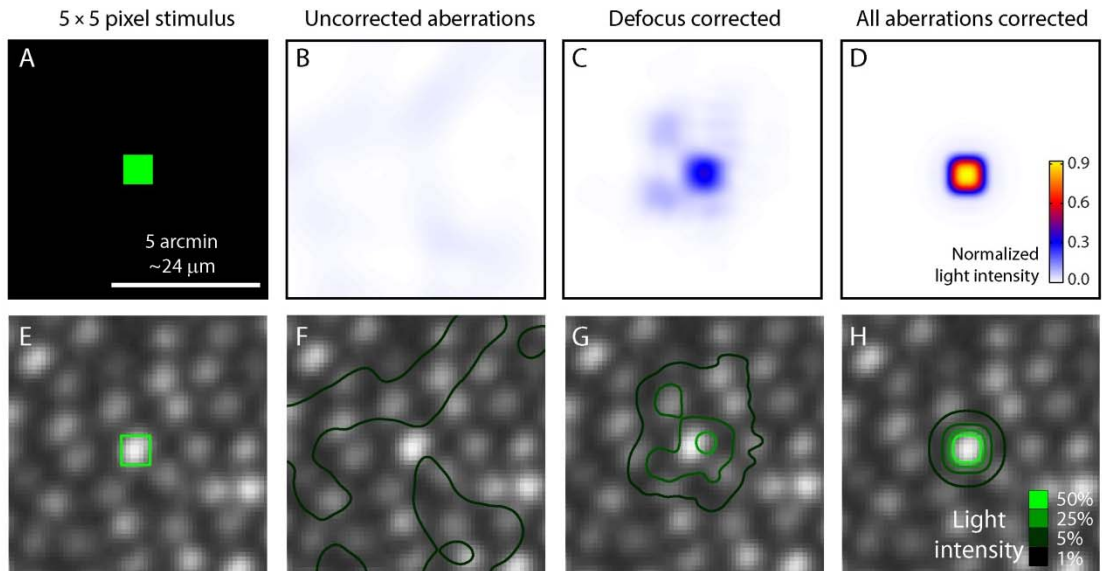


**Figure 11. Calculated light distribution of delivered stimulus without and with AOSLO correction.** Top row contains theoretical distributions of light energy from a square stimulus (A) delivered to the retina without any optical corrections (B), with just defocus corrected but retaining high-order aberrations (C), and with all optical corrections (D). Bottom row shows the above distributions as corresponding intensity contours (E-H) superimposed on a cone mosaic at  $3.5^\circ$  eccentricity. Aberration data were measured with the AOSLO from one of the subjects used in our experiments.



Expressed in image space, this equates to a diameter of 2.6 pixels, or  $\sim 1.9 \mu\text{m}$  on the retina (Sincich 2016). Left optically uncorrected, the aberrations present in the eye would cause the light from a  $5 \times 5$  pixel stimulus to be delivered over a retinal area of  $460 \mu\text{m}^2$  at the 1% intensity contour, containing only 48% of the light energy (Figure 11B, F; all not shown in panel F). This diffuse area never exceeds 5% of the light intensity anywhere and is much larger than that of an individual cone. Upon correction of defocus aberration only, the light becomes more concentrated, but  $\sim 70\%$  of the light still falls outside of the targeted cone diameter (Figure 11C, G). Finally, with all aberrations corrected using AOSLO, the 5% intensity contour covers  $33 \mu\text{m}^2$  on the retina and contains 88% of light energy (Figure 11D, H), with the remainder spread out over a very wide area, as expected from a PSF. With full AOSLO correction, cone-targeted microstimulation becomes possible.

In theory, therefore, the spatial distribution of the stimulus on the retina places most of the light over a single cone. However, repeated stimulation of the same cone is also necessary. Consequently, the stimulus geometry must also be characterized with respect to spatial delivery errors that occur during the course of each set of stimulus trials. These errors can occur even after fixational eye movements have been accounted for by real-time eye tracking and video stabilization software. In order to deliver a targeted stimulus to a retina that is in motion, the software reads the incoming video raster in real-time, and compares select portions of the raster to a predefined reference frame. Then, as the raster approaches the retinal location where stimuli are to be delivered, the software predicts the motion of the eye just prior to stimulus delivery. In the current AOSLO system, the stimulus delivery positional error has a standard deviation of about 0.15

arcmin (Arathorn *et al.* 2007; Yang *et al.* 2010; Sincich 2016). These delivery errors are accounted for in our experiments in Chapters 2 and 3.

As further evidence of high spatial fidelity in stimulus delivery in an AOSLO system, threshold experiments were performed in which one stimulus targeted cone and a second stimulus targeted an adjacent gap between cones. Perceptual thresholds were ~50% higher when the microstimuli were delivered between cones (Harmening *et al.* 2014). This finding was largely explained by a simple model of the geometry of cone light capture, where photoreceptor waveguiding would predict that coupling efficiency will be maximal at the cone center, and decrease with increasing distance from the center (see Figure 8 from Harmening *et al.* 2014). This effect has also been seen physiologically in the primate retina (Field *et al.* 2010), and in the primate lateral geniculate nucleus—the main neural target of retinal projections (Sincich *et al.* 2009). These experiments demonstrate how exquisitely sensitive the visual system is to the exact spatial position of stimuli, even down to the micron scale.

#### *Psychophysical testing and variability*

Using the real-time retinal eye tracking, vasculature mapping, chromatic aberration correction, and stimulus delivery accuracy described above, we are poised to determine how robust psychophysical threshold functions can be obtained using cone-sized stimuli. Threshold has been measured in this system using two methods of threshold estimation: a classic method of constant stimuli or an adaptive Bayesian staircase method. These threshold estimations have been obtained for single cones out to

about 5° eccentricity, with threshold rising consistently as eccentricity is increased (Harmening *et al.* 2014). Beyond 5°, multiple cones need to be stimulated simultaneously for a perceptual threshold to be measured. While this finding is only valid for a luminance increment threshold task operating within the range of light intensity that we can deliver, this increase in threshold with retinal eccentricity is consistent with prior studies using a constantly sized stimulus (Wilson 1970; Lie 1980; Inui *et al.* 1981). For threshold to be measured at the perceptual level beyond 5° eccentricity, summation of input across multiple cones is generally necessary (Anderson *et al.* 1991; Volbrecht *et al.* 2000; Drasdo *et al.* 2007).

While increment threshold measurements can be obtained from cone-sized stimuli, many forms of variability, such as stimulus delivery error, system noise, and subject inconsistency can impact psychophysical performance. Much of this variability can be traced back to errors in stimulus delivery and system noise; however, it is important to consider the possibility that human subjects may have some intrinsic inconsistency when performing threshold tasks repeatedly. Any of these errors may manifest as variability in threshold, where a measured threshold is not consistent throughout the course of the experiment. This type of variability needs to be distinguished from physiological variability, where the functional weighting of cones may not all be identical. As previously discussed, each retinal ganglion cell in the peripheral retina samples from a number of cone photoreceptors. When the functional connectivity between cones and ganglion cells was measured in explant macaque retina, each of the cones within the stimulated receptive field expressed a different synaptic weight (Field *et al.* 2010; Li *et al.* 2014). Similar results were found using an AOSLO

system while recording from macaque LGN *in vivo* (Sincich *et al.* 2009). These findings raise the possibility that differential cone weighting in the retina could be detectable at the perceptual level. One of the key experiments in this dissertation is to examine that possibility.

A final piece of evidence demonstrating the efficacy of microstimulation through AOSLO to generate cone-specific response comes from the likely occasional encounter with an S cone. The stimulus wavelength band used in these experiments was  $543 \pm 11$  nm, a range that is equally absorbed by L and M cone opsins. To produce an equivalent response with this wavelength of stimulation, an S cone would need ~400 times more light than would an L or M cone (Stockman *et al.* 2000). This would exceed the range of light that is deliverable with our AOSLO. If an S cone was targeted for stimulation under these experimental conditions, the subject would likely respond “not seen” to every trial. Given the relative sparsity of S cones in the human retina (Curcio *et al.* 1991; Roorda *et al.* 1999) this scenario was not anticipated to be encountered often. However, as we will see in *Chapter 2*, it is likely that we did encounter an occasional S cone, where no measurable threshold could be obtained, even though an adjacent cone readily produced thresholds. Such data provide additional evidence that positional delivery accuracy is high enough to probe functional responses on the cellular scale.

With all of the discussed issues taken into account, we are now ready to probe further into the functional responses arising from targeted cone-sized stimuli. Our experiments seek to understand two things: (1) perceptual response to an increase in light delivered to a single photoreceptor at threshold, and (2) perceptual change to an increase in light delivered to two photoreceptors at the same time. Because cone signals flow

through other cells in an ON pathway, intensity response curves from cone photoreceptors alone can only be one component in understanding the psychophysical response. The intensity response curves of ON cone bipolar cells and ON midget and parasol retinal ganglion cells must also be contributing to the perceptual sensation.

## COMPREHENSIVE BIBLIOGRAPHY

- Ahnelt, P. and H. Kolb (1994). Horizontal cells and cone photoreceptors in human retina: a Golgi-electron microscopic study of spectral connectivity. *J Comp Neurol* **343**(3): 406-427.
- Ahnelt, P. and H. Kolb (1994). Horizontal cells and cone photoreceptors in primate retina: a Golgi-light microscopic study of spectral connectivity. *J Comp Neurol* **343**(3): 387-405.
- Ahnelt, P. K., H. Kolb and R. Pflug (1987). Identification of a subtype of cone photoreceptor, likely to be blue sensitive, in the human retina. *J Comp Neurol* **255**(1): 18-34.
- Anderson, S. J. and D. C. Burr (1991). Spatial summation properties of directionally selective mechanisms in human vision. *J Opt Soc Am A* **8**(8): 1330-1339.
- Arathorn, D. W., Q. Yang, C. R. Vogel, Y. Zhang, P. Tiruveedhula and A. Roorda (2007). Retinally stabilized cone-targeted stimulus delivery. *Opt Express* **15**(21): 13731-13744.
- Arnett, D. W. (1972). Spatial and temporal integration properties of units in first optic ganglion of dipterans. *J Neurophysiol* **35**(4): 429-444.
- Atchison, D. A. and G. Smith (2005). Chromatic dispersions of the ocular media of human eyes. *J Opt Soc Am A Opt Image Sci Vis* **22**(1): 29-37.
- Barlow, H. B. (1953). Summation and inhibition in the frog's retina. *J Physiol* **119**(1): 69-88.

- Barlow, H. B. (1957). Increment thresholds at low intensities considered as signal/noise discriminations. *J Physiol* **136**(3): 469-488.
- Barlow, H. B. (1958). Temporal and spatial summation in human vision at different background intensities. *J Physiol* **141**(2): 337-350.
- Baumgardt, E. and B. Hillmann (1961). Duration and size as determinants of peripheral retinal response. *J Opt Soc Am* **51**: 340-344.
- Baylor, D. A. (1987). Photoreceptor signals and vision. Proctor lecture. *Invest Ophthalmol Vis Sci* **28**(1): 34-49.
- Baylor, D. A., M. G. Fuortes and P. M. O'Bryan (1971). Receptive fields of cones in the retina of the turtle. *J Physiol* **214**(2): 265-294.
- Baylor, D. A., B. J. Nunn and J. L. Schnapf (1984). The photocurrent, noise and spectral sensitivity of rods of the monkey *Macaca fascicularis*. *J Physiol* **357**: 575-607.
- Baylor, D. A., B. J. Nunn and J. L. Schnapf (1987). Spectral sensitivity of cones of the monkey *Macaca fascicularis*. *J Physiol* **390**: 145-160.
- Benardete, E. A., E. Kaplan and B. W. Knight (1992). Contrast gain control in the primate retina: P cells are not X-like, some M cells are. *Vis Neurosci* **8**(5): 483-486.
- Blackwell, H. R. (1963). Neural theories of simple visual discriminations. *J Opt Soc Am* **53**: 129-160.
- Bloch, A. M. (1885). Expérience sur la vision. *Comptes Rendus de Séances de la Société de Biologie (Paris)* **37**: 493-495.

- Boycott, B. B., J. E. Dowling and H. Kolb (1969). Organization of the primate retina: Light Microscopy. *Philosophical Transactions of the Royal Society of London. Series B, Biological Sciences* **255**(799): 109-184.
- Boycott, B. B., J. M. Hopkins and H. G. Sperling (1987). Cone connections of the horizontal cells of the rhesus monkey's retina. *Proc R Soc Lond B Biol Sci* **229**(1257): 345-379.
- Boycott, B. B. and H. Wässle (1991). Morphological Classification of Bipolar Cells of the Primate Retina. *Eur J Neurosci* **3**(11): 1069-1088.
- Brindley, G. S. (1954). The summation areas of human colour-receptive mechanisms at increment threshold. *J Physiol* **124**(2): 400-408.
- Bruce, K. S., W. M. Harmening, B. R. Langston, W. S. Tuten, A. Roorda and L. C. Sincich (2015). Normal Perceptual Sensitivity Arising From Weakly Reflective Cone Photoreceptors. *Invest Ophthalmol Vis Sci* **56**(8): 4431-4438.
- Burns, M. E. and V. Y. Arshavsky (2005). Beyond counting photons: trials and trends in vertebrate visual transduction. *Neuron* **48**(3): 387-401.
- Calkins, D. J., S. J. Schein, Y. Tsukamoto and P. Sterling (1994). M and L cones in macaque fovea connect to midget ganglion cells by different numbers of excitatory synapses. *Nature* **371**(6492): 70-72.
- Cao, L. H., D. G. Luo and K. W. Yau (2014). Light responses of primate and other mammalian cones. *Proc Natl Acad Sci U S A* **111**(7): 2752-2757.
- Cleland, B. G. and C. Enroth-cugell (1968). Quantitative aspects of sensitivity and summation in the cat retina. *J Physiol* **198**(1): 17-38.



- Crook, J. D., M. B. Manookin, O. S. Packer and D. M. Dacey (2011). Horizontal cell feedback without cone type-selective inhibition mediates "red-green" color opponency in midget ganglion cells of the primate retina. *J Neurosci* **31**(5): 1762-1772.
- Curcio, C. A., K. A. Allen, K. R. Sloan, C. L. Lerea, J. B. Hurley, I. B. Klock and A. H. Milam (1991). Distribution and morphology of human cone photoreceptors stained with anti-blue opsin. *J Comp Neurol* **312**(4): 610-624.
- Dacey, D. M. (1990). The dopaminergic amacrine cell. *J Comp Neurol* **301**(3): 461-489.
- Dacey, D. M. (1993). Morphology of a small-field bistratified ganglion cell type in the macaque and human retina. *Vis Neurosci* **10**(6): 1081-1098.
- Dacey, D. M. (1993). The mosaic of midget ganglion cells in the human retina. *J Neurosci* **13**(12): 5334-5355.
- Dacey, D. M. (1994). Physiology, morphology and spatial densities of identified ganglion cell types in primate retina. *Ciba Found Symp* **184**: 12-28; discussion 28-34, 63-70.
- Dacey, D. M. (1999). Primate retina: cell types, circuits and color opponency. *Prog Retin Eye Res* **18**(6): 737-763.
- Dacey, D. M. and B. B. Lee (1994). The 'blue-on' opponent pathway in primate retina originates from a distinct bistratified ganglion cell type. *Nature* **367**(6465): 731-735.
- Dacey, D. M., B. B. Lee, D. K. Stafford, J. Pokorny and V. C. Smith (1996). Horizontal cells of the primate retina: cone specificity without spectral opponency. *Science* **271**(5249): 656-659.

- Dacheux, R. F. and E. Raviola (1990). Physiology of HI horizontal cells in the primate retina. *Proc R Soc Lond B Biol Sci* **239**(1295): 213-230.
- Dannheim, F. and S. M. Drance (1971). Studies of spatial summation of central retinal areas in normal people of all ages. *Can J Ophthalmol* **6**(4): 311-319.
- Dartnall, H. J., J. K. Bowmaker and J. D. Mollon (1983). Human visual pigments: microspectrophotometric results from the eyes of seven persons. *Proc R Soc Lond B Biol Sci* **220**(1218): 115-130.
- Darwin, C. R. (1859). *On the origin of species by means of natural selection, or the preservation of favoured races in the struggle for life*. London, John Murray.
- de Monasterio, F. M. (1978). Center and surround mechanisms of opponent-color X and Y ganglion cells of retina of macaques. *J Neurophysiol* **41**(6): 1418-1434.
- de Monasterio, F. M. (1978). Properties of concentrically organized X and Y ganglion cells of macaque retina. *J Neurophysiol* **41**(6): 1394-1417.
- De Monasterio, F. M. and P. Gouras (1975). Functional properties of ganglion cells of the rhesus monkey retina. *J Physiol* **251**(1): 167-195.
- DeVries, S. H., X. Qi, R. Smith, W. Makous and P. Sterling (2002). Electrical coupling between mammalian cones. *Curr Biol* **12**(22): 1900-1907.
- Drasdo, N., C. L. Millican, C. R. Katholi and C. A. Curcio (2007). The length of Henle fibers in the human retina and a model of ganglion receptive field density in the visual field. *Vision Res* **47**(22): 2901-2911.
- Dubra, A., Y. Sulai, J. L. Norris, R. F. Cooper, A. M. Dubis, D. R. Williams and J. Carroll (2011). Noninvasive imaging of the human rod photoreceptor mosaic

- using a confocal adaptive optics scanning ophthalmoscope. *Biomed Opt Express* **2**(7): 1864-1876.
- Easter, S. S., Jr. (1968). Excitation in the goldfish retina: evidence for a non-linear intensity code. *J Physiol* **195**(2): 253-271.
- Enroth-Cugell, C. and J. G. Robson (1966). The contrast sensitivity of retinal ganglion cells of the cat. *J Physiol* **187**(3): 517-552.
- Euler, T., S. Haverkamp, T. Schubert and T. Baden (2014). Retinal bipolar cells: elementary building blocks of vision. *Nat Rev Neurosci* **15**(8): 507-519.
- Famiglietti, E. V., Jr., A. Kaneko and M. Tachibana (1977). Neuronal architecture of on and off pathways to ganglion cells in carp retina. *Science* **198**(4323): 1267-1269.
- Fankhauser, F. and T. Schmidt (1960). [The optimal conditions for the study of spatial summation with fixed stimuli according to the method of quantitative light-perception perimetry]. *Ophthalmologica* **139**: 409-423.
- Field, G. D., J. L. Gauthier, A. Sher, M. Greschner, T. A. Machado, L. H. Jepson, J. Shlens, D. E. Gunning, K. Mathieson, W. Dabrowski, L. Paninski, A. M. Litke and E. J. Chichilnisky (2010). Functional connectivity in the retina at the resolution of photoreceptors. *Nature* **467**(7316): 673-677.
- Freund, H. J., G. Grunewald and G. Baumgartner (1969). [Spatial summation within the receptive field center of lateral geniculate body neurons in the cat]. *Exp Brain Res* **8**(1): 53-65.
- Glezer, V. D. (1965). The receptive fields of the retina. *Vision Res* **5**(9): 497-525.
- Gouras, P. (1968). Identification of cone mechanisms in monkey ganglion cells. *J Physiol* **199**(3): 533-547.

- Graham, C. H., Brown, R. H., Mote, F. A. (1939). The relation of size of stimulus and intensity in the human eye: I. Intensity thresholds for white light. *Journal of Experimental Psychology* **24**(6): 555-573.
- Graham, C. H. C., C. (1937). Visual Acuity as a Function of Intensity and Exposure-Time. *The American Journal of Psychology* **49**(4): 654-661.
- Grimes, W. N. (2012). Amacrine cell-mediated input to bipolar cells: variations on a common mechanistic theme. *Vis Neurosci* **29**(1): 41-49.
- Grunert, U., P. R. Martin and H. Wässle (1994). Immunocytochemical analysis of bipolar cells in the macaque monkey retina. *J Comp Neurol* **348**(4): 607-627.
- Hallett, P. E., F. H. Marriott and F. C. Rodger (1962). The relationship of visual threshold to retinal position and area. *J Physiol* **160**: 364-373.
- Harmening, W. M., P. Tiruveedhula, A. Roorda and L. C. Sincich (2012). Measurement and correction of transverse chromatic offsets for multi-wavelength retinal microscopy in the living eye. *Biomed Opt Express* **3**(9): 2066-2077.
- Harmening, W. M., W. S. Tuten, A. Roorda and L. C. Sincich (2014). Mapping the perceptual grain of the human retina. *J Neurosci* **34**(16): 5667-5677.
- Hecht, S., S. Shlaer and M. H. Pirenne (1942). Energy, Quanta, and Vision. *J Gen Physiol* **25**(6): 819-840.
- Hofer, H., P. Artal, B. Singer, J. L. Aragon and D. R. Williams (2001). Dynamics of the eye's wave aberration. *J Opt Soc Am A Opt Image Sci Vis* **18**(3): 497-506.
- Hofer, H., J. Carroll, J. Neitz, M. Neitz and D. R. Williams (2005). Organization of the human trichromatic cone mosaic. *J Neurosci* **25**(42): 9669-9679.

- Hornstein, E. P., J. Verweij and J. L. Schnapf (2004). Electrical coupling between red and green cones in primate retina. *Nat Neurosci* **7**(7): 745-750.
- Horton, J. C. and H. Sherk (1984). Receptive field properties in the cat's lateral geniculate nucleus in the absence of on-center retinal input. *J Neurosci* **4**(2): 374-380.
- Humanski, R. A. and H. R. Wilson (1992). Spatial frequency mechanisms with short-wavelength-sensitive cone inputs. *Vision Res* **32**(3): 549-560.
- Ichinose, T., B. Fyk-Kolodziej and J. Cohn (2014). Roles of ON cone bipolar cell subtypes in temporal coding in the mouse retina. *J Neurosci* **34**(26): 8761-8771.
- Inui, T., O. Mimura and K. Kani (1981). Retinal sensitivity and spatial summation in the foveal and parafoveal regions. *J Opt Soc Am* **71**(2): 151-163.
- Jacoby, R., D. Stafford, N. Kouyama and D. Marshak (1996). Synaptic inputs to ON parasol ganglion cells in the primate retina. *J Neurosci* **16**(24): 8041-8056.
- Johnson, C. A., J. L. Keltner and F. Balestrery (1978). Effects of target size and eccentricity on visual detection and resolution. *Vision Res* **18**(9): 1217-1222.
- Johnson, M. A. (1986). Color vision in the peripheral retina. *Am J Optom Physiol Opt* **63**(2): 97-103.
- Jusuf, P. R., P. R. Martin and U. Grunert (2006). Synaptic connectivity in the midget-parvocellular pathway of primate central retina. *J Comp Neurol* **494**(2): 260-274.
- Kaplan, E. and R. M. Shapley (1982). X and Y cells in the lateral geniculate nucleus of macaque monkeys. *J Physiol* **330**: 125-143.
- Koenig, D. and H. Hofer (2011). The absolute threshold of cone vision. *J Vis* **11**(1).

- Kolb, H. (1970). Organization of the outer plexiform layer of the primate retina: electron microscopy of Golgi-impregnated cells. *Philos Trans R Soc Lond B Biol Sci* **258**(823): 261-283.
- Kolb, H. (1979). The inner plexiform layer in the retina of the cat: electron microscopic observations. *J Neurocytol* **8**(3): 295-329.
- Kolb, H. (1997). Amacrine cells of the mammalian retina: neurocircuitry and functional roles. *Eye (Lond)* **11** ( Pt 6): 904-923.
- Kolb, H. and L. Dekorver (1991). Midget ganglion cells of the parafovea of the human retina: a study by electron microscopy and serial section reconstructions. *J Comp Neurol* **303**(4): 617-636.
- Kolb, H., E. Fernandez, J. Schouten, P. Ahnelt, K. A. Linberg and S. K. Fisher (1994). Are there three types of horizontal cell in the human retina? *J Comp Neurol* **343**(3): 370-386.
- Kolb, H., P. Goede, S. Roberts, R. McDermott and P. Gouras (1997). Uniqueness of the S-cone pedicle in the human retina and consequences for color processing. *J Comp Neurol* **386**(3): 443-460.
- Kolb, H. and D. Marshak (2003). The midget pathways of the primate retina. *Doc Ophthalmol* **106**(1): 67-81.
- Kolb, H. and R. Nelson (1981). Amacrine cells of the cat retina. *Vision Res* **21**(11): 1625-1633.
- Koontz, M. A. and A. E. Hendrickson (1990). Distribution of GABA-immunoreactive amacrine cell synapses in the inner plexiform layer of macaque monkey retina. *Vis Neurosci* **5**(1): 17-28.

- Kouyama, N. and D. W. Marshak (1992). Bipolar cells specific for blue cones in the macaque retina. *J Neurosci* **12**(4): 1233-1252.
- Kuffler, S. W. (1953). Discharge patterns and functional organization of mammalian retina. *J Neurophysiol* **16**(1): 37-68.
- Lamb, T. D. and E. J. Simon (1976). The relation between intercellular coupling and electrical noise in turtle photoreceptors. *J Physiol* **263**(2): 257-286.
- Lee, B. B., J. Pokorny, V. C. Smith and J. Kremers (1994). Responses to pulses and sinusoids in macaque ganglion cells. *Vision Res* **34**(23): 3081-3096.
- Li, P. H., G. D. Field, M. Greschner, D. Ahn, D. E. Gunning, K. Mathieson, A. Sher, A. M. Litke and E. J. Chichilnisky (2014). Retinal representation of the elementary visual signal. *Neuron* **81**(1): 130-139.
- Liang, J., D. R. Williams and D. T. Miller (1997). Supernormal vision and high-resolution retinal imaging through adaptive optics. *J Opt Soc Am A Opt Image Sci Vis* **14**(11): 2884-2892.
- Lie, I. (1980). Visual detection and resolution as a function of retinal locus. *Vision Res* **20**(11): 967-974.
- Linsenmeier, R. A. and H. G. Jakiela (1979). Non-linear spatial summation in cat retinal ganglion cells at different background levels. *Exp Brain Res* **36**(2): 301-309.
- MacNeil, M. A., J. K. Heussy, R. F. Dacheux, E. Raviola and R. H. Masland (1999). The shapes and numbers of amacrine cells: matching of photofilled with Golgi-stained cells in the rabbit retina and comparison with other mammalian species. *J Comp Neurol* **413**(2): 305-326.

- MacNeil, M. A. and R. H. Masland (1998). Extreme diversity among amacrine cells: implications for function. *Neuron* **20**(5): 971-982.
- Mahajan, V. N. (2011). *Optical Imaging and Aberrations: Part II. Wave Diffraction Optics*. Bellingham, Washington, SPIE Press.
- Marc, R. E. (1982). Spatial organization of neurochemically classified interneurons of the goldfish retina-I. Local patterns. *Vision Res* **22**(5): 589-608.
- Marcos, S., S. A. Burns, P. M. Prieto, R. Navarro and B. Baraibar (2001). Investigating sources of variability of monochromatic and transverse chromatic aberrations across eyes. *Vision Res* **41**(28): 3861-3871.
- Mariani, A. P. (1981). A diffuse, invaginating cone bipolar cell in primate retina. *J Comp Neurol* **197**(4): 661-671.
- Mariani, A. P. (1984). Bipolar cells in monkey retina selective for the cones likely to be blue-sensitive. *Nature* **308**(5955): 184-186.
- Martin, J. A. and A. Roorda (2005). Direct and noninvasive assessment of parafoveal capillary leukocyte velocity. *Ophthalmology* **112**(12): 2219-2224.
- Martin, J. A. and A. Roorda (2009). Pulsatility of parafoveal capillary leukocytes. *Exp Eye Res* **88**(3): 356-360.
- McMahon, M. J., O. S. Packer and D. M. Dacey (2004). The classical receptive field surround of primate parasol ganglion cells is mediated primarily by a non-GABAergic pathway. *J Neurosci* **24**(15): 3736-3745.
- Naka, K. I. and P. W. Nye (1970). Receptive-field organization of the catfish retina: are at least two lateral mechanisms involved? *J Neurophysiol* **33**(5): 625-642.



- Nathans, J., D. Thomas and D. S. Hogness (1986). Molecular genetics of human color vision: the genes encoding blue, green, and red pigments. *Science* **232**(4747): 193-202.
- Nelson, R. and H. Kolb (1983). Synaptic patterns and response properties of bipolar and ganglion cells in the cat retina. *Vision Res* **23**(10): 1183-1195.
- Nishiwaki, H., Y. Ogura, H. Kimura, J. Kiryu, K. Miyamoto and N. Matsuda (1996). Visualization and quantitative analysis of leukocyte dynamics in retinal microcirculation of rats. *Invest Ophthalmol Vis Sci* **37**(7): 1341-1347.
- Paley, W. (1809). Natural Theology: or, Evidences of the Existence and Attributes of the Diety.
- Polyak, S. and E. N. Willmer (1949). Retinal structure and colour vision. *Doc Ophthalmol* **3**: 24-56.
- Riccò, A. (1877). Relazioni fra il minimo angolo visuale e l'intensità luminosa. *Ann Ottal.* **6**: 373-479.
- Rieke, F. and E. A. Schwartz (1996). Asynchronous transmitter release: control of exocytosis and endocytosis at the salamander rod synapse. *J Physiol* **493** ( Pt 1): 1-8.
- Rodieck, R. W. (1998). *The First Steps in Seeing*. Sunderland, Massachusetts, Sinauer Associates.
- Rolfs, M. (2009). Microsaccades: small steps on a long way. *Vision Res* **49**(20): 2415-2441.
- Roorda, A. and D. R. Williams (1999). The arrangement of the three cone classes in the living human eye. *Nature* **397**(6719): 520-522.

- Roufs, J. A. (1973). Dynamic properties of vision. 3. Twin flashes, single flashes and flickerfusion. *Vision Res* **13**(2): 309-323.
- Rynders, M., B. Lidkea, W. Chisholm and L. N. Thibos (1995). Statistical distribution of foveal transverse chromatic aberration, pupil centration, and angle psi in a population of young adult eyes. *J Opt Soc Am A Opt Image Sci Vis* **12**(10): 2348-2357.
- Scheffrin, B. E., M. L. Bieber, R. McLean and J. S. Werner (1998). The area of complete scotopic spatial summation enlarges with age. *J Opt Soc Am A Opt Image Sci Vis* **15**(2): 340-348.
- Schiller, P. H. (1982). Central connections of the retinal ON and OFF pathways. *Nature* **297**(5867): 580-583.
- Schiller, P. H. (1984). The connections of the retinal on and off pathways to the lateral geniculate nucleus of the monkey. *Vision Res* **24**(9): 923-932.
- Schiller, P. H. (1992). The ON and OFF channels of the visual system. *Trends Neurosci* **15**(3): 86-92.
- Schiller, P. H. and J. G. Malpeli (1977). Properties and tectal projections of monkey retinal ganglion cells. *J Neurophysiol* **40**(2): 428-445.
- Schnapf, J. L., T. W. Kraft and D. A. Baylor (1987). Spectral sensitivity of human cone photoreceptors. *Nature* **325**(6103): 439-441.
- Schnapf, J. L., B. J. Nunn, M. Meister and D. A. Baylor (1990). Visual transduction in cones of the monkey *Macaca fascicularis*. *J Physiol* **427**: 681-713.
- Schneeweis, D. M. and J. L. Schnapf (1999). The photovoltage of macaque cone photoreceptors: adaptation, noise, and kinetics. *J Neurosci* **19**(4): 1203-1216.

- Scholtes, A. M. and M. A. Bouman (1977). Psychophysical experiments on spatial summation at threshold level of the human peripheral retina. *Vision Res* **17**(7): 867-873.
- Shapley, R. and S. Hochstein (1975). Visual spatial summation in two classes of geniculate cells. *Nature* **256**(5516): 411-413.
- Sherrington, C. S. (1906). Observations on the scratch-reflex in the spinal dog. *J Physiol* **34**(1-2): 1-50.
- Shiells, R. A. and G. Falk (1990). Glutamate receptors of rod bipolar cells are linked to a cyclic GMP cascade via a G-protein. *Proc Biol Sci* **242**(1304): 91-94.
- Shiells, R. A., G. Falk and S. Naghshineh (1981). Action of glutamate and aspartate analogues on rod horizontal and bipolar cells. *Nature* **294**(5841): 592-594.
- Simonet, P. and M. C. Campbell (1990). The optical transverse chromatic aberration on the fovea of the human eye. *Vision Res* **30**(2): 187-206.
- Sincich, L. C., Sabesan, R, Tuten, W. S., Roorda, A., Harmening, W. M. (2016). Functional imaging of cone photoreceptors. *Human Color Vision*. R. Baraas, Marshall, J., Kremers, J. New York, Springer.
- Sincich, L. C., Y. Zhang, P. Tiruveedhula, J. C. Horton and A. Roorda (2009). Resolving single cone inputs to visual receptive fields. *Nat Neurosci* **12**(8): 967-969.
- Slaughter, M. M. and R. F. Miller (1981). 2-amino-4-phosphonobutyric acid: a new pharmacological tool for retina research. *Science* **211**(4478): 182-185.
- Snodderly, D. M., R. S. Weinhaus and J. C. Choi (1992). Neural-vascular relationships in central retina of macaque monkeys (*Macaca fascicularis*). *J Neurosci* **12**(4): 1169-1193.

- Spillmann, L., A. Ransom-Hogg and R. Oehler (1987). A comparison of perceptive and receptive fields in man and monkey. *Hum Neurobiol* **6**(1): 51-62.
- Stell, W. K. (1965). Correlation of retinal cytoarchitecture and ultrastructure in Golgi preparations. *Anat Rec* **153**(4): 389-397.
- Stockman, A., D. I. MacLeod and D. D. DePriest (1991). The temporal properties of the human short-wave photoreceptors and their associated pathways. *Vision Res* **31**(2): 189-208.
- Stockman, A. and L. T. Sharpe (2000). Tritanopic color matches and the middle- and long-wavelength-sensitive cone spectral sensitivities. *Vision Res* **40**(13): 1739-1750.
- Stone, J. and M. Fabian (1968). Summing properties of the cat's retinal ganglion cell. *Vision Res* **8**(8): 1023-1040.
- Szel, A., T. Diamantstein and P. Rohlich (1988). Identification of the blue-sensitive cones in the mammalian retina by anti-visual pigment antibody. *J Comp Neurol* **273**(4): 593-602.
- Tam, J., J. A. Martin and A. Roorda (2010). Noninvasive visualization and analysis of parafoveal capillaries in humans. *Invest Ophthalmol Vis Sci* **51**(3): 1691-1698.
- Tam, J., P. Tiruveedhula and A. Roorda (2011). Characterization of single-file flow through human retinal parafoveal capillaries using an adaptive optics scanning laser ophthalmoscope. *Biomed Opt Express* **2**(4): 781-793.
- Tessier-Lavigne, M. and D. Attwell (1988). The effect of photoreceptor coupling and synapse nonlinearity on signal:noise ratio in early visual processing. *Proc R Soc Lond B Biol Sci* **234**(1275): 171-197.

- Thibos, L. N., A. Bradley, D. L. Still, X. Zhang and P. A. Howarth (1990). Theory and measurement of ocular chromatic aberration. *Vision Res* **30**(1): 33-49.
- Thibos, L. N., M. Ye, X. Zhang and A. Bradley (1992). The chromatic eye: a new reduced-eye model of ocular chromatic aberration in humans. *Appl Opt* **31**(19): 3594-3600.
- Thoreson, W. B. and S. C. Mangel (2012). Lateral interactions in the outer retina. *Prog Retin Eye Res* **31**(5): 407-441.
- Tuten, W. S., P. Tiruveedhula and A. Roorda (2012). Adaptive optics scanning laser ophthalmoscope-based microperimetry. *Optom Vis Sci* **89**(5): 563-574.
- Uji, A., M. Hangai, S. Ooto, K. Takayama, N. Arakawa, H. Imamura, K. Nozato and N. Yoshimura (2012). The source of moving particles in parafoveal capillaries detected by adaptive optics scanning laser ophthalmoscopy. *Invest Ophthalmol Vis Sci* **53**(1): 171-178.
- Valeton, J. M. and D. van Norren (1983). Light adaptation of primate cones: an analysis based on extracellular data. *Vision Res* **23**(12): 1539-1547.
- Verweij, J., E. P. Hornstein and J. L. Schnapf (2003). Surround antagonism in macaque cone photoreceptors. *J Neurosci* **23**(32): 10249-10257.
- Verweij, J., M. Kamermans and H. Spekreijse (1996). Horizontal cells feed back to cones by shifting the cone calcium-current activation range. *Vision Res* **36**(24): 3943-3953.
- Volbrecht, V. J., E. E. Shrago, B. E. Scheffrin and J. S. Werner (2000). Spatial summation in human cone mechanisms from 0 degrees to 20 degrees in the superior retina. *J Opt Soc Am A Opt Image Sci Vis* **17**(3): 641-650.

- von Gersdorff, H. and G. Matthews (1994). Dynamics of synaptic vesicle fusion and membrane retrieval in synaptic terminals. *Nature* **367**(6465): 735-739.
- Wald, G. (1938). Area and Visual Threshold. *J Gen Physiol* **21**(3): 269-287.
- Wan, Q. F. and R. Heidelberger (2011). Synaptic release at mammalian bipolar cell terminals. *Vis Neurosci* **28**(1): 109-119.
- Wassle, H., B. B. Boycott and J. Rohrenbeck (1989). Horizontal Cells in the Monkey Retina: Cone connections and dendritic network. *Eur J Neurosci* **1**(5): 421-435.
- Wassle, H., U. Grunert, P. R. Martin and B. B. Boycott (1994). Immunocytochemical characterization and spatial distribution of midget bipolar cells in the macaque monkey retina. *Vision Res* **34**(5): 561-579.
- Wassle, H., L. Peichl and B. B. Boycott (1981). Dendritic territories of cat retinal ganglion cells. *Nature* **292**(5821): 344-345.
- Werblin, F. S. and J. E. Dowling (1969). Organization of the retina of the mudpuppy, *Necturus maculosus*. II. Intracellular recording. *J Neurophysiol* **32**(3): 339-355.
- Wiersma, C. A. (1966). Integration in the visual pathway of crustacea. *Symp Soc Exp Biol* **20**: 151-177.
- Wiesel, T. N. (1960). Receptive fields of ganglion cells in the cat's retina. *J Physiol* **153**: 583-594.
- Williams, D. R., D. I. MacLeod and M. M. Hayhoe (1981). Punctate sensitivity of the blue-sensitive mechanism. *Vision Res* **21**(9): 1357-1375.
- Wilson, M. E. (1970). Invariant features of spatial summation with changing locus in the visual field. *J Physiol* **207**(3): 611-622.

Yang, Q., D. W. Arathorn, P. Tiruveedhula, C. R. Vogel and A. Roorda (2010). Design of an integrated hardware interface for AOSLO image capture and cone-targeted stimulus delivery. *Opt Express* **18**(17): 17841-17858.

## CHAPTER 2

### CONE SIGNAL SUMMATION AND THRESHOLD VARIABILITY IN THE HUMAN RETINA

by

KADY S. BRUCE, WOLF M. HARMENING,  
WILLIAM S. TUTEN, AUSTIN ROORDA, LAWRENCE C. SINCICH

In preparation for publication  
Format adapted for dissertation



## ABSTRACT

While many factors affecting human psychophysical threshold have been studied, variation in cone functional weighting and cone signal integration have not been directly examined *in vivo*. Using an adaptive optics scanning laser ophthalmoscope (AOSLO) equipped with multiwavelength imaging and stimulation capabilities, we delivered cone-sized stimuli to individual photoreceptors in human subjects ( $n = 7$ ). Perceptual increment thresholds were measured from single cones and cone pairs using a Bayesian-based staircase method of threshold estimation. In 42 of 99 pairs, individual thresholds differed between cones ( $p < 0.05$ ), and differences in threshold as small as 14% were detectable. To address the source of observed variability in cone threshold, we examined several factors that could lead to differences in thresholds. We found that cone thresholds were consistent when measured over multiple testing days, that there is no relationship between cone reflectivity in AOSLO images and perceptual threshold ( $n = 494$  tests;  $p = 0.19$ ), and that systematic stimulus delivery errors did not explain variation (average error = 0.2 arcmin;  $R^2 = 8 \times 10^{-5}$ ). Individual cones in pairs were stimulated simultaneously and analyzed with respect to their signal summation. Lower thresholds were always observed, with 17 of 99 pairs manifesting linear summation, and 42 pairs integrating signals according to a two-detector model. The nature of signal integration was not correlated with the eccentricity of the tested cones, but was related to inter-cone distance (9 of 11 linear pairs were located within 1.5 cone spacings of one another), suggesting bipolar cells as mediating cone signal summation.

## INTRODUCTION

Because cone photoreceptors are the neurons that give us our primary experience of the visual world, they have been characterized extensively in terms of one unique trait—responsiveness to light (Baylor 1987). Much of the seminal physiological work has been demonstrated *in vitro*, where single photoreceptors can be isolated and studied under precise experimental conditions. To understand how photoreceptors function in concert, however, techniques must be developed by which retinal circuitry remains intact and photoreceptors can be stimulated and analyzed simultaneously. Recently, this has been accomplished in two ways: multi-electrode recordings and photoreceptor-targeted psychophysics.

Upon stimulation of a single cone photoreceptor, a series of biochemical events occur by which the incoming light signal is transmitted to downstream horizontal, bipolar, amacrine, and ganglion cells (Dacey 1999; Field *et al.* 2007; Lee *et al.* 2010). *In vitro* electrical recordings made from retinal ganglion cells lying atop a multi-electrode array have provided hints as to how signals arising from a single photoreceptor may be combined and integrated downstream (Sekirnjak *et al.* 2006; Field *et al.* 2010; Ala-Laurila *et al.* 2011; Greschner *et al.* 2011; Li *et al.* 2014). Signals from a single stimulated cone diverge into parallel retinal circuits, activating every major type of retinal ganglion cell (Wassle 2004; Field *et al.* 2007; Field *et al.* 2010; Ala-Laurila *et al.* 2011; Li *et al.* 2014). It has also been shown that single cone activation can drive neurons in the lateral geniculate nucleus (LGN) (Sincich *et al.* 2009), indicating that signals arising from one photoreceptor may be enough to drive perception (Koenig *et al.* 2011; Harmening *et*

*al.* 2014; Bruce *et al.* 2015; Sincich 2016). What remains less clear is how signals arising from multiple cones may sum their signals within the visual pathway, as this is likely to recruit unknown numbers of cells in the retina, as well as the central nervous system.

Both physiologically and psychophysically, it is well established that the visual system summates input signals spatially and temporally (Bloch 1885; Graham 1937; Wald 1938; Graham 1939; Barlow 1953; Brindley 1954; Barlow 1957; Barlow 1958; Fankhauser *et al.* 1960; Wiesel 1960; Baumgardt *et al.* 1961; Hallett *et al.* 1962; Blackwell 1963; Glezer 1965; Enroth-Cugell *et al.* 1966; Wiersma 1966; Cleland *et al.* 1968; Easter 1968; Stone *et al.* 1968; Freund *et al.* 1969; Naka *et al.* 1970; Wilson 1970; Dannheim *et al.* 1971; Arnett 1972; Roufs 1972; Scholtes *et al.* 1977; Johnson *et al.* 1978; Lie 1980; Inui *et al.* 1981; Johnson 1986; Spillmann *et al.* 1987; Scheffrin *et al.* 1998; Volbrecht *et al.* 2000), with a typical outcome of thresholds lowering as additional photoreceptors contribute to the visual signal. Riccò's Law, a psychophysical description of this phenomenon, states that signals arising from groups of receptors will sum according to probability when the system is operating at perceptual threshold (Riccò 1877). The size of Riccò's Area, over which signals sum linearly, has been shown to increase in size with retinal eccentricity, and is thought to correlate with the increasing size of ganglion cell receptive fields (Wilson 1970; Dannheim *et al.* 1971; Lie 1980; Inui *et al.* 1981; Johnson 1986; Volbrecht *et al.* 2000). One alternative to linear summation is the filtering of visual signals through a nonlinear operation, as might be expected when cells are transmitting signals along with noise independently (Rashbass 1970; Drongelen 2007). While both linear and nonlinear spatial summation have been demonstrated in the primate retina, it is unknown which type of signal summation holds true when stimuli are

precisely targeted at just two cones—the most simple application of spatial summation in the retina.

Combining precise delivery of microstimuli to cones with traditional psychophysical methodologies represents a technical challenge. Here, we use an adaptive optics scanning laser ophthalmoscope (AOSLO), which allows for simultaneous retinal imaging and psychophysics to be conducted in the intact human eye at a resolution approaching the diffraction limit (Roorda *et al.* 2002; Yang *et al.* 2010; Harmening *et al.* 2014). Combined with high-speed, real-time retinal tracking to compensate for eye motion (Yang *et al.* 2010), we sought to characterize how light delivery largely confined to individual and paired cones generates specific types of signals that lead to visual perception.

## METHODS

Experiments on human volunteers ( $n = 7$ ; 6 males, 1 female; aged 21-53) were conducted under a protocol approved by the Institutional Review Board at the University of Alabama Birmingham, in accordance with the Declaration of Helsinki. Written, informed consent was required of all subjects in order to participate in the research. All participants had 20/20 or better best corrected visual acuity, clear optics, and normal color vision (assessed using Hardy-Rand-Rittler plates and a Nagel anomaloscope).

## *AOSLO imaging*

The retinal cone mosaic was imaged using a multiwavelength AOSLO using methods described in detail previously (Roorda *et al.* 2002; Tuten *et al.* 2012; Harmening *et al.* 2014). Briefly, the light source for the AOSLO was a supercontinuum laser (SuperK Extreme; NKT Photonics; Birkerød, Denmark) bandpass filtered to provide an infrared (IR) imaging light ( $842 \pm 25$  nm; ranging from 120-250  $\mu$ W) and a visible green stimulation light ( $543 \pm 11$  nm). Filters were from Semrock Inc., Rochester, New York. The stimulation wavelength was chosen because it minimized the sensitivity difference between long and medium wavelength sensitive cones (Baylor *et al.* 1987). To image cone photoreceptors, a focused spot of IR light was raster scanned across a patch of retina via horizontal and vertical scanning mirrors. The IR imaging light reflected back through the optical system was sampled using a Shack-Hartmann wavefront sensor to measure wavefront aberrations. The aberrated wavefront was then compensated for using a 140-actuator, 5.5  $\mu$ m stroke micro-electromechanical systems (MEMS) deformable mirror (Boston Micromachines, Cambridge, MA, USA) operating in a closed loop at 16 Hz. Positional signals from the scanning mirrors were combined with the voltage output of a photomultiplier tube to create a  $512 \times 512$  pixel imaging video at 30 frames per second. For all retinal imaging and psychophysical testing, a 5.6 mm beam diameter and  $1.28^\circ$  imaging field were used ( $\sim$ 400 image pixels per degree of visual angle).

## *Microstimulation with AOSLO*

Acousto-optic modulators (AOMs) operating at 50 MHz allowed for independent 10-bit modulation of light in the imaging and stimulation channels. Switching of the AOMs at 20 MHz allowed a stimulus to be delivered at the pixel scale which composed the retinal image. To compensate for the retinal eye motion present during active fixation, real-time video stabilization software was used (Arathorn *et al.* 2007; Yang *et al.* 2010). This allowed for targeted stimulus delivery to preselected retinal locations, with cumulative delivery errors averaging less than a cone diameter (Harmening *et al.* 2014). By placing a digital marker in the retinal imaging video at the specific pixel location corresponding to the time of the AOM-triggered stimulus delivery, the actual location of the stimulus on the retina could be recorded for each trial.

For the present experiments, a  $5 \times 5$  pixel square stimulus (45 arcsec,  $\sim 3.6 \mu\text{m}$ ) of 543 nm light was flashed for a duration of  $\sim 130 \mu\text{sec}$  onto a constant background of  $\sim 4.3 \text{ cd/m}^2$  during each trial. In a diffraction-limited system, the incident beam aperture (5.75 mm) yields a PSF with Airy disc diameter of 24 arcsec, when calculated using the stimulation wavelength (543 nm) (Mahajan 2011). Expressed in image space, this equates to a diameter of 2.6 pixels, or  $\sim 1.9 \mu\text{m}$  on the retina (Sincich 2016). After accounting for the point spread function of the corrected optics under these imaging conditions and positional scatter in stimulus delivery, this stimulus subtended less than  $8 \mu\text{m}$  on the retina (at the 5% intensity contour), roughly corresponding to the diameters of cone inner segments over  $1.4 - 4.7^\circ$ —the range of eccentricities studied here (Curcio *et al.* 1992;

Scoles *et al.* 2014). Microstimuli like these targeted to cones more eccentric than  $\sim 5^\circ$  were generally not seen by our subjects.

Because our experiments used two wavelengths, one for imaging and one for stimulation, we addressed chromatic dispersion in each subject. The methods for doing so have been extensively described elsewhere (Harmening *et al.* 2012). Briefly, longitudinal chromatic aberration (LCA) arises when aligned beams of different wavelengths are focused in different axial planes. LCA is relatively consistent among individuals (Atchison *et al.* 2005), and was corrected by adjusting the relative vergences of the fiber optic point sources as they entered the optical path. Transverse chromatic aberration (TCA) causes beams of differing wavelength to be focused at different locations in the transverse plane of the retina, and is more idiosyncratic than LCA. TCA depends in part on the position of the imaging and stimulation beams relative to the eye's entrance pupil, making it difficult to infer micron-scale chromatic offsets solely from the pupil position of each subject. To measure such offsets, we employed an objective measurement of TCA from recorded retinal videos both before and after each experiment, in order to assess whether any lateral shift in the stimulus occurred during the course of testing (Harmening *et al.* 2012). Maximum correctable TCA offsets ranged up to 16 pixels in the image, corresponding to shifts of up to 2.4 arcmin ( $\sim 11.5 \mu\text{m}$ ) if left uncorrected. If measured offsets drifted during the experiment by more than one half cone width at the eccentricity being examined, the data were discarded.

In psychophysical testing, repeated stimulation under constant conditions is necessary. Consequently, the stimulus geometry must also be characterized with respect to spatial delivery errors that occur during the course of each set of stimulus trials. These

errors can occur even after fixational eye movements have been accounted for by real-time eye tracking and video stabilization software. In the current AOSLO system, the stimulus delivery positional error has a standard deviation of about 0.15 arcmin (Arathorn *et al.* 2007; Yang *et al.* 2010; Sincich 2016). To account for potential positional errors in delivery, the actual light delivery of the stimulus was summed over all trials (~100 trials per condition, per experiment) and integrated with the PSF-convolved nominal stimulus definition. The resulting light delivery distribution represents the final estimation of actual light distribution across a single experiment.

### *Psychophysical procedures*

Subjects were practiced at the psychophysical task and AOSLO-based microstimulation before any data collection began. Mydriasis was achieved using 1% tropicamide. Bite bars custom fitted for each subject were used to minimize pupil motion. Retinal locations being imaged were selected by having the subject fixate on an amber-colored light-emitting diode (LED) positioned outside of the 1.28° imaging field. Following TCA measurement and dark adaptation of at least 15 minutes, the experiment trials began. Retinal stimulation sites were chosen on an approximately horizontal meridian within the retina. Six subjects had testing sites located temporal to the fovea, and 1 subject had a nasally located site. Eccentricity was determined using a large montage of scaled AOSLO images that included the fovea, calibrated using a grid of known dimensions imaged within a model eye. Eccentricity was anchored at the subject's preferred fixational locus, determined using a 5 sec video of fixation upon a flashing 1



arcmin target. At each test site, vasculature maps were made in order to avoid potential light disruption arising from the overlying retinal blood vessels and capillaries (Tam *et al.* 2011; Harmening *et al.* 2014; Bruce *et al.* 2015). If a tested cone was found to lie underneath retinal vasculature as determined by the vessel map, the data were discarded.

Visual sensitivity was measured using a Bayesian staircase method of increment threshold estimation (King-Smith *et al.* 1994). Subjects reporting seeing or not seeing a small green stimulus square flashed during a single video frame. Stimulus delivery was accompanied by an audible cue. All trials were self-paced. There were 3 stimulus conditions, each containing 20 trials: stimulation of one cone, of a nearby second cone, or of both cones simultaneously. All trials were randomly interleaved, and thresholds were measured 4-6 times per cone (240-360 total trials) per experiment.

Throughout the study, threshold values are expressed in arbitrary units (a.u.) ranging from 0 to 1, where 0 corresponds to a stimulus condition containing only the constant  $1.28^\circ$  background field. A value of 1 represents the background field plus the maximum deliverable light intensity of the  $5 \times 5$  pixel test stimulus on the retina. In radiometric terms, this value of 1 was typically  $\sim 15$  nW incident at the cornea for the  $1.28^\circ$  imaging field, equaling  $\sim 4.72$  log quanta for a single frame containing the stimulus. The background light level, a product of residual light leak through the green channel AOM, was  $\sim 4.3$  cd/m<sup>2</sup> (in photopic units), equaling  $\sim 4,100$  rhodopsin isomerizations per second per rod (Geller *et al.* 1993). This effectively eliminated any rod contribution to the visual response (Aguilar 1954; Alpern *et al.* 1970; Tamura *et al.* 1991). The background light produced  $\sim 2.74$  log quanta incident on the cornea for an area comparable to the size and duration of the stimulus. Using these estimates, if a threshold was measured to be 0.5

a.u., the stimulus contained  $\sim 17$  times more photons than the background field over the same stimulus area. Occasionally, subjects reporting never seeing the stimulus (possibly due to targeting an S cone); if this occurred when the experiment required a response from a cone, a new cone was selected that did yield a measurable response.

#### *Inter-cone distance experiments*

In one set of experiments, the distance between targeted cones was intentionally varied at several retinal sites in 5 subjects. To measure the effect of cone spacing on summation at threshold, one anchor cone was common to each tested pair, while the second cone was selected by systematically varying the inter-cone distance. In 4 of the subjects, this procedure was repeated at 2 retinal eccentricities. In order to quantify cone spacing values across eccentricities where cone diameter and spacing increase with distance from the fovea, mean cone spacing values were obtained by measuring the inter-cone distance of 500 cones, centered over the area of testing. The inter-cone distance of each tested cone pair, measured in pixels from the AOSLO image, was normalized by the mean cone spacing value at each testing site; thus the metric was converted to number of cones between a pair rather than absolute distance.

#### *Cone weighting and summation calculations*

Cone photoreceptors have been demonstrated to exhibit variable synaptic weighting onto downstream ganglion cells (Field *et al.* 2010; Li *et al.* 2014). In order to

adequately consider variable cone thresholds, we used a weighted formula to compute two types of summation: linear summation according to a probability model and nonlinear summation according to a two-detector model. This weighting function accounts for, in cases where cones have different thresholds, the cone with the lower threshold dominating the response when the pair are stimulated simultaneously. Cone weights were thus computed as follows:

$$w_1 = 1 - (\theta_1 / (\theta_1 + \theta_2))$$

$$w_2 = 1 - (\theta_2 / (\theta_1 + \theta_2))$$

where  $w_i$  = functional weight of cone  $i$  and  $\theta_i$  = threshold obtained for cone  $i$ . For linear summation, the predicted threshold for the 2-cone condition was estimated from the weighted average of the individual cone thresholds:

$$\theta_{1+2} = (w_1 \theta_1 + w_2 \theta_2) / 2$$

This type of summation implies that the signals to be added each contain negligible noise, and that the detector itself is the main source of noise in the threshold measurement. For nonlinear summation, the predicted threshold for the 2-cone condition was estimated as follows:

$$\theta_{1+2} = (w_1 \theta_1 + w_2 \theta_2) / \sqrt{2}$$

This formula is derived from the idea that the detection of summed signals from independent detectors—each carrying independent noise—would improve as a function of the square root of the number of detectors (Drongelen 2007, p. 41). Because we generally examined cone pairs in our experiments, we refer to this type of nonlinear summation as a two-detector model.

In order to classify the style of summation, threshold data from each pair had to pass two statistical tests. For a pair to be classified as linear, for example, the  $\theta_{l+2}$  values had to be significantly no different from the linear prediction ( $p > 0.05$ ) and significantly different from the two-detector prediction ( $p < 0.05$ ), all based on the Wilcoxon rank-sum test because the data were not normally distributed (as determined by a Lilliefors test). The  $\theta_{l+2}$  statistics had to be reversed in the case of two-detector summation.

### *Cone reflectance quantification*

To determine if cone reflectivity had any impact on threshold, we measured the reflectivity of tested cones with a method described previously (Bruce *et al.* 2015). Briefly, during the course of a psychophysical experiment, a 1 sec retinally stabilized infrared video of 30 frames is recorded for each trial. These 30 frames were averaged into a single image, after eliminating any blank frames or those with uncorrected eye-motion artifacts that are readily detected by automated image analysis. Averaged images stemming from all individual trials were then summed into one image and normalized to the brightest value, representing the cone reflectivity during the course of the experiment. Reflectivity of the targeted cones was then measured by centering a  $3 \times 3$  pixel square onto a manual estimation of the pixel that was most centered within the cone (this was not necessarily the brightest pixel) (Pallikaris *et al.* 2003). The mean pixel value within the  $3 \times 3$  pixel square was then compared to the mean pixel value of a  $100 \times 100$  pixel square centered on the same location, and cone reflectance was quantified in standard deviations (SDs) from the field mean.

## RESULTS

In each subject, a reference montage was created of the cone mosaic covering the fovea and areas surrounding sites that were selected for testing (Figure 1A, B). The montages were used to identify testing locations near the horizontal meridian of the retina, where retinal vessels are smallest and present the least potential interference for stimuli. Cones were resolved at subcellular resolution up to within  $\sim 0.25^\circ$  of the fovea, and showed typical variation in reflectivity profiles—a characteristic which has been shown to change on a frame-by-frame basis during imaging (Roorda *et al.* 2002; Pallikaris *et al.* 2003; Rha *et al.* 2006; Putnam *et al.* 2010; Bruce *et al.* 2015).

While the fundus photograph and the AOSLO images allow for visualization of the larger blood vessels overlying the photoreceptor layer (as they create dark shadows), the IR images alone do not provide a full representation of the existing capillaries within any retinal area being studied (Snodderly *et al.* 1992). To ensure that our tested cone pairs did not lie beneath capillaries, which may distort the incoming stimulus light, we generated vascular maps for each tested retinal location (Figure 1C, D). All tested cone pairs were located in retinal areas free from vascular interference.

### *Threshold variability for microstimuli delivered to single cones*

It has been previously demonstrated *in vitro* that cone inputs to downstream retinal ganglion cells can carry unequal synaptic weights in the transduction of equivalent visual stimuli (Field *et al.* 2010; Li *et al.* 2014). Using a psychophysical approach, we

hypothesized that unequal synaptic weighting of cones may be observable in a threshold measurement if a stimulus could be reliably delivered to the same cone. Variability in increment threshold for cones tested with identical stimuli and experimental conditions has been noted before (Harmening *et al.* 2014; Bruce *et al.* 2015), but never characterized in detail. With optimal adaptive optics (AO) wavefront correction, a  $5 \times 5$  pixel stimulus (the size used here) convolved with the PSF will produce a light intensity profile where the 5% intensity contour encompasses an area of  $\sim 33 \mu\text{m}^2$  on the retina, containing 88% of all light energy (Figure 2A, C, left panels). While the stimulus defined in image pixels is smaller than the cone in the AO image, once convolved with the PSF it roughly matches the diameter of imaged cones at  $2.7^\circ$  eccentricity. This suggests that most of the delivered light was constrained to a retinal area the size of a single cone, although there still remains a small amount of uncontrollable light scatter, spread over a large area—given the PSF.

It is important to realize that testing one cone each day would not necessarily yield consistent thresholds, as many factors such as variation in light levels in the instrument and subject performance day-to-day can readily alter threshold. Thus, to allow a more controlled measurement of threshold, we studied two nearby cones in each experiment and examined relative increment thresholds. Three cones were tested as pairs on separate days in Subject 1. On one day, increment thresholds for the neighboring cones were significantly different by the end of the trials (Figure 2B; cone 1:  $0.52 \pm 0.13$ , cone 2:  $0.29 \pm 0.01$ ,  $p = 0.008$ , Wilcoxon rank-sum test). On another day, we conducted a second experiment in Subject 1 where one targeted cone was the same as in the previous experiment, and the second cone was a different neighbor. Here, the cones exhibited

increment thresholds that were similar (Figure 2D; cone 1:  $0.40 \pm 0.02$ , cone 2:  $0.43 \pm 0.08$ ,  $p = 0.80$ , Wilcoxon rank-sum test). These results suggest that perceptual thresholds can be cone specific, varying from one cone to the next, even for adjacent cones.

To assess the prevalence of nearby cones exhibiting different thresholds, we looked at the distribution of threshold variability throughout the population of tested cone pairs ( $n = 99$ ; Figure 3). Over these cone pairs, 57 had thresholds that were statistically similar to one another, while 42 had cones with different thresholds (Figure 3A, black circles;  $p < 0.05$ , Wilcoxon rank-sum test). The frequency distribution of the pair-wise cone threshold differences compiled into a population histogram showed that differences in threshold as small as 14% can be detected psychophysically. These results indicate that threshold variability among cone pairs is common, detectable among nearly half of the cones tested using psychophysical methods.

In any perceptual testing, it is important to consider the possibility that human subjects will have some degree of intrinsic inconsistency when performing threshold tasks repeatedly. To examine the possibility that differences in cone thresholds were caused by subject performance inconsistency, we conducted a set of experiments where the same set of cones were returned to over multiple days (Figure 4). Here, we specifically targeted triplets of cones in two subjects, tested in the same way as described previously. The threshold of each cone was measured 3-5 times during each day's experiment. To control for small day-to-day changes in stimulus light levels, thresholds were normalized to the mean of the triplet. Figure 4A shows a cone triplet in Subject 2 that demonstrated similar relative thresholds, and this similarity was consistent over 3 experiments spanning 5 days. In the triplet tested in Subject 3, two cones had consistently

similar thresholds and one cone had a consistently higher threshold (Figure 4B). The high-threshold cone needed about 40% more light in the stimulus in order to be detected. In a third triplet, one cone was encountered in Subject 2 that consistently had a threshold that was beyond the range of deliverable light (Figure 4C). Given that the other two cones had reliably measured thresholds across two days, this result suggests that the cone with the unreachable threshold was an S type. Given the 543 nm wavelength of the stimulus, an S cone would need ~400 times more light than would an L or M cone to reach a comparable threshold (Stockman *et al.* 2000). This would exceed the range of light deliverable with our AOLSO. If an S cone was targeted for stimulation under these experimental conditions, the subject would likely respond “not seen” to every trial. Given the relative sparsity of S cones in the human retina (Curcio *et al.* 1991; Roorda *et al.* 1999) this scenario was not anticipated to be encountered often.

Taken together, the results shown in Figure 4 indicate that the variation in cone functional weighting can be tapped psychophysically, and can be reliably assessed using the present technology. However, other factors may be introducing variability in these experiments. As noted previously, cone reflectivity varies on a cone-by-cone basis, and can change rapidly over time (Roorda *et al.* 2002; Harmening *et al.* 2014; Bruce *et al.* 2015). Could it be possible that the reflectivity of a cone is correlated with perceptual threshold, given the waveguiding properties of cones? To investigate this question, we measured the reflectivity of each cone in a tested pair for each set of trials. Because reflectivity varies from moment-to-moment and day-to-day, single cone reflectivity and threshold were normalized to the mean values of each tested pair (Figure 5A). In the population of tested cone pairs, the mean threshold was 1.6% higher in cones with less



versus more reflectivity, but this difference was not significant ( $p = 0.19$ , two-tailed  $t$ -test). Although this data had an increased  $n$  over our previously reported subset (Bruce *et al.* 2015), significance was still not reached. It is clear from this scatterplot that reflectivity cannot account for the wide threshold variation seen psychophysically.

A second factor may have led artificially to a wide variation in threshold. In cone pairs where the threshold differed, a systematic offset in the delivery of light to one of the cones in a pair could have resulted in a higher threshold. This is a distinct possibility because directing light intentionally away from the cone center leads to increased thresholds (Harmening *et al.* 2014). To see if a repeated error in stimulus delivery was responsible for the observed variation in cone thresholds, we examined where the centroid of the summed light delivery fell relative to each cone center for the 42 cone pairs that exhibited different thresholds (Figure 6). On average, the stimuli fell within 1.3 pixels (0.2 arcmin) of the cone centers, and showed no relationship between threshold and distance from cone center ( $R^2 = 8 \times 10^{-5}$ ). This analysis provides additional support that the consistent and repeatable differences in threshold between neighboring cones appears to arise from the transmission of the cone signal itself.

### *Two-cone signal summation*

For each cone pair represented in the data presented above, there was third trial condition—stimulation of both cones. This condition was included to directly examine how increasing the number of stimulated detectors in the visual system might affect threshold. In the population of cone pairs tested, the increment perceptual threshold

measured in the 2-cone condition was always lower than that of the single cone conditions, and also showed considerable variation.

To further characterize the nature of cone signal summation, we examined each pair with respect to two possible ways the signal could theoretically combine downstream. The first outcome, linearity, would occur if the signals from both stimulated cones summed directly onto one downstream detector. Linearity would dictate that only  $1/2$  as much light needs to be delivered to each of the two cones as is necessary for a single cone to reach threshold. One example of such linear summation is shown in Figure 7A, B. The second possible outcome, two-detector summation, would occur if each cone signal was passed to different downstream detectors, which would independently introduce noise into the summed signal. Here, two-cone threshold would be reached with  $1/\sqrt{2}$  the amount of light required for single cone thresholds (Drongelen 2007). This outcome was found in the pair shown in Figure 7C, D. Notably, cone 1 in Figure 6 manifested different summation strategies depending on which cone it was paired with, suggesting that downstream connectivity differences in the retina can be detected psychophysically. Across the population, one of the two types of summation could be measured in 60% of the pairs (linearity = 17/99 cone pairs; two-detector = 42/99 cone pairs).

Receptive field sizes increase steadily as a function of eccentricity in most retinal cell types, including ganglion cells (Watanabe 1986; Rodieck 1998; Dacey 1999). This increase in field size is accompanied by more cones converging onto a single receptive field. If ganglion cells are acting as the detector in summation, the idea of increased convergence with eccentricity led us to hypothesize that linear summation would be more

prevalent at greater eccentricities, because the likelihood of two cones sending signals to separate ganglion cells would be lower. To see if this was true, we plotted the summation data as a function of eccentricity (Figure 8). There did not appear to be any correlation between the nature of summation and increased distance from the fovea.

The lack of an eccentricity effect with respect to summation style suggests that the cell class at which summation is occurring is one that does not scale with receptive field size as distance from the fovea increases. To probe this idea more directly, we designed a set of experiments to systematically vary the distance between targeted cones at different eccentricities. In 5 subjects, a single anchor cone was selected to be common in each cone pair tested ( $n = 56$  of the 99 total cone pairs). The second cone was then varied systematically to increase inter-cone distance (Figure 9). In order to compare data across eccentricities, where cone diameter and spacing both get larger as distance from the fovea increases, a mean cone spacing value was computed at each site (described in Methods). This allowed us to normalize the distance between targeted cones in terms of cone spacing. When the ratio of the two-cone threshold and the mean weighted single cone thresholds was plotted with respect to inter-cone cone distance, 9 of the 11 linear pairs tested using an anchor cone were located within 1.5 cone spacings of one another (Figure 10), corresponding to a range of  $\sim 5\text{-}7.5\ \mu\text{m}$  on the retina. In contrast, two-detector summation was found throughout the range of intercone distances. The clustering of linearity amongst just neighboring cones suggests that the mechanisms of summation leading to detection are occurring at a cell type with receptive fields smaller than ganglion cells—very possibly bipolar cells.

## DISCUSSION

The signals originating from single cones have been demonstrated elsewhere to be sufficient for the activation of multiple cell types, namely bipolar cells, ganglion cells, and cells in the lateral geniculate nucleus (LGN) (Baylor *et al.* 1977; Hofer *et al.* 2005; Sincich *et al.* 2009; Field *et al.* 2010; Ala-Laurila *et al.* 2011; Soo *et al.* 2011; Li *et al.* 2014). If each downstream cell type has multiple cones contributing to its receptive field, the strength of input in single cones can be analyzed against one another with respect to the downstream cell's response. In this way, variable functional weighting from single cones has been shown in ganglion cells (Field *et al.* 2010; Li *et al.* 2014) and in LGN neurons (Sincich *et al.* 2009), but has never been directly examined psychophysically. Variability in functional weight among the cone population could manifest psychophysically as variability in threshold, if neural signals passing from the LGN through cortex to perception are not wholly diluted by other signals. For the detection task we used, our results on threshold variability suggest that such signal preservation along the visual pathway is indeed operating. Variation in cone weights, abiding by the principle of univariance, means that an equivalent response—from a ganglion cell or at the perceptual level—can be generated if the input strength of each cone is taken into account. Because we were testing at threshold, the input strength of a cone is simply mirrored by the relative threshold level. The range of variability we found was within the range found *in vitro* (where differences as large as 75% from the pair-wise mean can be estimated for single cones from Figure 1 in Li *et al.* 2014), supporting the idea that both types of experiments tapped into the same cone weighting phenomenon.

It is possible that some of the variation in cone weight is due to a factor yet unexamined, arising from the waveguiding nature of cones. A cone's ability to funnel light through the inner segment and into the outer segment is dependent, in part, on the size and shape of the photoreceptor (Roorda *et al.* 2002; Lakshminarayanan 2010). Could local variation in inner segment dimensions account for the variation we observed in threshold? To examine this, the diameter and isotropy of inner segments were measured from human retinal wholemount histological material and used to estimate light coupling efficiency in outer segments with an optical model (Defenderfer *et al.* 2016). For groups of neighboring cones, light coupling varied by a factor of 10 less than the variation observed psychophysically. Because shape differences yielded such a minor variation in light coupling among cones, these results suggest that synaptic weighting is likely to account for most of the variation in perceptual thresholds. This idea is supported by the data presented here, which eliminates other confounds that could have produced variable thresholds: day-to-day inconsistency, inter-subject differences, cone reflectivity, and stimulus delivery errors.

The possibility remains that the variation in increment thresholds measured here are not arising from the photoreceptors at all, but are instead a product of downstream retinal neurons. While there is good evidence that functional weights vary between cones and ganglion cells (Chichilnisky *et al.* 1999; Field *et al.* 2010; Li *et al.* 2014), it is still unclear at which synapse this is occurring. There may be differential synaptic weighting at cone-bipolar cell synapses as well as at bipolar-ganglion cell synapses. Since we always examined relative thresholds, the variation could arise from cones with the same weights passing their signals along two different retinal circuits, either separate bipolar

cells or separate ganglion cells, or some combination. *In vitro* experiments would be required to reconcile these possibilities definitively. At present, it is worth noting that in the complete cone maps produced to date, cones near the edges of the receptive field centers do not always have the lowest cone weights (Field *et al.* 2010; Li *et al.* 2014), as might be expected from synapses formed at the distal tips of ganglion cell dendrites. This observation makes it more likely that threshold variation originates at the cone-bipolar cell synapse.

Assuming that differential weighting does originate with each cone, long-held ideas about the two-dimensional profiles of receptive fields may need modification—particularly near the fovea. Thinking of an ON center ganglion cell as an example, the field center is usually depicted as a perfectly smooth Gaussian profile of sensitivity. Instead, this two-dimensional sensitivity profile should mirror the variability seen in individual cones, which would create a “bumpy” profile, likely still with a central peak. The smoothness seen historically is partly due to uncorrected high order aberrations in earlier physiological experiments; as AOSLO-based physiology moves forward, the receptive fields of visual neurons will reveal much more sensitivity texture than previously realized (Sincich *et al.* 2009). Clinically, cone threshold variability may also need to be taken into account. Microperimetry is often used as a test of cone function, most recently in conjunction with AOSLO imaging (Tuten *et al.* 2012). Traditionally, there are three test spot sizes, called Goldman I, II, and III (Midena 2007). At 4°, the Goldman I test spot covers ~4-5 cones. Cone threshold variability would increase the noise in such measurements of retinal function, increasingly so as the test moves away from the fovea, potentially confounding proper assessment of visual function.

The summation experiments were performed to examine how signals from two cones add together. We found that pairs of cones always sum their signals when stimulated simultaneously, leading to a lower threshold than when they were targeted individually. Notably, the summation was not always linear, which suggests that at least two detection mechanisms are available. We first pursue the idea that the summation is occurring in the retina.

In the linear case, the interpretation is straightforward: the signals from each cone contain a relatively low degree of noise and are added together by one detector operating in a linear regime against the background light intensity. Is the detector a bipolar cell, or a ganglion cell? The answer rests on what type of ganglion cell is likely to be mediating the summed signal. Because the experiments utilized a briefly flashed low contrast stimulus, it seems likely that any perceptual effect is occurring through parasol retinal ganglion cells, which in turn suggests that diffuse bipolar cells are the site of summation. Over a wide range of eccentricities, ON diffuse bipolar cells uniformly contact about 6 cones (Boycott *et al.* 1969; Kolb 1970; Boycott *et al.* 1991; Kolb *et al.* 1993). For any pair of randomly selected adjacent cones, there is a good chance that they would be connected to the same diffuse bipolar cell, and because they respond with graded membrane potentials, linear summation is likely to occur here, followed by transmission to a single parasol ganglion cell. This circuit also explains the two-detector summation cases. With diffuse bipolars contacting just 6 cones, the chance that any two neighboring cones contacted different bipolars is also reasonably high. Because two bipolars may act like uncorrelated sources of noise, their summation at a single ganglion cell will follow

the two-detector model, as the noise will cancel but more signal will be required from each cone to reach threshold.

The experiments where inter-cone distance was intentionally varied were designed to hone in on the cell type mediating summation. Our data indicated that linear summation generally occurred when cones were within 1.5 cone spacings of one another—regardless of eccentricity. In these instances, summation is probably occurring at the bipolar cell level, since ganglion cells (of all types) increase in size with eccentricity, which would have predicted no correlation between the prevalence of linear summation and the distance between cones. By contrast, two-detector summation was prevalent at all inter-cone distances, which accords with summation at the ganglion cell, since two bipolar cells were likely to be channeling the signals (Figure 11). Summation style, in other words, may be able to pick out different sites in the retinal circuit that mediate perceptual threshold.

Could two-cone summation not be computed in the retina, but somewhere further downstream such as the LGN? This seems unlikely for several reasons. One is that it would require signals from separate ganglion cells to arrive at LGN neurons and be summed in two distinct ways. It has been shown that LGN neurons in the cat and in primate generally have one predominant input from one ganglion cell, which can be optimally driven by a small stimulus (Cleland *et al.* 1971; Mastronarde 1987; Mastronarde 1987; Usrey *et al.* 1999; Sincich *et al.* 2007). For many of our cone pairs, threshold was about equal. This would require that two cones made segregated connections with two ganglion cells, which in turn have equal synaptic weighting at a single LGN neuron, but this is not supported by physiological evidence. Second, it is



unclear how LGN neurons could distinguish between ganglion cells carrying inputs from neighboring cones and produce two styles of summation as a function of eccentricity. Future physiology experiments replicating the stimulus paradigm used here should be able to provide firmer evidence about the nature of cone summation beyond the retina.

It remains to examine how our findings relate to other psychophysical studies of spatial summation. The most relevant of these centers on Riccò's Law, wherein the product of stimulus intensity and area is a constant up to a certain size, beyond which summation is no longer linear (Riccò 1877). Many studies have found that Riccò's area increases in size steadily with eccentricity, and roughly scales with retinal ganglion cell dendritic fields (Wilson 1970; Dannheim *et al.* 1971; Lie 1980; Inui *et al.* 1981; Johnson 1986; Volbrecht *et al.* 2000). In an experiment designed to probe L cone summation at threshold, the authors concluded that parasol ganglion cells appear to set the size of Riccò's area (Volbrecht *et al.* 2000). In their data, the diameter over which a stimulus would be summed linearly was  $\sim 11$  arcmin at  $2^\circ$  eccentricity, an area that would encompass dozens of cones. How can this be reconciled with the prevalence of nonlinear summation among adjacent cones we found here? In the experiments cited above, the stimuli spanned many cones, were many milliseconds in duration, and could not have been projected onto the same cones for each trial. Under these conditions, horizontal cells would have been strongly engaged, and different ganglion cells would have been tested over the complete set of trials, with the perceptual outcome reflecting their average behavior as a population. Because so many additional neural circuits must be activated in these experimental conditions, the summation result is not readily comparable to our cone-targeted experiments. To bridge that comparison, it would be useful to examine

cone summation with an AOSLO approach over a large range of cone numbers, to see how threshold is affected by each additional cone being stimulated. It is likely that inhibitory effects from horizontal cells would be revealed (Thoreson *et al.* 2012), which would greatly alter the function relating threshold to stimulus size. Until then, it appears that classical Riccò's area experiments and cone-targeted microstimulation experiments probe different features of the retinal circuit.

## REFERENCES

- Aguilar, M. S., W. S. (1954). Saturation of the rod mechanism of the retina at high levels of saturation. *Opt Acta Int J Opt* **1**: 59-65.
- Ala-Laurila, P., M. Greschner, E. J. Chichilnisky and F. Rieke (2011). Cone photoreceptor contributions to noise and correlations in the retinal output. *Nat Neurosci* **14**(10): 1309-1316.
- Alpern, M., W. A. Rushton and S. Torii (1970). The attenuation of rod signals by backgrounds. *J Physiol* **206**(1): 209-227.
- Arathorn, D. W., Q. Yang, C. R. Vogel, Y. Zhang, P. Tiruveedhula and A. Roorda (2007). Retinally stabilized cone-targeted stimulus delivery. *Opt Express* **15**(21): 13731-13744.
- Arnett, D. W. (1972). Spatial and temporal integration properties of units in first optic ganglion of dipterans. *J Neurophysiol* **35**(4): 429-444.
- Atchison, D. A. and G. Smith (2005). Chromatic dispersions of the ocular media of human eyes. *J Opt Soc Am A Opt Image Sci Vis* **22**(1): 29-37.
- Barlow, H. B. (1953). Summation and inhibition in the frog's retina. *J Physiol* **119**(1): 69-88.
- Barlow, H. B. (1957). Increment thresholds at low intensities considered as signal/noise discriminations. *J Physiol* **136**(3): 469-488.
- Barlow, H. B. (1958). Temporal and spatial summation in human vision at different background intensities. *J Physiol* **141**(2): 337-350.

- Baumgardt, E. and B. Hillmann (1961). Duration and size as determinants of peripheral retinal response. *J Opt Soc Am* **51**: 340-344.
- Baylor, D. A. (1987). Photoreceptor signals and vision. Proctor lecture. *Invest Ophthalmol Vis Sci* **28**(1): 34-49.
- Baylor, D. A. and R. Fettiplace (1977). Kinetics of synaptic transfer from receptors to ganglion cells in turtle retina. *J Physiol* **271**(2): 425-448.
- Baylor, D. A., B. J. Nunn and J. L. Schnapf (1987). Spectral sensitivity of cones of the monkey *Macaca fascicularis*. *J Physiol* **390**: 145-160.
- Blackwell, H. R. (1963). Neural theories of simple visual discriminations. *J Opt Soc Am* **53**: 129-160.
- Bloch, A. M. (1885). Expérience sur la vision. *Comptes Rendus de Séances de la Société de Biologie (Paris)* **37**: 493-495.
- Boycott, B. B., J. E. Dowling and H. Kolb (1969). Organization of the primate retina: Light Microscopy. *Philosophical Transactions of the Royal Society of London. Series B, Biological Sciences* **255**(799): 109-184.
- Boycott, B. B. and H. Wassle (1991). Morphological Classification of Bipolar Cells of the Primate Retina. *Eur J Neurosci* **3**(11): 1069-1088.
- Brindley, G. S. (1954). The summation areas of human colour-receptive mechanisms at increment threshold. *J Physiol* **124**(2): 400-408.
- Bruce, K. S., W. M. Harmening, B. R. Langston, W. S. Tuten, A. Roorda and L. C. Sincich (2015). Normal Perceptual Sensitivity Arising From Weakly Reflective Cone Photoreceptors. *Invest Ophthalmol Vis Sci* **56**(8): 4431-4438.

- Chichilnisky, E. J. and D. A. Baylor (1999). Receptive-field microstructure of blue-yellow ganglion cells in primate retina. *Nat Neurosci* **2**(10): 889-893.
- Cleland, B. G., M. W. Dubin and W. R. Levick (1971). Simultaneous recording of input and output of lateral geniculate neurones. *Nat New Biol* **231**(23): 191-192.
- Cleland, B. G. and C. Enroth-cugell (1968). Quantitative aspects of sensitivity and summation in the cat retina. *J Physiol* **198**(1): 17-38.
- Curcio, C. A., K. A. Allen, K. R. Sloan, C. L. Lerea, J. B. Hurley, I. B. Klock and A. H. Milam (1991). Distribution and morphology of human cone photoreceptors stained with anti-blue opsin. *J Comp Neurol* **312**(4): 610-624.
- Curcio, C. A. and K. R. Sloan (1992). Packing geometry of human cone photoreceptors: variation with eccentricity and evidence for local anisotropy. *Vis Neurosci* **9**(2): 169-180.
- Dacey, D. M. (1999). Primate retina: cell types, circuits and color opponency. *Prog Retin Eye Res* **18**(6): 737-763.
- Dannheim, F. and S. M. Drance (1971). Studies of spatial summation of central retinal areas in normal people of all ages. *Can J Ophthalmol* **6**(4): 311-319.
- Defenderfer, M., A. Meadway, K. S. Bruce and L. C. Sincich (2016). Photoreceptor shape variation does not account for perceptual threshold variation in single cones. *Society for Neuroscience*. San Diego, CA.
- Drongelen, W. v. (2007). *Signal Processing for Neuroscientists*, Academic Press: 35-67.
- Easter, S. S., Jr. (1968). Excitation in the goldfish retina: evidence for a non-linear intensity code. *J Physiol* **195**(2): 253-271.

- Enroth-Cugell, C. and J. G. Robson (1966). The contrast sensitivity of retinal ganglion cells of the cat. *J Physiol* **187**(3): 517-552.
- Fankhauser, F. and T. Schmidt (1960). [The optimal conditions for the study of spatial summation with fixed stimuli according to the method of quantitative light-perception perimetry]. *Ophthalmologica* **139**: 409-423.
- Field, G. D. and E. J. Chichilnisky (2007). Information processing in the primate retina: circuitry and coding. *Annu Rev Neurosci* **30**: 1-30.
- Field, G. D., J. L. Gauthier, A. Sher, M. Greschner, T. A. Machado, L. H. Jepson, J. Shlens, D. E. Gunning, K. Mathieson, W. Dabrowski, L. Paninski, A. M. Litke and E. J. Chichilnisky (2010). Functional connectivity in the retina at the resolution of photoreceptors. *Nature* **467**(7316): 673-677.
- Freund, H. J., G. Grunewald and G. Baumgartner (1969). [Spatial summation within the receptive field center of lateral geniculate body neurons in the cat]. *Exp Brain Res* **8**(1): 53-65.
- Geller, A. M. and P. A. Sieving (1993). Assessment of foveal cone photoreceptors in Stargardt's macular dystrophy using a small dot detection task. *Vision Res* **33**(11): 1509-1524.
- Glezer, V. D. (1965). The receptive fields of the retina. *Vision Res* **5**(9): 497-525.
- Graham, C. H., Brown, R. H., Mote, F. A. (1939). The relation of size of stimulus and intensity in the human eye: I. Intensity thresholds for white light. *Journal of Experimental Psychology* **24**(6): 555-573.
- Graham, C. H. C., C. (1937). Visual Acuity as a Function of Intensity and Exposure-Time. *The American Journal of Psychology* **49**(4): 654-661.

- Greschner, M., J. Shlens, C. Bakolitsa, G. D. Field, J. L. Gauthier, L. H. Jepson, A. Sher, A. M. Litke and E. J. Chichilnisky (2011). Correlated firing among major ganglion cell types in primate retina. *J Physiol* **589**(Pt 1): 75-86.
- Hallett, P. E., F. H. Marriott and F. C. Rodger (1962). The relationship of visual threshold to retinal position and area. *J Physiol* **160**: 364-373.
- Harmening, W. M., P. Tiruveedhula, A. Roorda and L. C. Sincich (2012). Measurement and correction of transverse chromatic offsets for multi-wavelength retinal microscopy in the living eye. *Biomed Opt Express* **3**(9): 2066-2077.
- Harmening, W. M., W. S. Tuten, A. Roorda and L. C. Sincich (2014). Mapping the perceptual grain of the human retina. *J Neurosci* **34**(16): 5667-5677.
- Hofer, H., J. Carroll, J. Neitz, M. Neitz and D. R. Williams (2005). Organization of the human trichromatic cone mosaic. *J Neurosci* **25**(42): 9669-9679.
- Inui, T., O. Mimura and K. Kani (1981). Retinal sensitivity and spatial summation in the foveal and parafoveal regions. *J Opt Soc Am* **71**(2): 151-163.
- Johnson, C. A., J. L. Keltner and F. Balestrery (1978). Effects of target size and eccentricity on visual detection and resolution. *Vision Res* **18**(9): 1217-1222.
- Johnson, M. A. (1986). Color vision in the peripheral retina. *Am J Optom Physiol Opt* **63**(2): 97-103.
- King-Smith, P. E., S. S. Grigsby, A. J. Vingrys, S. C. Benes and A. Supowit (1994). Efficient and unbiased modifications of the QUEST threshold method: theory, simulations, experimental evaluation and practical implementation. *Vision Res* **34**(7): 885-912.
- Koenig, D. and H. Hofer (2011). The absolute threshold of cone vision. *J Vis* **11**(1).

- Kolb, H. (1970). Organization of the outer plexiform layer of the primate retina: electron microscopy of Golgi-impregnated cells. *Philos Trans R Soc Lond B Biol Sci* **258**(823): 261-283.
- Kolb, H., L. Zhang and L. Dekorver (1993). Differential staining of neurons in the human retina with antibodies to protein kinase C isozymes. *Vis Neurosci* **10**(2): 341-351.
- Lakshminarayanan, V., Enoch, JM (2010). Biological Waveguides. *Handbook of Optics, Vol III: Vision and Vision Optics*. M. Bass. New York, McGraw Hill.
- Lee, B. B., P. R. Martin and U. Grunert (2010). Retinal connectivity and primate vision. *Prog Retin Eye Res* **29**(6): 622-639.
- Li, P. H., G. D. Field, M. Greschner, D. Ahn, D. E. Gunning, K. Mathieson, A. Sher, A. M. Litke and E. J. Chichilnisky (2014). Retinal representation of the elementary visual signal. *Neuron* **81**(1): 130-139.
- Lie, I. (1980). Visual detection and resolution as a function of retinal locus. *Vision Res* **20**(11): 967-974.
- Mahajan, V. N. (2011). *Optical Imaging and Aberrations: Part II. Wave Diffraction Optics*. Bellingham, Washington, SPIE Press.
- Mastrorarde, D. N. (1987). Two classes of single-input X-cells in cat lateral geniculate nucleus. I. Receptive-field properties and classification of cells. *J Neurophysiol* **57**(2): 357-380.
- Mastrorarde, D. N. (1987). Two classes of single-input X-cells in cat lateral geniculate nucleus. II. Retinal inputs and the generation of receptive-field properties. *J Neurophysiol* **57**(2): 381-413.



- Midena, E. (2007). *Perimetry and the Fundus: An Introduction to Microperimetry*. Thorofare, NJ, SLACK, Inc.
- Naka, K. I. and P. W. Nye (1970). Receptive-field organization of the catfish retina: are at least two lateral mechanisms involved? *J Neurophysiol* **33**(5): 625-642.
- Pallikaris, A., D. R. Williams and H. Hofer (2003). The reflectance of single cones in the living human eye. *Invest Ophthalmol Vis Sci* **44**(10): 4580-4592.
- Putnam, N. M., D. X. Hammer, Y. Zhang, D. Merino and A. Roorda (2010). Modeling the foveal cone mosaic imaged with adaptive optics scanning laser ophthalmoscopy. *Opt Express* **18**(24): 24902-24916.
- Rashbass, C. (1970). The visibility of transient changes of luminance. *J Physiol* **210**(1): 165-186.
- Rha, J., R. S. Jonnal, K. E. Thorn, J. Qu, Y. Zhang and D. T. Miller (2006). Adaptive optics flood-illumination camera for high speed retinal imaging. *Opt Express* **14**(10): 4552-4569.
- Riccò, A. (1877). Relazioni fra il minimo angolo visuale e l'intensità luminosa. *Ann Ottal.* **6**: 373-479.
- Rodieck, R. W. (1998). *The First Steps in Seeing*. Sunderland, Massachusetts, Sinauer Associates.
- Roorda, A., F. Romero-Borja, W. J. Dornally, 3rd, H. Queener, T. Hebert and M. Campbell (2002). Adaptive optics scanning laser ophthalmoscopy. *Opt Express* **10**(9): 405-412.
- Roorda, A. and D. R. Williams (1999). The arrangement of the three cone classes in the living human eye. *Nature* **397**(6719): 520-522.

- Roorda, A. and D. R. Williams (2002). Optical fiber properties of individual human cones. *J Vis* **2**(5): 404-412.
- Roufs, J. A. (1972). Dynamic properties of vision. I. Experimental relationships between flicker and flash thresholds. *Vision Res* **12**(2): 261-278.
- Scheffrin, B. E., M. L. Bieber, R. McLean and J. S. Werner (1998). The area of complete scotopic spatial summation enlarges with age. *J Opt Soc Am A Opt Image Sci Vis* **15**(2): 340-348.
- Scholtes, A. M. and M. A. Bouman (1977). Psychophysical experiments on spatial summation at threshold level of the human peripheral retina. *Vision Res* **17**(7): 867-873.
- Scoles, D., Y. N. Sulai, C. S. Langlo, G. A. Fishman, C. A. Curcio, J. Carroll and A. Dubra (2014). In vivo imaging of human cone photoreceptor inner segments. *Invest Ophthalmol Vis Sci* **55**(7): 4244-4251.
- Sekirnjak, C., P. Hottowy, A. Sher, W. Dabrowski, A. M. Litke and E. J. Chichilnisky (2006). Electrical stimulation of mammalian retinal ganglion cells with multielectrode arrays. *J Neurophysiol* **95**(6): 3311-3327.
- Sincich, L. C., D. L. Adams, J. R. Economides and J. C. Horton (2007). Transmission of spike trains at the retinogeniculate synapse. *J Neurosci* **27**(10): 2683-2692.
- Sincich, L. C., Sabesan, R, Tuten, W. S., Roorda, A., Harmening, W. M. (2016). Functional imaging of cone photoreceptors. *Human Color Vision*. R. Baraas, Marshall, J., Kremers, J. New York, Springer.
- Sincich, L. C., Y. Zhang, P. Tiruveedhula, J. C. Horton and A. Roorda (2009). Resolving single cone inputs to visual receptive fields. *Nat Neurosci* **12**(8): 967-969.

- Snodderly, D. M., R. S. Weinhaus and J. C. Choi (1992). Neural-vascular relationships in central retina of macaque monkeys (*Macaca fascicularis*). *J Neurosci* **12**(4): 1169-1193.
- Soo, F. S., G. W. Schwartz, K. Sadeghi and M. J. Berry, 2nd (2011). Fine spatial information represented in a population of retinal ganglion cells. *J Neurosci* **31**(6): 2145-2155.
- Spillmann, L., A. Ransom-Hogg and R. Oehler (1987). A comparison of perceptive and receptive fields in man and monkey. *Hum Neurobiol* **6**(1): 51-62.
- Stockman, A. and L. T. Sharpe (2000). Tritanopic color matches and the middle- and long-wavelength-sensitive cone spectral sensitivities. *Vision Res* **40**(13): 1739-1750.
- Stone, J. and M. Fabian (1968). Summing properties of the cat's retinal ganglion cell. *Vision Res* **8**(8): 1023-1040.
- Tam, J., P. Tiruveedhula and A. Roorda (2011). Characterization of single-file flow through human retinal parafoveal capillaries using an adaptive optics scanning laser ophthalmoscope. *Biomed Opt Express* **2**(4): 781-793.
- Tamura, T., K. Nakatani and K. W. Yau (1991). Calcium feedback and sensitivity regulation in primate rods. *J Gen Physiol* **98**(1): 95-130.
- Thoreson, W. B. and S. C. Mangel (2012). Lateral interactions in the outer retina. *Prog Retin Eye Res* **31**(5): 407-441.
- Tuten, W. S., P. Tiruveedhula and A. Roorda (2012). Adaptive optics scanning laser ophthalmoscope-based microperimetry. *Optom Vis Sci* **89**(5): 563-574.

- Usrey, W. M., J. B. Reppas and R. C. Reid (1999). Specificity and strength of retinogeniculate connections. *J Neurophysiol* **82**(6): 3527-3540.
- Volbrecht, V. J., E. E. Shrago, B. E. Scheffrin and J. S. Werner (2000). Spatial summation in human cone mechanisms from 0 degrees to 20 degrees in the superior retina. *J Opt Soc Am A Opt Image Sci Vis* **17**(3): 641-650.
- Wald, G. (1938). Area and Visual Threshold. *J Gen Physiol* **21**(3): 269-287.
- Wassle, H. (2004). Parallel processing in the mammalian retina. *Nat Rev Neurosci* **5**(10): 747-757.
- Watanabe, M. (1986). [Visual information processing from the retina to the prefrontal cortex]. *Shinrigaku Kenkyu* **56**(6): 365-378.
- Wiersma, C. A. (1966). Integration in the visual pathway of crustacea. *Symp Soc Exp Biol* **20**: 151-177.
- Wiesel, T. N. (1960). Receptive fields of ganglion cells in the cat's retina. *J Physiol* **153**: 583-594.
- Wilson, M. E. (1970). Invariant features of spatial summation with changing locus in the visual field. *J Physiol* **207**(3): 611-622.
- Yang, Q., D. W. Arathorn, P. Tiruveedhula, C. R. Vogel and A. Roorda (2010). Design of an integrated hardware interface for AOSLO image capture and cone-targeted stimulus delivery. *Opt Express* **18**(17): 17841-17858.

## FIGURES

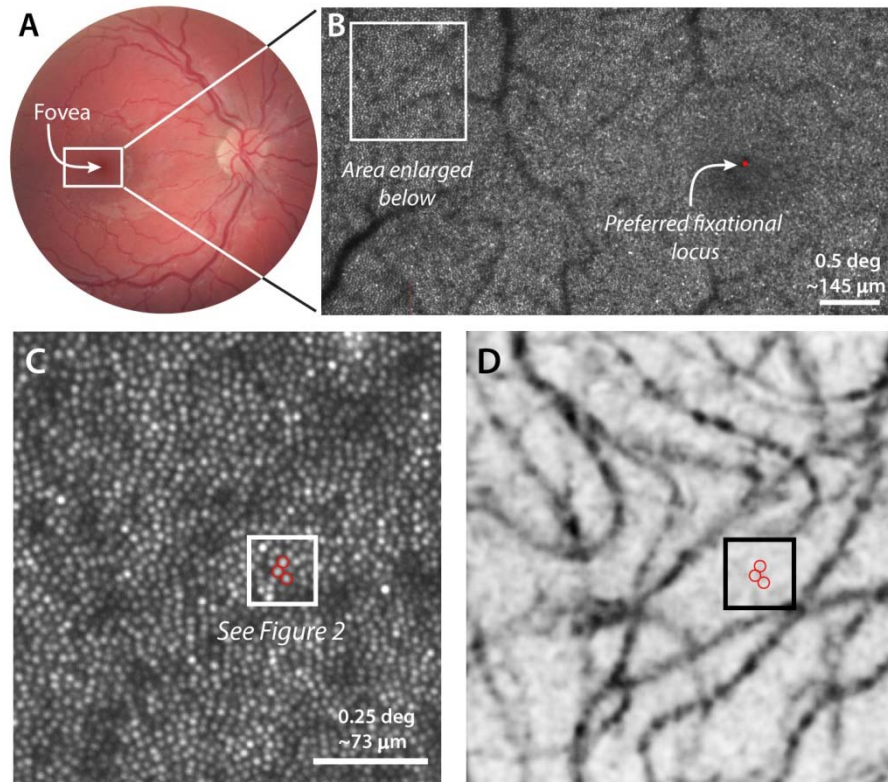


**Figure 1. Retinal areas targeted for microstimulation are chosen to avoid vasculature.** (A) Fundus photograph of the right eye of Subject 1. Outlined area shown magnified in (B), where AOSLO images are montaged to determine the eccentricity of testing locations relative to fixational locus (red dot). Outlined area shown magnified in panel C, where cone photoreceptors appear as bright spots within an AOSLO image (eccentricity = 2.7°). (D) Vasculature map covering the same retinal area as in C. Cones chosen for targeted microstimulation are free from overlying vasculature (red circles). Outlined area in panels C and D are magnified further in Figures 2 and 7.

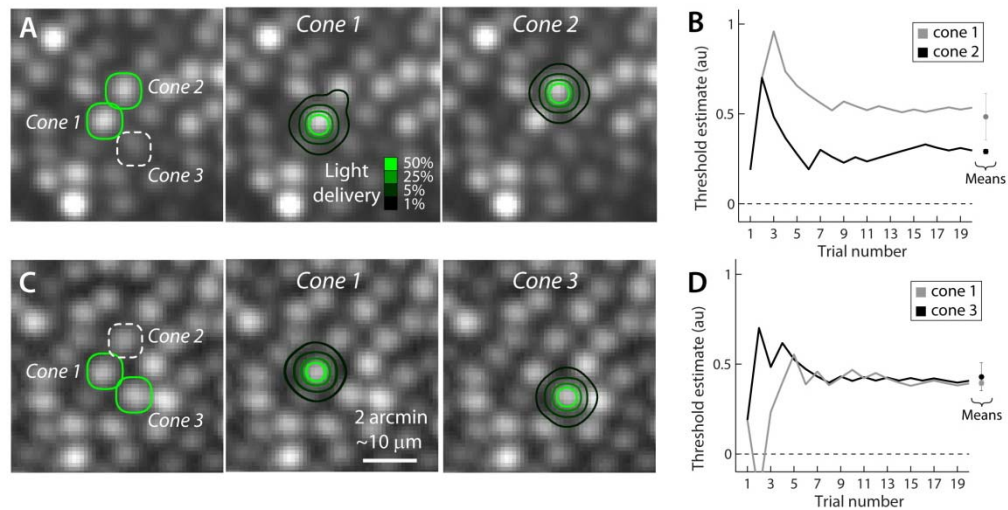


**Figure 2. Example cone pairs with similar and different thresholds.** (A) Green contour in left panel shows stimulus with optimal AOSLO wavefront correction, representing the 5% intensity contour that contains 88% of all light energy. When the PSF convolved stimulus is integrated over all the delivery locations for each stimulus condition, the light delivery contours show that most of the light fell within the diameter of the imaged cone (middle and right panels, taken from outlined area in Figure 1C). (B) Staircases for increment threshold estimation from a single experimental run are shown for cones 1 and 2. Threshold means are at right for each cone, demonstrating a difference in threshold (cone 1 mean =  $0.52 \pm 0.13$ , cone 2 mean =  $0.29 \pm 0.01$ ,  $p = 0.008$ ; Wilcoxon rank-sum test). (C) On a separate day, cones 1 and 3 were tested as a pair, with light delivery contours calculated as in A. (D) Staircase threshold estimations exhibiting similar thresholds (cone 1 mean =  $0.40 \pm 0.02$ , cone 3 mean =  $0.43 \pm 0.08$ ;  $p = 0.8$ ; Wilcoxon rank-sum test).

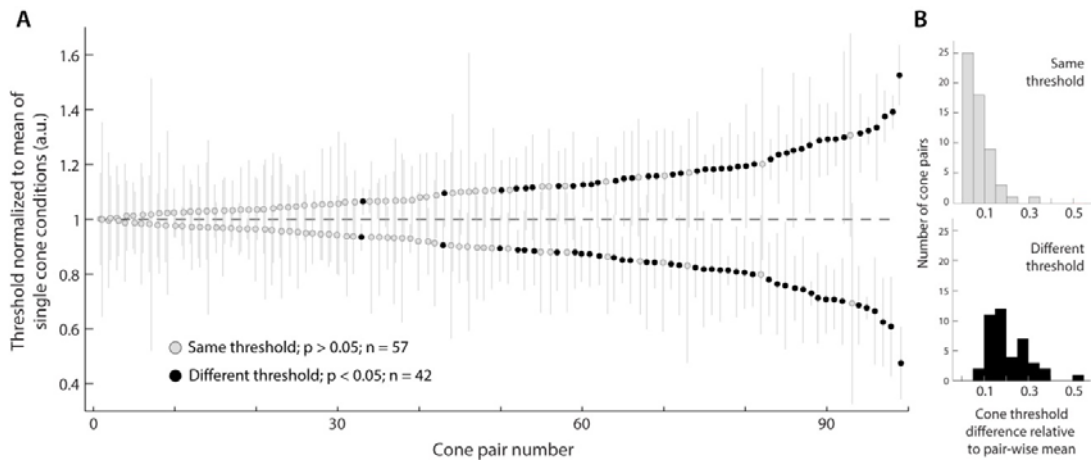


**Figure 3. Individual cones exhibit variation in perceptual threshold. (A)** Mean experimental individual cone thresholds are shown, normalized to the pair-wise mean ( $\pm 1$  SD). Data are rank-ordered by relative threshold difference between cones in the pair. Of 99 cone pairs tested, 57 exhibited statistically indistinguishable thresholds (gray), while 42 had different thresholds (black;  $p < 0.05$ ). **(B)** Population histograms of pair-wise cone threshold differences, indicating that differences as low as 14% can be detected psychophysically.

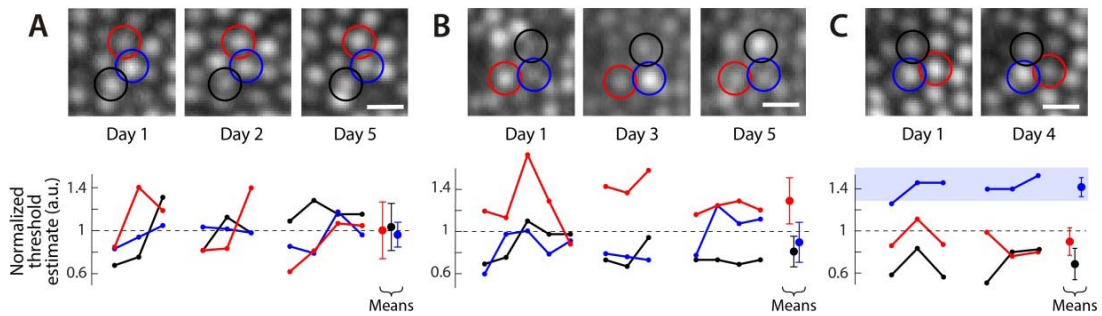


**Figure 4. Cone thresholds are consistent over time.** AOSLO images of identical cone triplets in Subject 2 (**A**, **C**) and Subject 3 (**B**) studied over 2-3 days. Cones targeted for stimulation are circled in each image, and the thresholds from each are coded by color. Data are grouped by test day and were normalized to the mean threshold of the triplet. Each cone was tested 3-5 times per experiment (small dots). Mean single-cone thresholds ( $\pm 1$  SD) across all days are shown on the right within each panel. In **A** all cones had similar increment thresholds, while in **B** the cone circled in red had a consistently higher threshold than the other two cones in its triplet. In **C** the cone circled in blue had thresholds beyond the range of deliverable light (indicated by blue shading), which suggests it is an S cone, given the stimulus conditions.



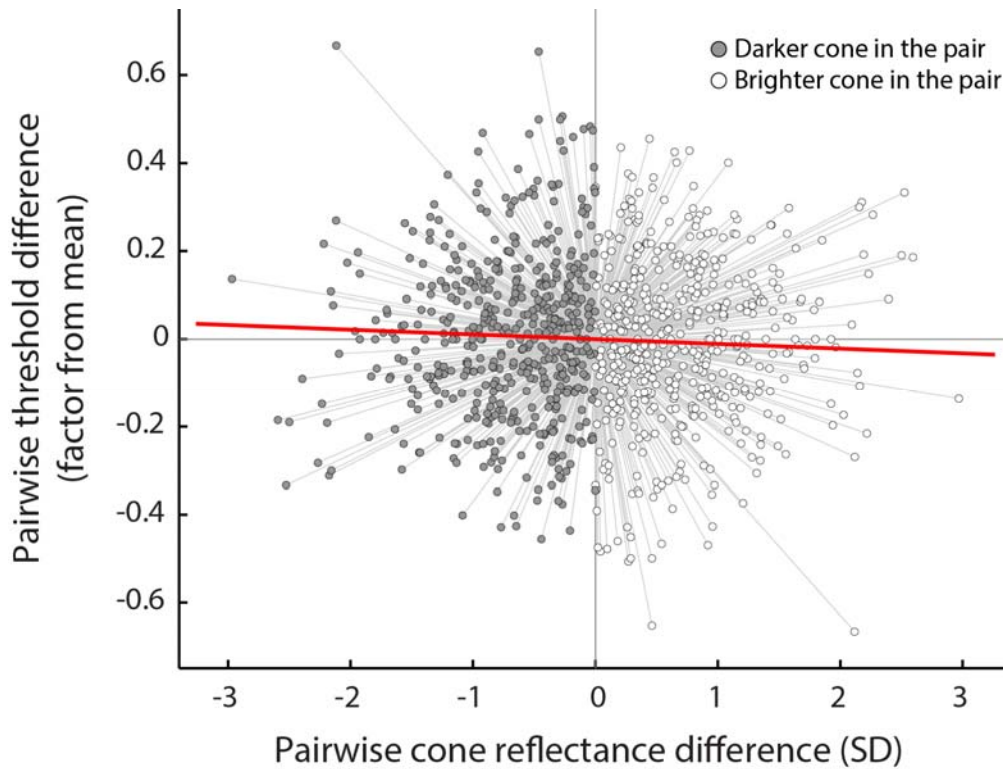


**Figure 5. Cone reflectance is unrelated to threshold.** For cone pairs, reflectance values for each cone during each staircase were normalized to the mean of the pair (indicated by connecting gray lines), expressed in SDs from the pairwise mean. Darker shading represents the less reflective cone in each pair ( $n = 494$  experiments). Cone thresholds from individual experimental runs were normalized to the mean of each cone pair, and plotted as a factor from the pairwise mean. The mean threshold difference between dark and bright cones in a pair was 1.6%, a value below significance ( $p = 0.19$ ; two-tailed  $t$ -test). Red line is a linear regression through the data.

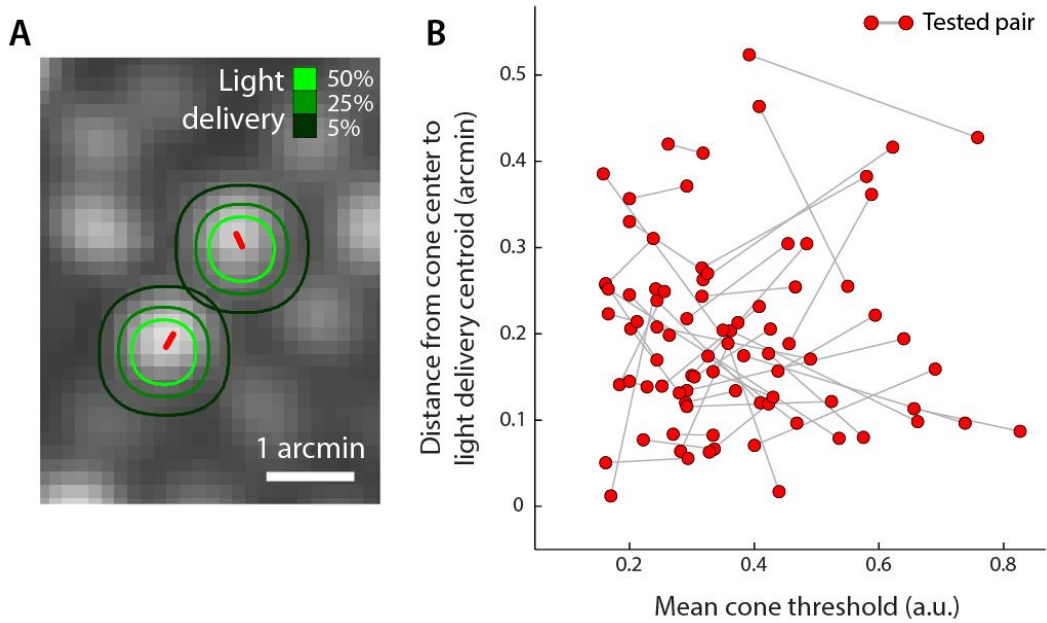


**Figure 6. Threshold differences do not arise from systematic errors in stimulus delivery.** (A) The center of each cone was identified and compared to the centroid of the summed light delivery in order to determine the relative offset of stimulus delivery onto targeted cones (here, the cone pair from Figure 2A). Red lines connect the cone center and stimulus centroid (B) For the 42 cone pairs (red circles connected by a gray line) that exhibited different thresholds (see Figure 3), stimuli fell within 1.3 pixels (0.2 arcmin) of the cone centers on average. No relationship between threshold and distance from cone center was observed ( $R^2 = 8 \times 10^{-5}$ ).

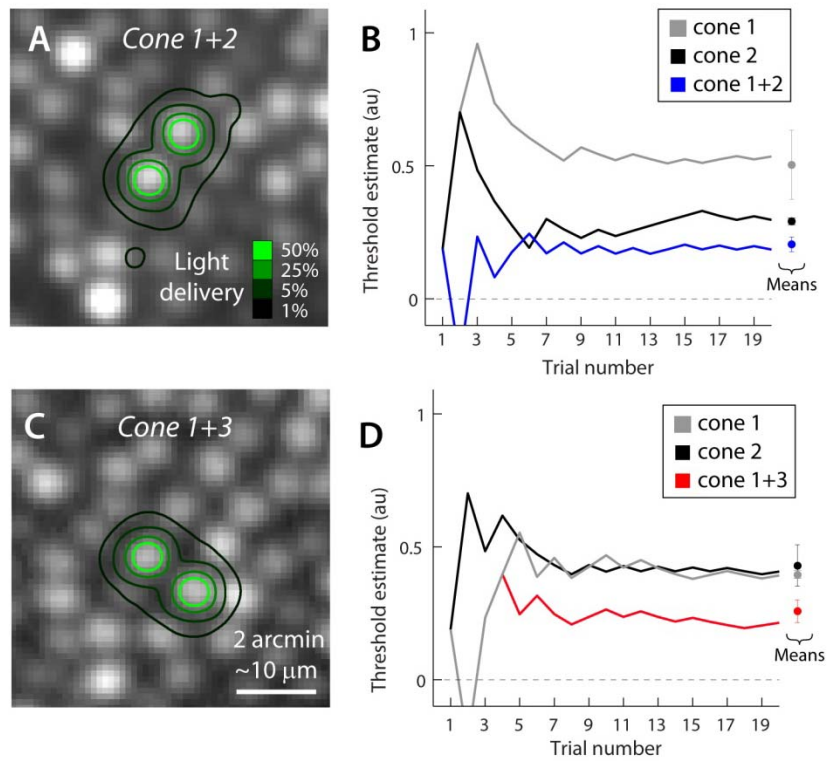


**Figure 7. Cone pairs can exhibit two styles of signal summation.** Neighboring cones in Subject 1 were tested simultaneously to assess the nature of cone signal summation (see single-cone examples from these cone pairs in Figure 2). Light delivery contours with two  $5 \times 5$  pixel stimuli are shown in (A, C). (B) Staircases for increment threshold estimation from Figure 2B incorporating the two-cone condition, demonstrating signal integration consistent with a linear model of summation (cone 1+2 mean =  $0.21 \pm 0.03$ ). (D) Staircases from Figure 2D adding the two-cone condition, here fitting a two-detector model of summation (cone 1+3 mean =  $0.26 \pm 0.04$ ).

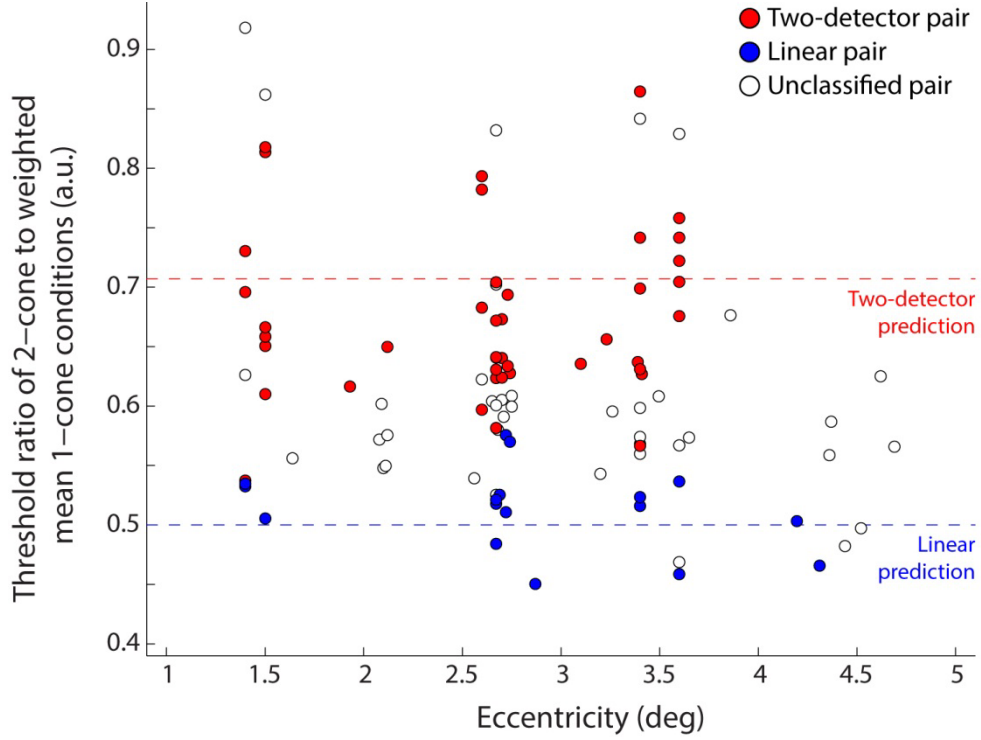


**Figure 8. Style of cone signal summation does not vary with eccentricity.** Individual points represent the threshold ratio of the 2-cone threshold to the mean weighted single-cone thresholds ( $n = 99$  cone pairs). Red circles represent cone pairs that exhibited signal integration consistent with a model of two-detector summation ( $n = 42$ ). Blue circles denote pairs where the signal integration fit a linear model of summation ( $n = 17$ ). White circles indicate pairs whose signal integration was not attributable to either model ( $n = 40$ ). Dashed lines indicate model predictions.

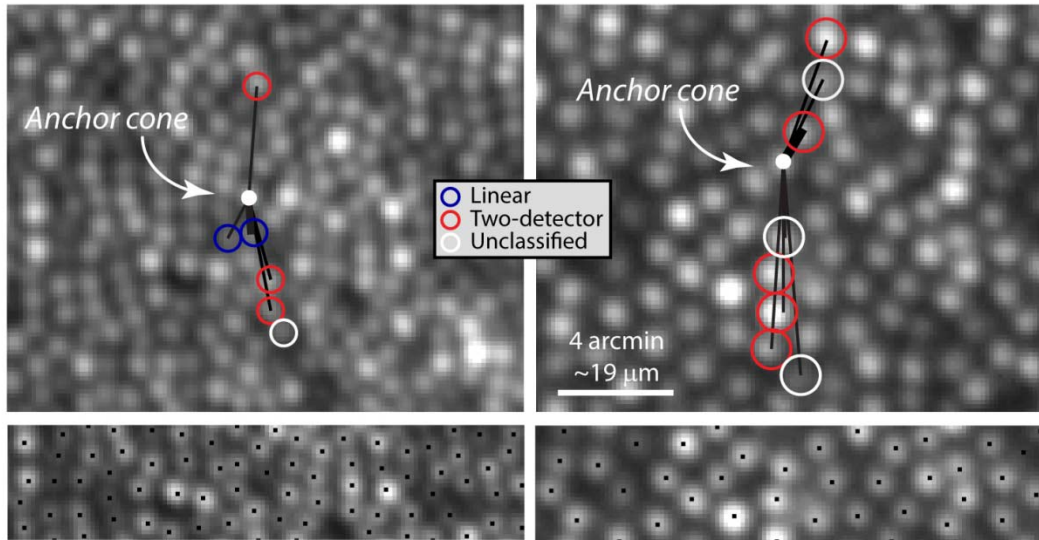


**Figure 9. Summation style depends on distance between cones.** (Top) At each site tested, an anchor cone was selected. The second cone in each tested pair was chosen at different distances from the anchor cone. Type of summation is color-coded according to legend. Data from Subject 4 at different eccentricities:  $1.4^\circ$  at left,  $3.4^\circ$  at right. Scale bar applies to both panels. (Bottom) Because tested eccentricities varied, it was necessary to obtain an average cone spacing value at each site to normalize for inter-cone distance. This was done by identifying the centers of 500 cones at each site (black dots, subsample shown), centered on the tested cone pairs, to create a metric of cone spacing rather than absolute distance.

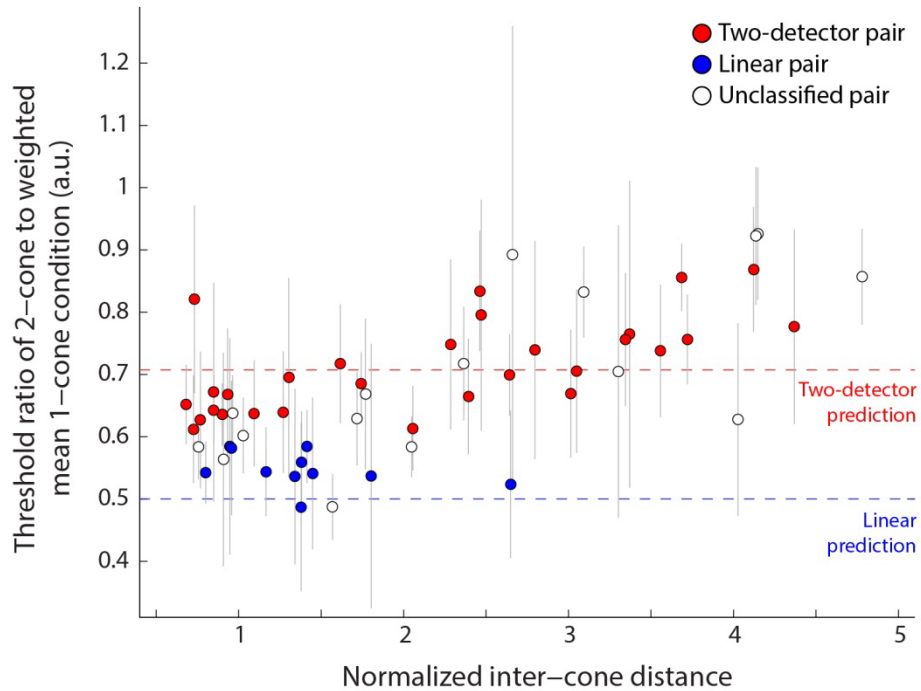


**Figure 10. Linear summation occurs with closely spaced cones.** Individual points represent the ratio of the two-cone threshold to the mean weighted single-cone thresholds for a single experiment ( $\pm 1$  SD;  $n = 56$  cone pairs tested with an anchor cone). Red circles represent pairs with signal integration that adhered to the two-detector model of summation ( $n = 29$ ). Blue circles indicate cone pairs with signal integration that fit a linear model of summation ( $n = 11$ ). White circles were pairs with signal summation not attributable to either model ( $n = 16$ ). Dashed lines represent the model predictions.

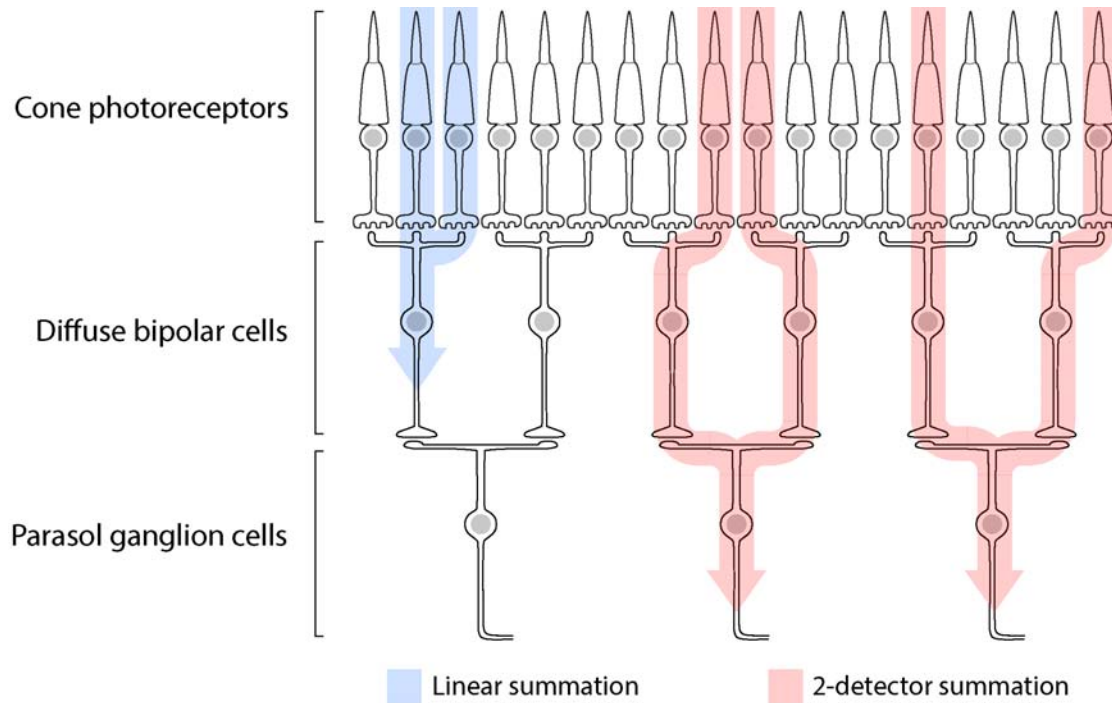


**Figure 11. Cone signal pathway determines style of summation.** Two models of summation are shown, with linear summation occurring at the level of the bipolar cell (blue) and two-detector summation occurring in the ganglion cells (red). Two-detector summation could occur when cones are nearest neighbors, if each cone synapsed onto an individual bipolar cell. As inter-cone distance increases, the likelihood of independent bipolar cell activation increases.

### CHAPTER 3

#### NORMAL PERCEPTUAL SENSITIVITY ARISING FROM WEAKLY REFLECTIVE CONE PHOTORECEPTORS

by

KADY S. BRUCE, WOLF M. HARMENING, BRADLEY R. LANGSTON,  
WILLIAM S. TUTEN, AUSTIN ROORDA, LAWRENCE C. SINCICH

*Investigative Ophthalmology and Visual Science*

Volume 56, Number 8, pages 4431-4438

Copyright 2015

by

The Association for Research in Vision and Ophthalmology

Used by permission

Format adapted for dissertation



## **Abstract**

**Purpose:** To determine the light sensitivity of poorly reflective cones observed in retinas of normal subjects, and to establish a relationship between cone reflectivity and perceptual threshold.

**Methods:** Five subjects (4 male, 1 female) with normal vision were imaged longitudinally (7-26 imaging sessions, representing 82-896 days) using adaptive optics scanning laser ophthalmoscopy (AOSLO) to monitor cone reflectance. Ten cones with unusually low reflectivity, as well as ten normally reflective cones serving as controls, were targeted for perceptual testing. Cone-sized stimuli were delivered to the targeted cones and luminance increment thresholds were quantified. Thresholds were measured 3-5 times per session for each cone in the 10 pairs, all located 2.2-3.3° from the center of gaze.

**Results:** Compared to other cones in the same retinal area, 3 of 10 monitored dark cones were persistently poorly reflective, while 7 occasionally manifested normal reflectance. Tested psychophysically, all 10 dark cones had thresholds comparable to those from normally reflecting cones measured concurrently ( $p = 0.49$ ). The variation observed in dark cone thresholds also matched the wide variation seen in a large population ( $n = 56$  cone pairs, 6 subjects) of normal cones; in the latter, no correlation was found between cone reflectivity and threshold ( $p = 0.0502$ ).

**Conclusions:** Low cone reflectance cannot be used as a reliable indicator of cone sensitivity to light in normal retinas. To improve assessment of early retinal pathology, other diagnostic criteria should be employed along with imaging and cone-based microperimetry.

## **Introduction**

Adaptive optics scanning laser ophthalmoscopy (AOSLO) has provided valuable insight about retinal structure at the cellular level in many diseases. Consequently, clinical interest in using AOSLO imaging to examine disease is likely to continue growing (Carroll, Kay et al. 2013). Although AOSLO has been employed to image numerous retinal structures, it is most commonly used to visualize cone photoreceptors because of their intrinsic ability to reflect incoming light (Williams 2011). In retinal disease, cones may be dysmorphic, atrophied, or missing from the mosaic. These factors will contribute to poor reflectance and possibly increased cone spacing in AOSLO images, both of which are metrics commonly used to gauge disease progression. For instance, patients with type 1 diabetes, glaucoma, and Stargardt disease all showed a decrease of cone density (Chen, Ratnam et al. 2011, Choi, Zawadzki et al. 2011, Lombardo, Parravano et al. 2014) , while patients with acute macular retinopathy and severe head trauma showed a reduction in cone reflectivity (Stepien, Martinez et al. 2012, Hansen, Cooper et al. 2013). These retinopathies represent a small sample of the potential diseases that may cause cone photoreceptors to appear abnormal in adaptive optics imaging (Carroll, Neitz et al. 2004, Choi, Doble et al. 2006, Makous, Carroll et al. 2006, Wolfing, Chung et al. 2006, Duncan, Zhang et al. 2007, Roorda, Zhang et al. 2007, Choi, Zawadzki et al. 2008, Carroll, Rossi et al. 2010, Merino, Duncan et al. 2011, Talcott, Ratnam et al. 2011, Ratnam, Vastinsalo et al. 2013, Syed, Sundquist et al. 2013, Dubis, Cooper et al. 2014). Consequently, it is important to establish how cone reflectivity is related to functional light sensitivity.

The intrinsic waveguiding properties of cones are well established (Lakshminarayanan 2010), and depend upon the normally cylindrical shape of the inner and outer segments. If retinal diseases cause either of the segments to become atrophic or dysmorphic, the cones are likely to appear dark within an AOSLO image. However, in normal retinas it has been reported that there are occasional cones that exhibit unusually low reflectance (Liang, Williams et al. 1997, Pallikaris, Williams et al. 2003, Genead, Fishman et al. 2011). These cones appear as a dark space within an otherwise regular mosaic, much in the same way that a diseased cone might. It is important to realize that in all subjects imaged with AOSLO, regardless of disease state, cone reflectivity in AOSLO images varies considerably from moment-to-moment, as well as from day-to-day. This variation in reflectivity is not completely understood and may arise from multiple factors, including natural morphological variation within cells, refractive index changes associated with photocurrent dynamics, and the coherence properties of the imaging light (Roorda, Romero-Borja et al. 2002, Pallikaris, Williams et al. 2003, Jonnal, Rha et al. 2007, Bedggood and Metha 2013). Consistent with the earlier reports, we have observed cones within AOSLO images that exhibit low reflectivity in the perifoveal region. Given that these poorly reflective cones exist in pathological and non-pathological states, this raises the question of whether persistently dark cones in normal subjects represent dysfunctional photoreceptors. If so, dark cones may serve as a useful harbinger of retinal disease at the earliest stages.

Here we sought to determine the light sensitivity of persistently dark cones found in the retinas of normal subjects. To do so, selected dark cones were first imaged longitudinally using an AOSLO system in a laboratory setting, in order to see how the

reflectivity of the cones changed over time scales longer than a single imaging session. Second, the dark cones were targeted for psychophysical testing, where a cone-sized stimulus was delivered to selected cones in the retinal mosaic and increment thresholds were determined (Harmening, Tuten et al. 2014). Finally, we examined whether there was any relationship between cone reflectivity and the perceptual thresholds measured with such microstimulation.

## **Methods**

Our multi-site, experimental cohort study was approved prospectively by the Institutional Review Boards of the University of Alabama at Birmingham and the University of California, Berkeley, and conformed to the tenets of the Declaration of Helsinki.

Written, informed consent was required by all subjects to participate in the research. All participating subjects had 20/20 or better best corrected visual acuity, clear optics, and had normal color vision. Exclusion criteria included highly irregular corneal shape and visual acuity that could not be optically compensated; however, no prospective subjects were excluded.

### *Retinal imaging*

Cones were imaged using multiwavelength AOSLOs (UAB and UCB) with infrared light ( $842 \pm 25$  nm). In each system, the light source was a supercontinuum laser (SuperK Extreme; NKT Photonics) bandpass filtered to provide the infrared imaging light and the visible stimulation light ( $543 \pm 11$  nm) in separate imaging channels. The rationale for choosing 543 nm for the stimulation wavelength was to minimize the sensitivity differences between the long and medium wavelength sensitive cones. For

imaging, specific details pertaining to AOSLO systems have been described elsewhere (Roorda, Romero-Borja et al. 2002, Zhang, Poonja et al. 2006, Harmening, Tiruveedhula et al. 2012) . Briefly, light in both channels was projected into the eye via vertical and horizontal scanning mirrors. Infrared light reflected back through the optical system was sampled by a Shack-Hartmann wavefront sensor for measurement of wavefront aberrations. The aberrated wavefront in both light channels was then compensated using a MEMs deformable mirror (Boston Micromachines, Cambridge MA), with the wavefront being continuously corrected in a closed loop operating at 16 Hz.

#### *Single cone microstimulation with AOSLO*

Microstimulation involves delivering a cone-sized stimulus onto a single targeted cone. Comprehensive methods have been recently described elsewhere (Harmening, Tuten et al. 2014). For the present experiments, we used a  $5 \times 5$  pixel square (35 arcsec,  $\sim 3.6 \mu\text{m}$ ) of 543 nm light, flashed for a duration of  $\sim 130 \mu\text{s}$  on a constant background of  $\sim 4.3 \text{ cd/m}^2$ . Taking into account the point spread function of the eye's optics under these imaging conditions, and the small scatter in stimulus delivery (Harmening, Tuten et al. 2014), this stimulus size (at the 5% intensity contour) subtended less than  $8 \mu\text{m}$  on the retina (less than 2 arcmin for a typical human eye assuming  $290 \mu\text{m/deg}$  (Wyszecki 1982)), closely matching the inner segment diameter of the cones at the eccentricities studied ( $2.2\text{-}3.3^\circ$ ) (Curcio, Sloan et al. 1990). This eccentricity range is optimal for microstimulation because the cone spacing is large enough to be minimally affected by positional delivery errors, yet the sites were within the  $\sim 5^\circ$  limit where such stimuli presented through this system can be seen (Harmening, Tuten et al. 2014). Because the

imaging and stimulation were performed with different wavelengths, transverse chromatic aberrations were both measured and corrected in each subject (Harmening, Tiruveedhula et al. 2012). This measurement was made before and after each experiment, to assess whether any lateral shift in the stimulus occurred during the experiment. If measured offsets drifted by more than one half cone width, the data were discarded. Fixational eye movements present in all subjects was compensated for using real-time eye tracking (Yang, Arathorn et al. 2010), allowing retinally stabilized stimulus delivery with cumulative delivery errors of less than a cone diameter (Harmening, Tuten et al. 2014).

### *Psychophysical experiments*

Pupils were dilated with 1% tropicamide. Bite bars custom fitted for each subject were used to minimize pupil motion. Retinal locations being imaged were selected by having the subject fixate on a light-emitting diode positioned outside of a 1.2° imaging field. Following transverse chromatic aberration measurement and 15 minute dark adaptation, the psychophysical experiments commenced self-paced. Subjects used a keyboard to initiate each trial and to provide a response. Five subjects (4 male, 1 female) were participants in the experiments testing dark cones explicitly, and 1 additional male subject was included in the normal cone psychophysical testing. All subjects (aged 22-51) had normal color vision (assessed by Hardy, Rand & Rittler plates and a Nagel anomaloscope) and no known retinal pathology based on comprehensive optometric eye exams. Luminance increment thresholds for the flashed microstimuli were measured using a Bayesian staircase method of threshold estimation (King-Smith, Grigsby et al.

1994). Increment threshold was chosen as the test for light sensitivity because, at threshold, the stimulus is necessarily the least amount of light required to be perceived. Light levels representing threshold were converted to arbitrary units, ranging from 0 to 1, in order to control for day-to-day variations in stimulus intensity and allow comparisons between experiments. To provide a sense of the stimulus intensity in radiometric terms, we calculate that a typical  $5 \times 5$  pixel stimulus (lasting  $\sim 240 \mu\text{sec}$ ) included  $\sim 12$  log quanta at maximum intensity, presented on a background of  $\sim 8$  log quanta incident at the cornea (Harmening, Tuten et al. 2014). Two cones, one dark and a neighboring one with normal reflectivity to serve as a control, were targeted for stimulus delivery. All trials were randomly interleaved between each cone in a tested pair, and threshold was measured 3-5 times for each cone location (60-100 total trials) per experiment. Because of stimulus light level fluctuations, and also because threshold rises steeply with eccentricity, we analyzed the data with respect to relative threshold (between the two targeted cones) rather than raw threshold. Before any psychophysical data were used for analysis, subjects had practiced the task to the point where reasonably consistent thresholds were obtained upon repeated measurements.

Ten cone pairs (one normally reflective and one poorly reflective) were monitored for both longitudinal imaging and psychophysical testing ( $n = 5$  subjects). Six of these pairs were studied in one subject (age 23), with the remaining pairs in one subject each. Dark cones were initially selected as a cone-sized dark space within an otherwise normal cone mosaic. In 3 cases, the dark cone never increased appreciably in brightness. In 7 cases the cone occasionally reflected enough light to be visible; in these cases, the selected center was chosen based upon the cone's location on such imaging days. In

cases where the dark cone was never visible, cone locations were estimated by choosing a point in the center of the cone-sized gap among neighboring cones. The 10 poorly reflective cones tracked longitudinally were tested only when they were darker than the field mean in the AOSLO image; this was required because some of these monitored cones occasionally exhibited normal reflectivity.

To validate the results obtained from the psychophysical testing of the dark/normal cone pairs, a larger population of normal cone pairs was also tested psychophysically. In these pairs, each of the cones in the pair exhibited normal reflectivity (n=56 cone pairs, 6 subjects). These normal/normal cone pairs were tested in the same manner as described above.

#### *Identification of retinal vessels*

Retinal blood vessels and capillaries lying in front of the photoreceptors could, in principle, disrupt the light reflecting from the cones or interfere with stimulation light being delivered to the cones. In order to avoid these artifacts, vasculature maps were made for each targeted retinal location (Tam, Martin et al. 2010). These maps were compiled using video processing tools to extract blood motion contrast cues from 30 second AOSLO videos taken with 710 or 840 nm light. By examining the vasculature maps that corresponded to the cone images at each site, we could select dark or normally reflective cones that were not associated with light path interference caused by retinal vessels.



### *Reflectance quantification and longitudinal imaging*

To obtain the AOSLO images used for reflectance quantification, two methods were used. First, for the majority of the cases, reflectivity data was obtained from images acquired during unrelated psychophysical experiments performed in the areas of interest. During each trial of a psychophysical experiment, a 1 second retinally-stabilized infrared video of 30 frames was recorded (Arathorn, Yang et al. 2007). These frames were averaged, after eliminating any blank frames or those with patent uncorrected eye-motion artifacts which are readily detected by automated image analysis. All single-trial average frames were then summed into one image, normalized to the brightest value, representing the cone reflectivity during one experiment. From these normalized images we quantified reflectivity for cones of interest. Second, if there were no prior psychophysical experiments performed in a selected retinal location, a 5 second retinally-stabilized infrared video was taken (150 frames). These frames were also averaged to obtain a brightest-value normalized image (after manually removing frames with motion artifacts). Beyond the difference in total number of averaged frames, all cone reflectivity measurements were done in the same manner.

For the longitudinally monitored cone pairs, cone reflectance was quantified by first calculating the average pixel value for a  $3 \times 3$  pixel square centered on each cone (Pallikaris, Williams et al. 2003). Dark cone locations were identified manually by choosing a point in the center of the cone-sized gap among neighboring cones (for persistently dark cones), or in the cone center if the cone was visible (for intermittently dark cones). For normally reflective cones, the center of the cone was chosen based on manual estimation of the pixel which was most centered within the cone (occasionally,

this was not the brightest pixel). Because the mean reflectance value of an AOSLO image varies over time, we compared the mean pixel value of each cone to the mean pixel value of a  $101 \times 101$  pixel field also centered on the cone. Reflectance was measured in standard deviations (SDs) from the field mean, to control for variations in image quality, laser power, and photomultiplier gain. Finally, for each of the 10 targeted dark/normal cone pairs, the same area of retina in each subject was repeatedly imaged over time to quantify cone reflectivity longitudinally (7-26 imaging sessions, representing 82-896 days).

To identify multiple cones within large fields, custom image processing was performed on normalized images using a custom local peak-finding routine in Matlab (Mathworks, Natick, MA). As this procedure did not always identify every cone correctly, especially those darker than the field mean, the processed images were surveyed manually and misidentified locations were corrected. In instances where cones were darkened due to interference by blood vessels and no peak was detected, cone locations were estimated based on local spacing. Individual cone reflectance was then quantified as described above.

## **Results**

### *Imaging characteristics of poorly reflective cones*

AOSLO images show considerable variation in reflectivity on a cone-by-cone basis. Examining 5 imaged fields of retina from 5 normal subjects, cones ranged in reflectance by a factor of 0.5-2.9 from the mean field reflectance ( $n = 4,377$  cones from  $\sim 169,000 \mu\text{m}^2$  of retina), a range that is consistent with previous reports (Roorda,

Romero-Borja et al. 2002, Pallikaris, Williams et al. 2003, Rha, Jonnal et al. 2006, Putnam, Hammer et al. 2010). Some of the variation at the dark end of this range is likely to be associated with retinal blood vessels, which cover a substantial portion of the retinal surface (Snodderly, Weinhaus et al. 1992). To estimate what percentage of cones within an AOSLO image may be poorly reflective because of light path interference by retinal vessels, we compared the cone field to its overlying vasculature (Figure 1). A map of the cones which had gray scale values below the mean image gray level was created (Figure 1C), and then compared against the vascular map made at the same retinal location (Figure 1D). As expected, most of the poorly reflective cones were associated with vessels. Of the 2,179 cones identified in the patch of retina shown in Figure 1, 346 cones (16%) had gray levels which fell below the image mean (red dots), while 1,833 had gray levels at or above the image mean (black dots). However, a small number of these relatively dark cones were not obviously associated with vessels (blue circles). Such dark cones not associated with blood vessels were found in every subject (Figure 2), in nearly every 1.2° field examined. Given their poor reflectivity, this subset of cones could represent either optical anomalies, present only at the time of imaging, or indicate possibly dysfunctional cones.

To learn if these unoccluded cones were only spuriously dark, we examined a longitudinal series of images to determine the persistence of the reflectivity. The reflectivity of 10 cone pairs, one dark and one normally reflective (depicted in Figure 2D-M), was measured on multiple days. For each cone pair, there was 7 to 26 individual imaging sessions, over lengths of time spanning 82 to 896 days. Of these 10 dark cones, 3 never exhibited reflectivity that was higher than the mean image value (Figure 2D-F),

and were considered persistently dark. Figure 3A shows data for one cone that remained dark, despite neighboring cones that varied in brightness from day to day. The remaining 7 cases occasionally exhibited reflectance that was higher than the mean field reflectance, thereby confirming the presence of a cone in these locations (often this required viewing images on a logarithmic gray scale to reveal the dim signal, as in Figure 3). Data for one such intermittently dark cone is shown in Figure 3B, highlighting the fact that on most days the cone was darker than the mean image reflectivity.

#### *Psychophysical testing of poorly reflective cones*

Because a small number of cones persisted in having anomalously low reflectance, we tested each of the 10 monitored dark cones psychophysically to determine if they were functional, using a staircase method to measure increment thresholds. All poorly reflective cones were tested for light sensitivity only when they were darker than the field mean in the AOSLO image. For the persistently dark cones, the stimulus was targeted at a manual estimate of where the cone center would be, given the position of neighboring cones (Figure 4A). Testing one of the 3 persistently dark cases, the targeted dark cone location showed an increment threshold that was similar to the increment threshold obtained from its paired normally reflective cone (Figure 4B). Data from one of the intermittently dark cones showed an increment threshold that was slightly lower than that of a nearby normally reflective cone (Figure 4C). Because thresholds measured with such microstimuli can vary between cones for a number of reasons (discussed in (Harmening, Tuten et al. 2014)), we compared the thresholds from the 10 dark cones to the 10 normally reflective cones as a population. To make this comparison, individual

cone thresholds were normalized to the mean of each pairwise run of trials, to control for the effects of inter-subject variability and visual field eccentricity on threshold. As a population, the dark cones did not have higher thresholds than the normally reflective cones that were tested at the same time ( $p = 0.49$ , Wilcoxon rank-sum test, Figure 4D). Persistent and intermittently dark cones showed equivalent variation in threshold versus their paired normal cones.

To confirm that these thresholds were genuinely no different from normally reflective cones, we compared the dark/normal cone paired thresholds to a larger population of normally reflective cone pairs (56 cone pairs, 6 subjects). Threshold data were normalized as before; in addition, cone reflectivity was also normalized to the mean of each tested pair (Figure 5). In this population of normally reflective cone pairs, the mean threshold was 3.6% higher in cones with less versus more reflectivity, a difference that was not significant ( $p = 0.0502$ , Wilcoxon rank-sum test). Had this correlation between cone reflectivity and threshold attained significance, it would still have been greatly outweighed by the ~80% variation in the thresholds observed in the normally reflective cone pairs. The targeted dark/normal cone pairs (Figure 5, red points) exhibited the same variability in threshold and followed the same trend as the normally reflective cone pairs (Figure 5, gray points). To better illustrate this variability, we modified Figure 5 to highlight measurements taken from 5 normally reflecting cone pairs, each tested 5 times (Figure 6). These highlighted pairs vary greatly in measured threshold, with little discernable tendency for the brighter cone to have the lower threshold. Also, as a population, there was no appreciable difference in absolute light levels for the dark/normal versus normal/normal pair thresholds, suggesting there was no

local retinal effect on threshold (Figure 7). The range of reflectivity in these dark/normal cone pairs is on the extremes of the normal/normal cone pairs, as expected, since the inclusion of a dark cone increases the difference in reflectivity between cones in a pair.

## **Discussion**

Our results suggest that cones which appear dark in AOSLO images and are not occluded by blood vessels remain normally sensitive to light, specifically when measured by luminance increment thresholds. One possible explanation for this is that residual scattered light from our stimulus is being detected by cones that surround the targeted cone. Light reaching these cones may arise from intraocular scatter or residual errors in our optical correction. In the case of normal intraocular scatter, experimental results and a model presented in Harmening *et al.* (2014) showed that this does not play a detectable role in determining increment thresholds for cone-sized stimuli. Regarding imperfections in optical correction, in the diffraction-limited case, the resultant point spread function implies a very wide but very shallow intensity profile around the targeted cone. Less than 1% of the delivered light falls onto each of the 6 surrounding cones while more than 80% of the light lands within the targeted cone's inner segment profile (Harmening, Tuten et al. 2014). Even if the optical correction was not completely diffraction-limited, this would likely raise the light delivered to surrounding cones by only a few percent. Thus, if the targeted dark cone was functionally compromised, and the neighboring cones were responsible for detecting the stimulus light, the measured increment threshold would still be greatly increased compared to the paired normally reflective control cone. Instead, the dark cones and paired normally reflective cones exhibited no difference in

their observed thresholds (Figure 4D), rendering it unlikely that neighboring cones could account for the increment thresholds measured from poorly reflective cones.

In the cases where the cones remained persistently dark, it might be hypothesized that the sites were actually small clusters of rod photoreceptors, which can occur occasionally at the eccentricities studied (Curcio, Sloan et al. 1990). Our AOSLOs cannot currently resolve rod photoreceptors, so they appear in the images as dark spaces surrounding the cones (Zhang, Poonja et al. 2006, Merino, Duncan et al. 2011). However, recent experiments have demonstrated that rod-filled gaps in the photoreceptor mosaic would not respond to the stimuli used here in the same manner as a cone photoreceptor would. On average, increment thresholds obtained from deliberately targeting microstimuli to the rod-sized gaps between cones was 48% higher than thresholds obtained when the stimuli were centered on a cone (Harmening, Tuten et al. 2014). This result was accounted for by the cones outlining the gap. Moreover, the stimulus conditions here and in the gap-targeting experiments had background light levels that were rod-saturating, making any rod-mediated contribution to the task negligible. Therefore our results are not likely to arise from any rod-mediated perception.

The question remains why a small set of cones with normal light sensitivity are poorly reflective on most days. Several independent factors may come into play. Waveguiding is one: small reflections that occur within the cone are efficiently directed back out of the eye because of the anatomical shape of the photoreceptors. This reflection is made more efficient because cones point toward the pupil due to phototropism (Lakshminarayanan 2010). Either waveguiding or cone pointing may be

disrupted for these unusual cones. Given their waveguiding nature, a scanned beam directed at a cone may vary in reflection efficiency on short time scales because of interference between reflections within the cone (Putnam, Hammer et al. 2010, Bedggood and Metha 2013, Harmening, Tuten et al. 2014, Jonnal, Kocaoglu et al. 2014). This effect is partially mitigated by flood-illuminated systems, though cone reflectance still varies (Liang, Williams et al. 1997, Pallikaris, Williams et al. 2003, Cooper, Dubis et al. 2011). Because the cones we have examined are persistently dark, these interference effects cannot readily account for any lasting state of poor reflectivity. Instead, the cause is likely to be of anatomical origin. Several possibilities exist. First, waveguiding may be inefficient because the cone may be dysmorphic. Without knowing more about the geometry of an occasionally misshaped cone, it is difficult to predict whether entering light will be proportional to reflected light, and therefore affect the relationship between threshold and reflectance systematically. Second, the reflections within a properly waveguiding cone may be reduced because the reflective interfaces within the cone (either between inner and outer segments or at the posterior tips of the outer segments) are permanently altered in some way. This anatomical anomaly would tend to separate the efficiency of light collection from light reflection. Finally, these uncommon dark cones may have aberrant orientations, pointing slightly away from the pupil rather than in the tightly aligned orientation most cones have (Roorda and Williams 2002, Pallikaris, Williams et al. 2003). All of these anatomical anomalies may persist over the time scales we have examined, and may be present in combination.

Regardless of the origin of the diminished reflectivity, it is not necessarily the case that a cone's reflectivity should positively correlate with its sensitivity. A cone that



is weakly reflecting solely due to aberrant orientation will suffer a corresponding loss in light coupling and consequent sensitivity. However, there are factors working against this correspondence. One of the primary sources of reflection arises from the inner/outer segment junction (Pallikaris, Williams et al. 2003, Jonnal, Rha et al. 2007, Gao, Cense et al. 2008), and this reflection is light which has never passed through the cone's visual pigment. Second, most of the light coupled into a cone is either transmitted or absorbed. The portion that is reflected is on the order of 1% of what passes through the outer segments (Berendschot, DeLint et al. 2003), and so may not be representative of the light that the cone detects. Considering all this, it is unsurprising that cone threshold is not significantly influenced by large—and often short term—changes in cone reflectivity (Figure 5).

As mentioned earlier, the presence of dark cones in AOSLO images of many retinal diseases is not surprising, given the pathological changes that the tissue manifests. In some instances, dark cones in diseased retinas may not indicate photoreceptor death (Jacob, Paques et al. 2015, Wang, Tuten et al. 2015). The possibility remains that dark cones in normal retinas cannot be considered homologues of dark cones in diseased retinas, so extrapolating functional tests from normal to diseased populations should not be done. In one study, a deuteranope with poorly reflective cones was found to have sensitivity deficits that suggested the mutation-affected cones were not functional (Makous, Carroll et al. 2006), whereas in another study examining a group of patients with retinal degenerations, functional tests appeared normal despite cone losses (Ratnam, Carroll et al. 2013). Thus more work is needed to understand how each type of visual

test (e.g. acuity, microstimulation) can be used to adequately characterize both normal and diseased retinas.

Because of its microscopic access to the photoreceptors, AOSLO imaging nonetheless has promise for becoming a powerful tool for early detection of disease and assessment of therapies. While many studies have examined the complex reflectance properties of cones, only recently has it been possible to probe cone function at the same microscopic scale. Cone-targeted microstimulation reveals that increment thresholds for individual cones vary considerably, even for adjacent cones when all other factors such as eccentricity and cone type are taken into account (Figure 5). Such psychophysical data are consistent with the fact that the functional “weighting” of cones can vary when measured more directly in physiological experiments (Sincich, Zhang et al. 2009, Field, Gauthier et al. 2010, Li, Field et al. 2014). The use of microstimulation to assess function in a clinical setting, therefore, will have to take into account the wide variation in cone thresholds as well as cone reflectivity. The results shown here suggest that cones with diminished visibility in an otherwise normal-appearing retina do not necessarily indicate a sensitivity deficit. With a clearer functional picture of what a normal retina can do with AOSLO-based microstimulation, it can now be appreciated that cone thresholds vary widely. This variation will have to be taken into consideration when testing for nascent disease in patients with suspected retinal disorders but no macroscopic pathology.

## Acknowledgements

We thank A. B. Metha and C. A. Curcio for good-natured and thoughtful comments on the paper.

*Funding/support:* DFG Ha 5323/3-1, Ha 5323/4-1, Ha 5323/5-1, NIH T35HL07473, EY022412, American Optometric Foundation Ezell Fellowship, EY021642, EY014375, EY007043, EY023591, EY003039, EY023581, Eyesight Foundation of Alabama

*Financial disclosures:* A.R. has a patent (USPTO#7118216) licensed to Canon USA Inc.

## References

1. Carroll J, Kay DB, Scoles D, Dubra A, Lombardo M. Adaptive optics retinal imaging--clinical opportunities and challenges. *Curr Eye Res.* 2013;38(7):709-21.
2. Williams DR. Imaging single cells in the living retina. *Vision Res.* 2011;51(13):1379-96.
3. Lombardo M, Parravano M, Lombardo G, et al. Adaptive optics imaging of parafoveal cones in type 1 diabetes. *Retina.* 2014;34(3):546-57.
4. Choi SS, Zawadzki RJ, Lim MC, et al. Evidence of outer retinal changes in glaucoma patients as revealed by ultrahigh-resolution in vivo retinal imaging. *Br J Ophthalmol.* 2011;95(1):131-41.
5. Chen Y, Ratnam K, Sundquist SM, et al. Cone photoreceptor abnormalities correlate with vision loss in patients with Stargardt disease. *Invest Ophthalmol Vis Sci.* 2011;52(6):3281-92.
6. Hansen SO, Cooper RF, Dubra A, Carroll J, Weinberg DV. Selective cone photoreceptor injury in acute macular neuroretinopathy. *Retina.* 2013;33(8):1650-8.
7. Stepien KE, Martinez WM, Dubis AM, et al. Subclinical photoreceptor disruption in response to severe head trauma. *Arch Ophthalmol.* 2012;130(3):400-2.
8. Syed R, Sundquist SM, Ratnam K, et al. High-resolution images of retinal structure in patients with choroideremia. *Invest Ophthalmol Vis Sci.* 2013;54(2):950-61.
9. Carroll J, Neitz M, Hofer H, Neitz J, Williams DR. Functional photoreceptor loss revealed with adaptive optics: an alternate cause of color blindness. *Proc Natl Acad Sci U S A.* 2004;101(22):8461-6.

10. Carroll J, Rossi EA, Porter J, et al. Deletion of the X-linked opsin gene array locus control region (LCR) results in disruption of the cone mosaic. *Vision Res.* 2010;50(19):1989-99.
11. Choi SS, Zawadzki RJ, Keltner JL, Werner JS. Changes in cellular structures revealed by ultra-high resolution retinal imaging in optic neuropathies. *Invest Ophthalmol Vis Sci.* 2008;49(5):2103-19.
12. Choi SS, Doble N, Hardy JL, et al. In vivo imaging of the photoreceptor mosaic in retinal dystrophies and correlations with visual function. *Invest Ophthalmol Vis Sci.* 2006;47(5):2080-92.
13. Duncan JL, Zhang Y, Gandhi J, et al. High-resolution imaging with adaptive optics in patients with inherited retinal degeneration. *Invest Ophthalmol Vis Sci.* 2007;48(7):3283-91.
14. Roorda A, Zhang Y, Duncan JL. High-resolution in vivo imaging of the RPE mosaic in eyes with retinal disease. *Invest Ophthalmol Vis Sci.* 2007;48(5):2297-303.
15. Merino D, Duncan JL, Tiruveedhula P, Roorda A. Observation of cone and rod photoreceptors in normal subjects and patients using a new generation adaptive optics scanning laser ophthalmoscope. *Biomed Opt Express.* 2011;2(8):2189-201.
16. Ratnam K, Carroll J, Porco TC, Duncan JL, Roorda A. Relationship between foveal cone structure and clinical measures of visual function in patients with inherited retinal degenerations. *Invest Ophthalmol Vis Sci.* 2013;54(8):5836-47.
17. Wolfing JI, Chung M, Carroll J, Roorda A, Williams DR. High-resolution retinal imaging of cone-rod dystrophy. *Ophthalmology.* 2006;113(6):1019 e1.

18. Talcott KE, Ratnam K, Sundquist SM, et al. Longitudinal study of cone photoreceptors during retinal degeneration and in response to ciliary neurotrophic factor treatment. *Invest Ophthalmol Vis Sci.* 2011;52(5):2219-26.
19. Dubis AM, Cooper RF, Aboshiha J, et al. Genotype-dependent variability in residual cone structure in achromatopsia: toward developing metrics for assessing cone health. *Invest Ophthalmol Vis Sci.* 2014;55(11):7303-11.
20. Makous W, Carroll J, Wolfing JI, et al. Retinal microscotomas revealed with adaptive-optics microflashes. *Invest Ophthalmol Vis Sci.* 2006;47(9):4160-7.
21. Lakshminarayanan V, Enoch, JM, *Biological Waveguides*, in *Handbook of Optics, Vol III: Vision and Vision Optics*, M. Bass, Editor. 2010, McGraw Hill: New York.
22. Pallikaris A, Williams DR, Hofer H. The reflectance of single cones in the living human eye. *Invest Ophthalmol Vis Sci.* 2003;44(10):4580-92.
23. Genead MA, Fishman GA, Rha J, et al. Photoreceptor structure and function in patients with congenital achromatopsia. *Invest Ophthalmol Vis Sci.* 2011;52(10):7298-308.
24. Liang J, Williams DR, Miller DT. Supernormal vision and high-resolution retinal imaging through adaptive optics. *J Opt Soc Am A Opt Image Sci Vis.* 1997;14(11):2884-92.
25. Jonnal RS, Rha J, Zhang Y, et al. In vivo functional imaging of human cone photoreceptors. *Opt Express.* 2007;15(24):16141-60.
26. Bedggood P, Metha A. Optical imaging of human cone photoreceptors directly following the capture of light. *PLoS One.* 2013;8(11):e79251.

27. Roorda A, Romero-Borja F, Donnelly WJ, 3rd, et al. Adaptive optics scanning laser ophthalmoscopy. *Opt Express*. 2002;10(9):405-12.
28. Harmening WM, Tuten WS, Roorda A, Sincich LC. Mapping the perceptual grain of the human retina. *J Neurosci*. 2014;34(16):5667-77.
29. Zhang Y, Poonja S, Roorda A. MEMS-based adaptive optics scanning laser ophthalmoscopy. *Opt Lett*. 2006;31(9):1268-70.
30. Harmening WM, Tiruveedhula P, Roorda A, Sincich LC. Measurement and correction of transverse chromatic offsets for multi-wavelength retinal microscopy in the living eye. *Biomed Opt Express*. 2012;3(9):2066-77.
31. Wyszecki G, Stiles, WS, *Color Science*. Second ed. 1982, New York: John Wiley & Sons.
32. Curcio CA, Sloan KR, Kalina RE, Hendrickson AE. Human photoreceptor topography. *J Comp Neurol*. 1990;292(4):497-523.
33. Yang Q, Arathorn DW, Tiruveedhula P, Vogel CR, Roorda A. Design of an integrated hardware interface for AOSLO image capture and cone-targeted stimulus delivery. *Opt Express*. 2010;18(17):17841-58.
34. King-Smith PE, Grigsby SS, Vingrys AJ, Benes SC, Supowit A. Efficient and unbiased modifications of the QUEST threshold method: theory, simulations, experimental evaluation and practical implementation. *Vision Res*. 1994;34(7):885-912.
35. Tam J, Martin JA, Roorda A. Noninvasive visualization and analysis of parafoveal capillaries in humans. *Invest Ophthalmol Vis Sci*. 2010;51(3):1691-8.
36. Arathorn DW, Yang Q, Vogel CR, et al. Retinally stabilized cone-targeted stimulus delivery. *Opt Express*. 2007;15(21):13731-44.

37. Putnam NM, Hammer DX, Zhang Y, Merino D, Roorda A. Modeling the foveal cone mosaic imaged with adaptive optics scanning laser ophthalmoscopy. *Opt Express*. 2010;18(24):24902-16.
38. Rha J, Jonnal RS, Thorn KE, et al. Adaptive optics flood-illumination camera for high speed retinal imaging. *Opt Express*. 2006;14(10):4552-69.
39. Snodderly DM, Weinhaus RS, Choi JC. Neural-vascular relationships in central retina of macaque monkeys (*Macaca fascicularis*). *J Neurosci*. 1992;12(4):1169-93.
40. Jonnal RS, Kocaoglu OP, Zawadzki RJ, et al. The cellular origins of the outer retinal bands in optical coherence tomography images. *Invest Ophthalmol Vis Sci*. 2014;55(12):7904-18.
41. Cooper RF, Dubis AM, Pavaskar A, et al. Spatial and temporal variation of rod photoreceptor reflectance in the human retina. *Biomed Opt Express*. 2011;2(9):2577-89.
42. Roorda A, Williams DR. Optical fiber properties of individual human cones. *J Vis*. 2002;2(5):404-12.
43. Gao W, Cense B, Zhang Y, Jonnal RS, Miller DT. Measuring retinal contributions to the optical Stiles-Crawford effect with optical coherence tomography. *Opt Express*. 2008;16(9):6486-501.
44. Berendschot TT, DeLint PJ, van Norren D. Fundus reflectance--historical and present ideas. *Prog Retin Eye Res*. 2003;22(2):171-200.
45. Wang Q, Tuten WS, Lujan BJ, et al. Adaptive optics microperimetry and OCT images show preserved function and recovery of cone visibility in macular telangiectasia type 2 retinal lesions. *Invest Ophthalmol Vis Sci*. 2015;56(2):778-86.



46. Jacob J, Paques M, Krivosic V, et al. Meaning of visualizing retinal cone mosaic on adaptive optics images. *Am J Ophthalmol.* 2015;159(1):118-123 e1.
47. Sincich LC, Zhang Y, Tiruveedhula P, Horton JC, Roorda A. Resolving single cone inputs to visual receptive fields. *Nat Neurosci.* 2009;12(8):967-9.
48. Field GD, Gauthier JL, Sher A, et al. Functional connectivity in the retina at the resolution of photoreceptors. *Nature.* 2010;467(7316):673-7.
49. Li PH, Field GD, Greschner M, et al. Retinal representation of the elementary visual signal. *Neuron.* 2014;81(1):130-9.

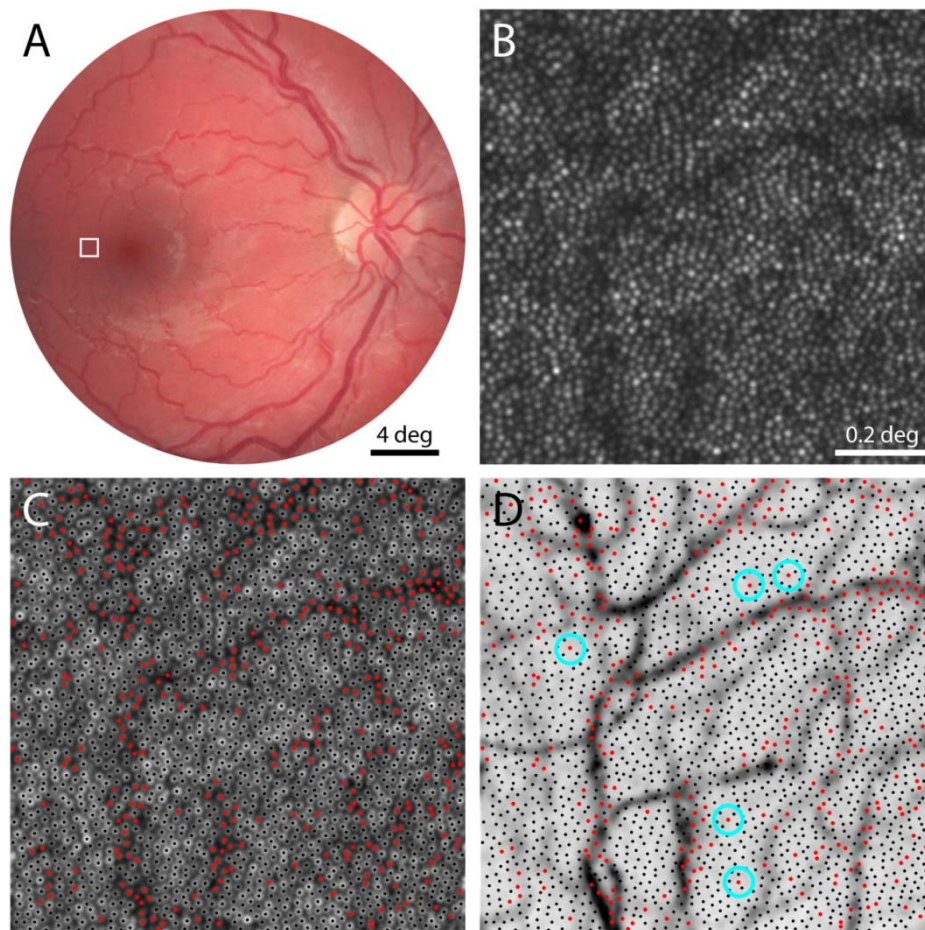


**Figure 1: Relationship between poorly reflective cones and retinal vasculature**

(A) Fundus photograph of the right eye of one subject. Outlined area shown magnified with AOSLO imaging in (B), where cone photoreceptors appear as bright spots (eccentricity =  $2.7^\circ$ ). (C) Same field of view as in (B), with gray levels represented logarithmically to facilitate identification of poorly reflective cones. Cones brighter than the mean image reflectivity are marked with black dots, and those with reflectivity below the mean are indicated with red spots. (D) Vasculature map of same retinal area with cone centers from (C) superimposed, showing that most dark cones are associated with blood vessels. Blue circles mark dark cones that are not situated near blood vessels.

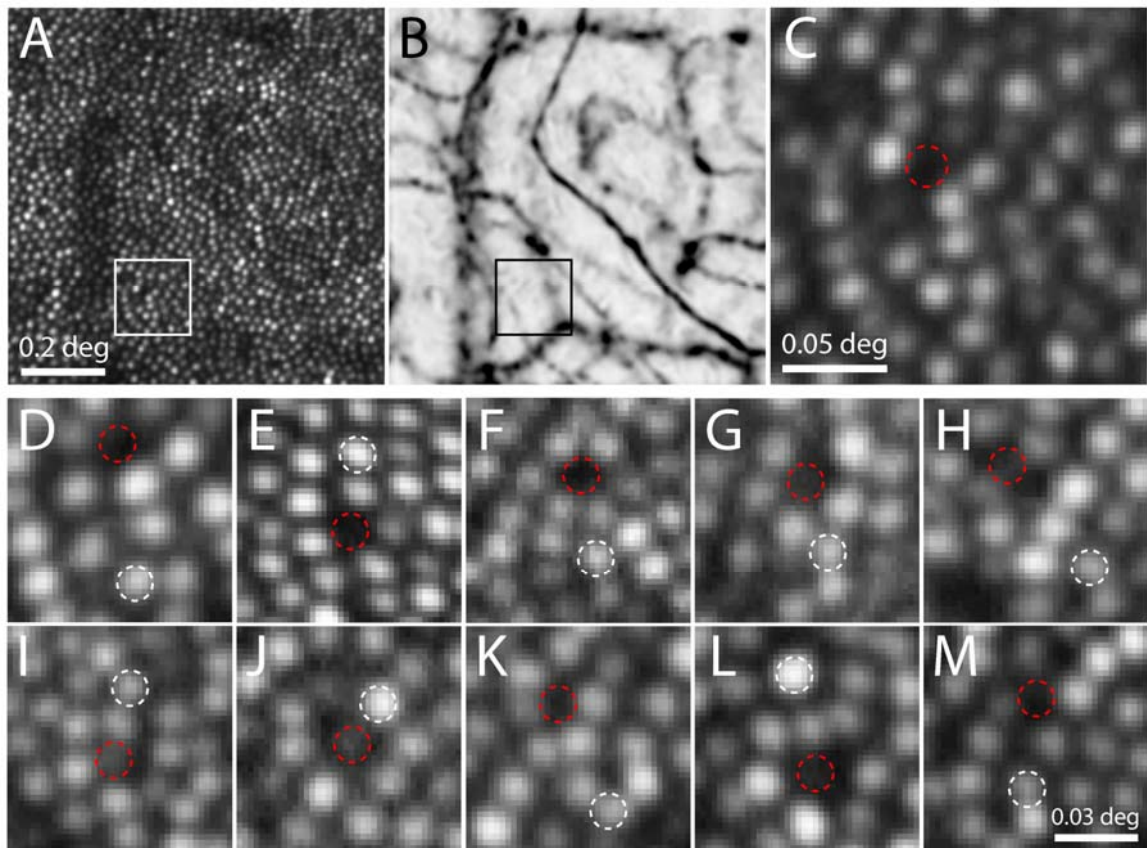


**Figure 2: Identifying dark cones for longitudinal imaging and functional testing.** AOSLO image (A) and vasculature map (B) from a second subject. Outlined area is magnified in (C), showing a dark gap in the cone mosaic where a cone could ordinarily fit (dashed circle), yet not situated under any blood vessels (eccentricity =  $3.3^\circ$ ). (D-M) Images of 10 cone pairs on the day they were selected for threshold testing in 5 subjects (white = normal cone, red = dark cone). Persistently dark cones are shown in panels D-F, and intermittently dark cones in panels G-M. All of these sites were confirmed to not reside under blood vessels.

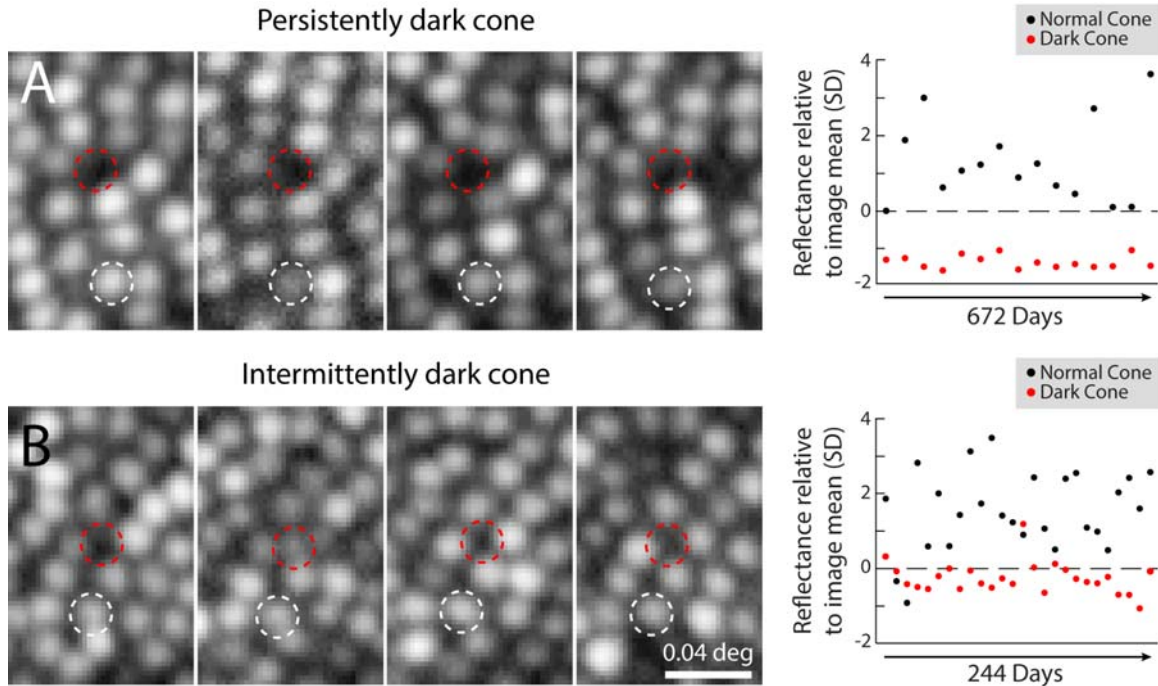


**Figure 3: Poor cone reflectivity can be persistent or intermittent.** (A) Longitudinal series of AOSLO images from a persistently dark cone in one subject, from the site illustrated in Figure 2A-C, shown on 4 separate imaging days (left). Dashed circles outline the same set of cones throughout (white = normal cone, red = dark cone), and indicate the locations where microstimulation was targeted for psychophysical testing. The normal cone varied in reflectivity, while the dark cone remained poorly reflective on all imaging days (right). (B) An intermittently dark cone, from the retinal area in Figure 1, is shown during 4 imaging days (left). In this case, the dark cone was intermittently visible (second panel from left), but did not vary as much as the normally reflective cone (right). All images in this figure are on a log intensity scale, to facilitate identification of relatively dark cones (note: this makes cone profiles appear larger; compare Figure 2). Reflectance measurements were not taken at equal time intervals.

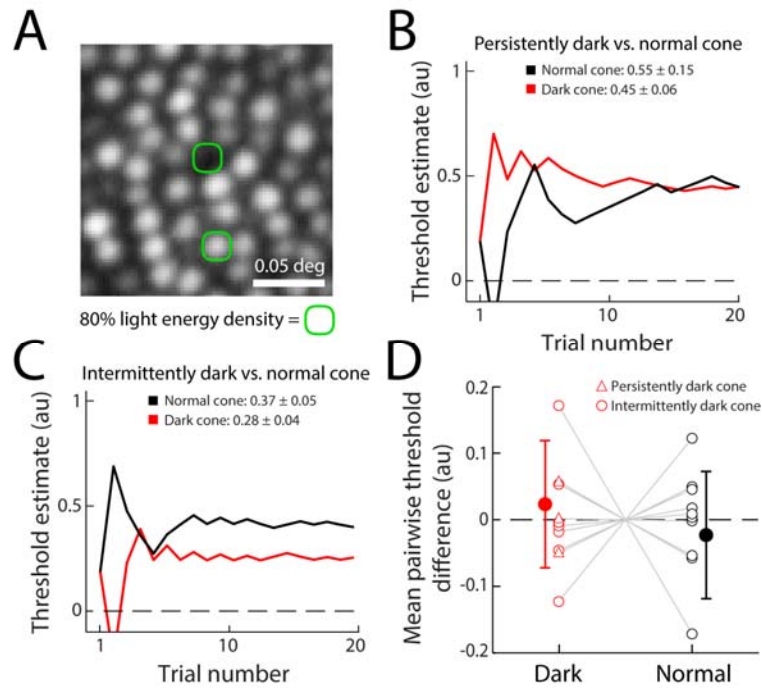


**Figure 4: Microstimulation increment thresholds show no difference in light sensitivity between dark and normally reflective cones.** (A) Schematic of the approximate size of the microstimuli. Green contour contains 80% of the integrated light energy delivered on the retina for a single stimulus flash. (B) Example staircase threshold estimates and mean values from repeated experiments for the persistently dark/normal cone pair shown in panel A and Figure 3A. Mean thresholds from 3 measurements ( $\pm 1$  SD) are indicated. (C) Example staircases for the intermittently dark/normal cone pair of Figure 3B, with mean thresholds from 5 experiments. Estimates in panels B-C are given in arbitrary units (au), spanning the range of deliverable light intensity. The threshold estimates are computed from the trial history. (D) Population mean threshold difference measured between 10 pairs of dark and normally reflective cones (filled data points). To compare thresholds across sites, each single-cone threshold was normalized to the mean of the cone pair thresholds for each run. Open data points represent the mean normalized thresholds computed from individual experiments. Dark and normal cone thresholds across the population did not differ significantly ( $p = 0.49$ ; error bars  $\pm 1$  SD).



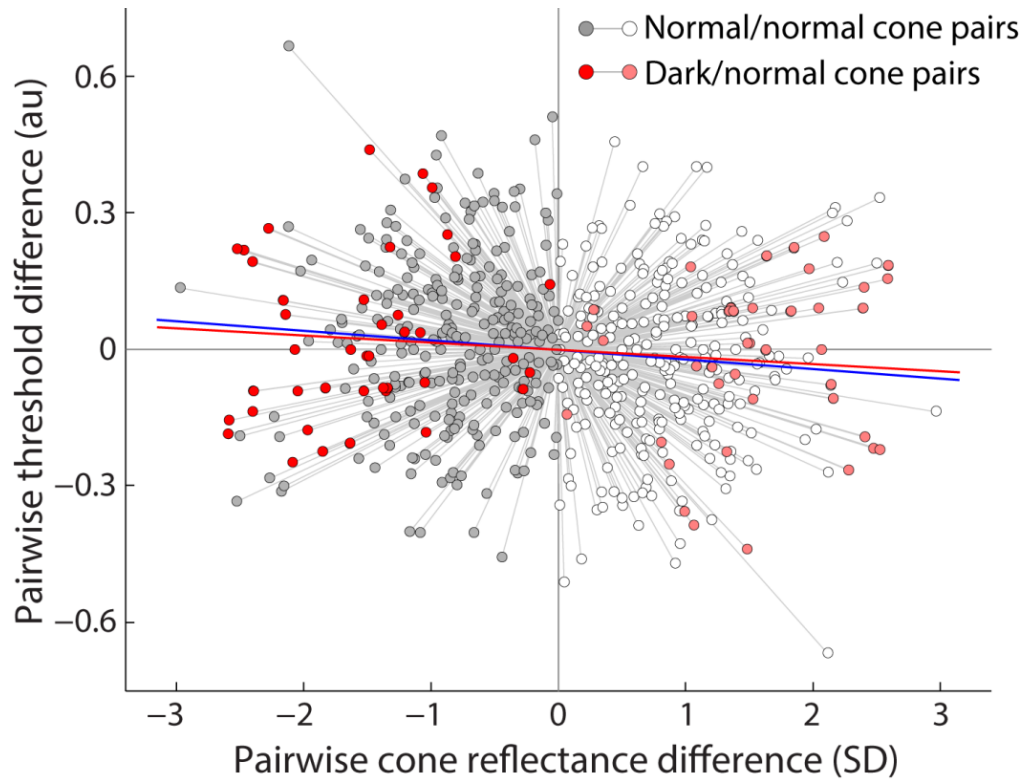
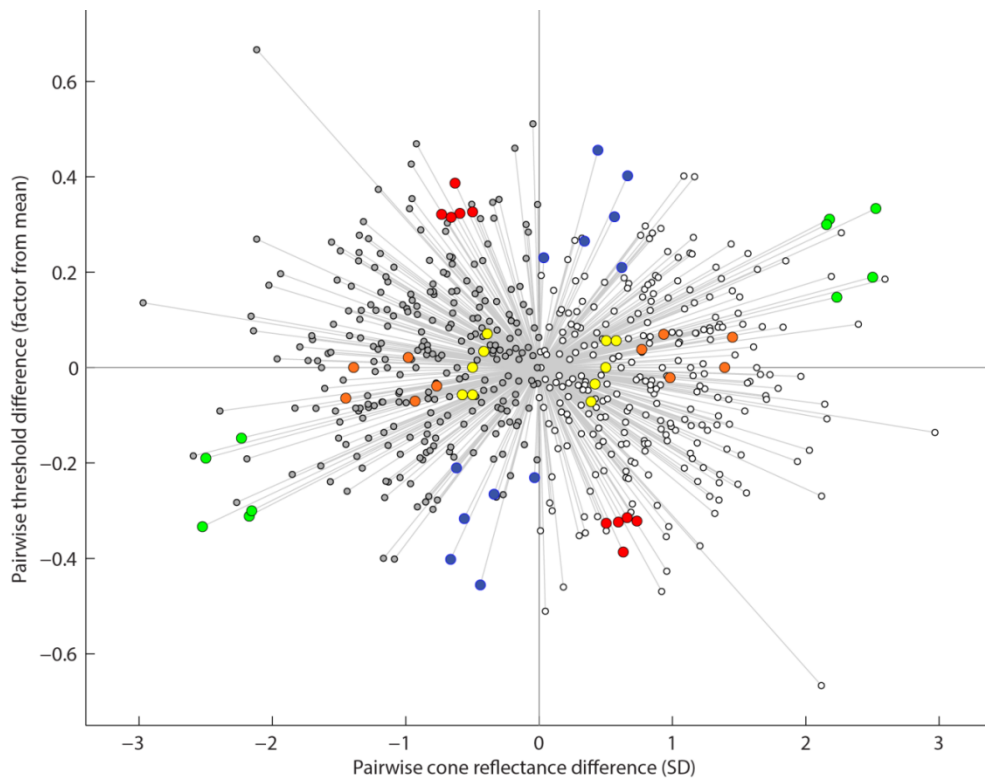


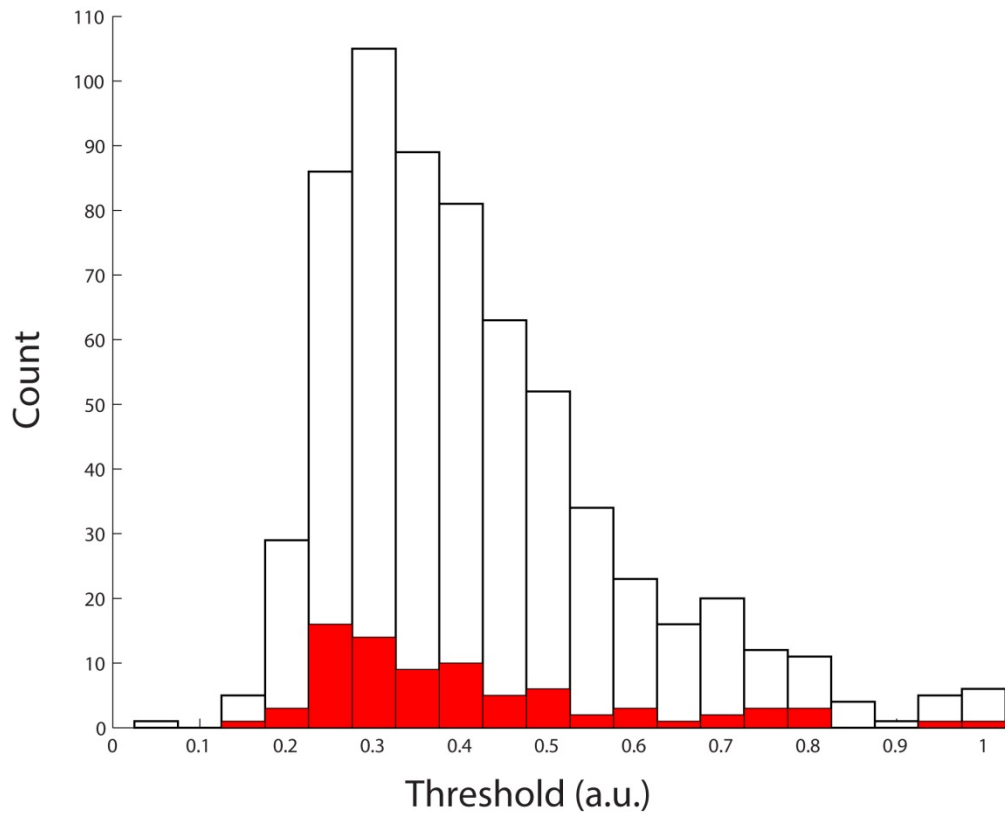
**Figure 5: Comparison of single-cone reflectance and threshold.** For both normal/normal (gray scale) and dark/normal (red scale) cone pairs, reflectance values for each cone were normalized to the mean reflectance of each pair during one experiment (indicated by connecting gray lines), expressed in SDs of the field gray level from the pairwise mean. Darker shading (towards the left) represents the less reflective cone in each pair. Cone thresholds were normalized to the mean of each cone pair, and plotted in arbitrary units from the pairwise mean. Linear regression reveals a 3.6% difference in mean threshold between normal cones with less versus more reflectivity (blue line,  $p = 0.0502$ , 284 paired threshold measurements). This trend was matched by dark/normal cone pairs, but also did not reach significance (red line,  $p = 0.49$ , 41 paired threshold measurements).

## APPENDIX

Three additional figures were generated in the process of responding to reviewer comments, and were not included in the published version of this work. Figure A3 was additionally used as part of a presentation at the annual meeting for the Association for Research in Vision and Ophthalmology.

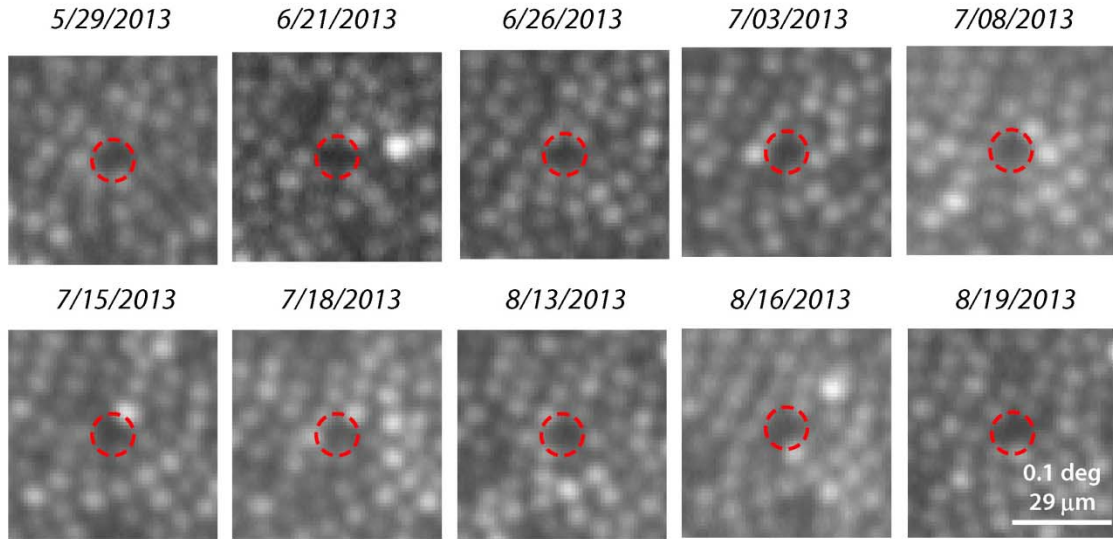


**Appendix Figure A1: Highlighting variability among normally reflective cone pairs.** Data from the normally reflective cone pairs shown in Figure 5 are duplicated here. Five individual cone pairs (each tested 5 times) are coded by color.



**Appendix Figure A2: Distribution of raw threshold measurements.** Frequency distribution of raw threshold measurements for normally reflective cone pairs (white) and dark/normal cone pairs (red). The two targeted populations exhibited little appreciable difference in the distributions of threshold.





**Appendix Figure A3: Persistently dark cone remains dark over time.** Persistently dark cone from Figure 2F (red) is shown over multiple imaging sessions spanning 82 days. The cone remains dark throughout.

APPENDIX A

UNIVERSITY OF ALABAMA AT BIRMINGHAM INTERNAL REVIEW BOARD  
APPROVALS AND PERMISSIONS



# Human Subjects Protocol (HSP)



Form Version: October 5, 2012

- **You are applying** for IRB review of the research described in this form.
- **To avoid delay**, respond to all items in order and include all required approvals and documents.
- **To complete the form**, click the underlined areas and type or paste in your text; double-click checkboxes to check/uncheck. For more tips, see [www.uab.edu/irb/forms](http://www.uab.edu/irb/forms).
- **Mail or deliver all materials to AB 470**, 701 20th Street South, Birmingham, AL 35294-0104.

## Indicate the type of review you are applying for:

- Convened (Full) IRB *or*
- Expedited—See the [Expedited Category Review Sheet](#), and indicate the category(ies) here: 1 2 3 4 5 6 7

**1. IRB Protocol Title:** Perception of visual microstimuli

## 2. Investigator, Contacts, Supervisors

**a. Name of Principal Investigator:** Lawrence Sincich

Degree(s)/Title: Ph.D. BlazerID: sincich

Dept/Div: Vision Sciences Mailing Address: WORB 638 UAB ZIP: 4390

Phone: 205-975-3446 Fax: 205-934-5725 E-mail: Sincich@uab.edu

**b. Name of Contact Person:** None Title: \_\_\_\_\_ Phone: \_\_\_\_\_

E-mail: \_\_\_\_\_ Fax: \_\_\_\_\_

Mailing Address (if different from that of PI, above): \_\_\_\_\_

## INVESTIGATOR ASSURANCE STATEMENT & SIGNATURE

By my signature as Principal Investigator, I acknowledge my responsibilities for this Human Subjects Protocol, including:

- Certifying that I and any Co-Investigators or Other Investigators comply with reporting requirements of the UAB Conflict of Interest Review Board;
- Certifying that the information, data, and/or specimens collected for the research will be used, disclosed and maintained in accordance with this protocol and UAB policies;
- Following this protocol without modification unless (a) the IRB has approved changes prior to implementation or (b) it is necessary to eliminate an apparent, immediate hazard to a participant(s);
- Verifying that all key personnel listed in the protocol and persons obtaining informed consent have completed initial IRB training and will complete continuing IRB training each year;
- Verifying that all personnel are licensed/credentialed for the procedures they will be performing, if applicable;
- Certifying that I and all key personnel have read the *UAB Policy/Procedure to Ensure Prompt Reporting of Unanticipated Problems Involving Risks to Subjects or Others to the IRB, Institutional Officials, and Regulatory Agencies* and understand the procedures for reporting;
- Applying for continuing review of the protocol at least annually unless directed by the IRB to apply more frequently;
- Conducting the protocol as represented here and in compliance with IRB determinations and all applicable local, state, and federal law and regulations; providing the IRB with all information necessary to review the protocol; refraining from protocol activities until receipt of initial and continuing formal IRB approval.

**Signature of Investigator:**\_\_\_\_\_

**Date:**\_\_\_\_\_

- c. List all staff who will be involved with the design, conduct, and reporting of the research, their degree(s) and job title, and any additional qualifications. Include individuals who will be involved in the consent process. *Repeat the table below for each individual.*

*Note. For studies involving investigational drugs, include all investigators who will be listed on FDA Form 1572 and attach a copy, if applicable. Send the IRB a copy of Form 1572 anytime you update the form with the FDA.*

Role: Co- -OR- Other –AND/OR-   
Consent Process

Full Name: **Lawrence Sincich**

Primary UAB Dept.: **Vision Sciences**  
(Employer if not UAB)

Degree(s) / Job Title: **Ph.D. / Assistant Professor**

Additional Qualifications pertinent to the study: **17 years of research on visual system**

Role:	<input type="checkbox"/> Co- -OR- <input checked="" type="checkbox"/> Other –AND/OR- <input type="checkbox"/> Consent Process
Full Name:	<b><u>Kady S. Bruce</u></b>
Primary UAB Dept.: (Employer if not UAB)	<b><u>Vision Sciences</u></b>
Degree(s) / Job Title:	<b><u>B.A. / 2<sup>nd</sup> year graduate student</u></b>
Additional Qualifications pertinent to the	<b><u>Trained to run the instrument used in the study.</u></b>

study:	
--------	--

Role:	<input type="checkbox"/> Co- -OR- <input checked="" type="checkbox"/> Other -AND/OR- <input type="checkbox"/> Consent Process
Full Name:	<b><u>John Laurent</u></b>
Primary UAB Dept.: (Employer if not UAB)	<b><u>Optometry</u></b>
Degree(s) / Job Title:	<b><u>O.D., Ph.D.</u></b>
Additional Qualifications pertinent to the study:	<b><u>Clinical optometrist who will provide initial eye exams for potential participants.</u></b>

d. Is the principal investigator a student, fellow, or resident?  Yes  No

**If Yes**, complete items below and obtain signature of faculty advisor or supervisor:

Supervisor's Name: \_\_\_\_\_

Degree(s) / Job Title: \_\_\_\_\_

Additional \_\_\_\_\_  
Qualifications  
pertinent to the  
study:

Telephone: \_\_\_\_\_

E-Mail: \_\_\_\_\_

**Signature:**

---

- e. Describe the principal investigator's activities related to this protocol and provisions made by the PI to devote sufficient time to conduct the protocol:

**PI will conduct the experiments, and supervise the student involvement. As the PI is presently the only person in the laboratory who is capable of running the instrument used in the experiments, he will necessarily devote adequate time to the study to ensure success.**

- f. Is medical supervision required for this research? Yes No

**If Yes**, who will provide the supervision?

PI will provide -OR- Name: **John Laurent OD PhD** Telephone: **205-975-7783**

If other than PI, obtain signature of person providing medical supervision:

Signature \_\_\_\_\_

- g. Describe the process that ensures that all persons assisting with the research are adequately informed about the protocol and their research-related duties and functions: **Ms. Bruce will be trained to perform the experiments after reading and understanding the protocol. The PI will participate in running the experiments initially, to ensure proper performance.**

### 3. Funding

Is this study funded? Yes No

**If No**, specify that costs of the study will be covered by funds from the UAB department or other source named: \_\_\_\_\_

**If Yes**, attach one copy of completed application or request for funding sent to sponsor, and complete a-d.

a. Title of Grant or Contract: \_\_\_\_\_

b. PI of Grant or Contract: \_\_\_\_\_

c. Office of Sponsored Programs Proposal Number: \_\_\_\_\_  
(or enter "Pending" and provide upon receipt from OSP)

d. Sponsor, Funding Route (check and describe all that apply):

- Gov't Agency or Agencies—Agency name(s): \_\_\_\_\_
- Department of Defense (DoD): Identify DoD component: \_\_\_\_\_
- Department of Energy (DOE)
- Department of Justice (DOJ)
- Department of Education
- NIH Coop. Group Trial—Group name: \_\_\_\_\_
- Private Nonprofit (e.g., Foundation)—Name: \_\_\_\_\_
- Industry, investigator-initiated—Name: \_\_\_\_\_ Describe the funding arrangement: \_\_\_\_\_
- Note. [Western IRB](#) reviews industry-sponsored protocols unless the investigator initiated the research, or the study qualifies for expedited review or involves gene therapy.*
- UAB Departmental/Division Funds—Specify: **IMPACT fund**

**4. Conflict of Interest—Human subjects research involving a disclosed financial interest is subject to IRB review following review by the [Conflict of Interest Review Board](#).**

The following definitions are used for Item #4:

***Immediate family*** means spouse or a dependent of the employee. *Dependent* is any person, regardless of his or her legal residence or domicile, who receives 50% or more of his or her support from the public official or public employee or his or her spouse or who resided with the public official or public employee for more than 180 days during the reporting period.

***Financial Interest Related to the Research*** means financial interest in the sponsor, product or service being tested, or competitor of the sponsor.

For each investigator and staff member involved in the design, conduct and reporting of the research (see Items 2.a. and 2.c.) answer the questions below: **(Repeat the section below for each individual)**

**Name:** Lawrence Sincich

Do you or your immediate family have any of the following? (check all that apply)



- An ownership interest, stock options, or other equity interest related to the investigator's responsibilities of any value.
- Compensation related to the research unless it meets two tests:
  - Less than \$5,000 in the past year when aggregated for the immediate family.
  - Amount will not be affected by the outcome of the research.
- Proprietary interest related to the research including, but not limited to, a patent, trademark, copyright, or licensing agreement.
- Board of executive relationship related to the research, regardless of compensation.

**Name: Kady S. Bruce**

Do you or your immediate family have any of the following? (check all that apply)

- An ownership interest, stock options, or other equity interest related to the investigator's responsibilities of any value.
- Compensation related to the research unless it meets two tests:
  - Less than \$5,000 in the past year when aggregated for the immediate family.
  - Amount will not be affected by the outcome of the research.
- Proprietary interest related to the research including, but not limited to, a patent, trademark, copyright, or licensing agreement.
- Board of executive relationship related to the research, regardless of compensation.

**Name: John Laurent**

Do you or your immediate family have any of the following? (check all that apply)

- An ownership interest, stock options, or other equity interest related to the investigator's responsibilities of any value.
- Compensation related to the research unless it meets two tests:
  - Less than \$5,000 in the past year when aggregated for the immediate family.
  - Amount will not be affected by the outcome of the research.
- Proprietary interest related to the research including, but not limited to, a patent, trademark, copyright, or licensing agreement.
- Board of executive relationship related to the research, regardless of

compensation.

**If you checked any of the above**, a financial interest disclosure has to be submitted to or currently be on file with the CIRB. A completed CIRB Evaluation has to be available before the IRB will conduct its review.

## 5. Locations Involved

a. Describe the facilities available for the conduct of the research. For research on UAB campus, include building names and room numbers: **Research Support Building room 350B**

b. Indicate all "performance sites" that will provide space, services, facilities, potential or actual participants, or other support for this protocol.

The Kirklin Clinic (TKC)

University of Alabama Hospital (UAHosp)

The Children's Hospital of Alabama (TCHA)

Callahan Eye Foundation Hospital (CEFH)

UAB Highlands

Jefferson County Dept. of Health (JCDH)

Birmingham Veterans Affairs Medical Center (BVAMC)

General Clinical Research Center (GCRC)—inpatient

General Clinical Research Center (GCRC)—outpatient

General Clinical Research Center (GCRC) at The Kirklin Clinic (TKC)

Other (i.e., Any performance site not listed above, including those covered by subcontracts related to this protocol)—Describe:

**Research Support Building 350B**

c. Is this study a clinical trial requiring clinical services at one of the performance sites listed in Item b above?  Yes  No

**If Yes**, Fiscal Approval Process (FAP)-designated units complete a FAP submission and send to [fap@uab.edu](mailto:fap@uab.edu). For more on the UAB FAP, see [www.uab.edu/osp/clinical-billing-review](http://www.uab.edu/osp/clinical-billing-review).

- d. Is this a field study? Yes No

**If Yes**, describe the community and include information about how the community will be involved in the design, implementation and analysis of the research. This would include focus groups, training local facilitators/community health advisors: \_\_\_\_\_

- e. Is the study to be undertaken within a school, business, or other institution that does not have an institutional review board?

Yes No

**If Yes**, attach a statement of any contacts with and approvals from the appropriate institution officials.

*Note. Documentation of all such approvals must be received by the UAB OIRB before IRB approval will be issued.*

- f. Has this protocol or project been reviewed by another IRB, similar review board, or departmental review committee(s) that authorizes the use of its patient populations? Yes No

**If Yes**, provide name of the review board(s): \_\_\_\_\_ and for each board listed, enter either the date of latest approval(s) or "PENDING": \_\_\_\_\_ or reasons not approved: \_\_\_\_\_. *If this protocol is subsequently rejected or disapproved by another review board, the UAB IRB must be notified promptly. Attach copies approvals/disapprovals.*

- g. Will any of the participants be from the Birmingham Veterans Affairs Medical Center? Yes No

**If Yes**, attach VA IRB approval or notification from the VA Research and Development Department that the study has been submitted to the VA IRB for review.

- h. Will the study be conducted at or recruit participants from the Jefferson County Department of Public Health (JCDH)? Yes No

**If Yes**, attach notification that the protocol has been approved by JCDH or the Alabama Department of Public Health IRB.

## 6. Multi-Site Studies

- a. Is the investigator the lead investigator of a multi-site study?

Yes No

b. Is UAB a coordinating site in a multi-site study? Yes No

c. If you answered **Yes** to *a* or *b*, describe the management of information obtained in multi-site research that might be relevant to the protection of participants. Include, at a minimum, the following items:

- o IRB approvals from other sites
- o Unanticipated problems involving risks to participants or others. (For example, if there is an unanticipated problem involving risks to participants or others, which site is responsible for reporting it?)
- o Interim results.
- o Protocol modifications. \_\_\_\_\_

**7. Drugs:** Will any drugs or supplements be used/studied in this protocol? Yes No

**If Yes**, attach the [Drug Review Sheet](#).

**8. Devices:** Will any devices be studied in this protocol or used for a purpose other than for which they were approved by the FDA?

Yes No

**If Yes**, attach the [Device Review Sheet](#).

### 9. Special Approvals

a. Does this project involve the use of radioisotopes? Yes No

**If Yes**, attach documentation of approval from the Radiation Safety Division.

b. Does this project include patients with contagious infections (e.g., mumps, measles, chickenpox, TB, meningitis)? Yes No

**If Yes**, attach documentation of approval from Chairman of the Infection Control Committee of the appropriate facilities.

c. Does this project involve obtaining remnant biopsy or surgical material from the Department of Pathology or any other source? Yes No

**If Yes**, attach documentation of approval from the entity or individual providing the materials (e.g., the [UAB Division of Anatomic Pathology Release of Pathologic Materials](#)).

- d. Does this project require obtaining any remnant clinical laboratory specimens, body fluids, or microbiological isolates from the Department of Pathology or any other source? Yes No

**If Yes**, attach documentation of approval from the entity or individual providing the materials (e.g., the [UAB Division of Laboratory Medicine Release of Pathologic Materials](#)).

- e. Does this project use stored (existing) specimens from a repository?  
Yes No

**If Yes**, attach documentation of approval for use of specimens, and describe how existing specimens are labeled: \_\_\_\_\_

## 10. Use of Specimens

Does this project involve collecting specimens from participants and storing them for future research? Yes No

**If Yes**, complete a-h. If no, skip to Item 11

- a. How will specimens be obtained, processed, distributed, and stored? \_\_\_\_\_
- b. How will specimens be labeled (e.g., unique identifier, medical record number, Social Security number, name, date of birth)? \_\_\_\_\_
- c. How will clinical data associated with the specimens be collected and stored? \_\_\_\_\_
- d. What participant-identifying information will be collected and linked to the specimens? \_\_\_\_\_
- e. What steps will be taken to maximize the confidentiality of linked identifiers? For example, procedures could include using a password-protected computer database to link identifiers, with limited personnel knowledgeable of the password, or coded identifiers released without the ability to link to clinical data (also called "stripped" or "anonymized" specimens). \_\_\_\_\_
- f. Will specimens be shared with other investigators in the future?  
Yes No

**If Yes**, what identifiers, clinical information and demographic information will be shared; or will the specimens be stripped of

identifiers (i.e., anonymized)? Also **if yes**, outline your procedure for assuring IRB approval for release and use prior to release of specimens. \_\_\_\_\_

*Note. Investigators who receive and/or use these specimens must document approval from the appropriate IRB(s) before the specimens may be released.*

g. Will biological samples be stored for future use? Yes No

**If Yes**, indicate whether they will be used for the disease under study in this protocol or research on other diseases. \_\_\_\_\_

h. Is genetic testing planned? Yes No

**If Yes**, describe the planned testing here and see "DNA/Genetic testing" in the Guidebook for consent requirements. \_\_\_\_\_

## 11. Gene Therapy

Does this project involve gene therapy or administering recombinant materials to humans? Yes No

**If Yes**, submit the [Gene Therapy Project Review Panel Report](#) –OR- If this is a vaccine trial that is exempt from the NIH Guidelines For Research Involving Recombinant DNA Molecules, submit the [Protocol Oversight Review Form For Clinical Vaccine Trials](#).

## 12. HIPAA Privacy and Security

Will the PI or others obtain, review, or make other use of participants' "personal health information" (i.e., information, whether oral or recorded in any form or medium that (a) is created or received by a health care provider and (b) relates to past, present, or future physical or mental health or condition of an individual; or provision of health care; or payment for provision of health care)? Yes No

**If Yes**, complete a-e as described.

a. Will the data/information be stored or managed electronically (on a computer)?

Yes No

- b. Is the principal investigator requesting that the UAB IRB waive patient HIPAA authorization from another institution or entity (e.g., insurance company, collaborating institution). Yes No

**If Yes**, attach copy of privacy notices from institution/entity, and provide the name of institution/entity: \_\_\_\_\_

- c. Indicate which, if any, of the listed entities below would provide information or maintain health information collected for this protocol and/or where health information that been collected will be stored/maintained.

- The Kirklin Clinic
- University of Alabama Hospital
- The Children's Hospital of Alabama
- Callahan Eye Foundation Hospital
- UAB Highlands
- Jefferson County Department of Health
- School of Dentistry
- School of Health Professions
- School of Medicine
- School of Nursing
- School of Optometry
- University of Alabama Health Services Foundation
- UAB Health Centers
- Viva Health
- Ophthalmology Services Foundation
- Valley Foundation
- Medical West - UAB Health System Affiliate

*Health System Information Systems:*

- HealthQuest

- Cerner Millennium (Lab, Radiology, UED, Surgery)
- EMMI - Master Member Index
- Horizon - IPV (IVR/CDA/CRIS)
- CareFlow Net
- Eclipsys (PIN)
- IMPACT
- None—**If None, skip to Item 13.**

d. Indicate which of the listed identifiers would be associated/linked with the protected health information (PHI) used for this protocol.

- Names
- Geographic subdivisions smaller than a State
- Elements of dates (except year) related to an individual
- Telephone numbers
- Fax numbers
- Email addresses
- Social security numbers
- Medical record numbers
- Health plan beneficiary numbers
- Account numbers
- Certificate/license numbers
- Vehicle identifiers and serial numbers
- Device identifiers and serial numbers
- Biometric identifiers
- Web universal resource locators (URLs)
- Internet protocol address numbers
- Full-face photographic images



Any other unique identifying number—Describe: \_\_\_\_\_

*Note. Codes are not identifying as long as the researcher cannot link the data to an individual*

None—**If None, skip to Item 13.**

e. Choose one plan to describe your use of the personal health information:

The data collected meet the specifications for a “limited data set”

—Attach [Data Use Agreement](#) or Business Associate Agreement

Research staff will obtain authorization from each patient to use the information

—Attach [Patient Authorization](#) form, complete except for patient name and IRB protocol number

PI requests Waiver of Patient Authorization to use the information

—Attach [Waiver of Authorization and Informed Consent](#) form

#### PROPOSED RESEARCH

- The IRB will not accept grant applications and/or sponsor's protocols in lieu of the items as outlined below.
- Do not separate responses from items. Instead, insert your response to each item below the item, keeping the information in the order of this form.
- Number each page of the Human Subjects Protocol (i.e., Page X of Y).

### 13. Purpose—in nontechnical, lay language

Summarize the purpose and objectives of this protocol, including any related projects, in one short paragraph.

**The purpose of our study is to characterize the detectability of small visual stimuli delivered to the eye under conditions where ocular aberrations have been corrected.**

### 14. Background—in nontechnical, lay language

Summarize in 2-3 paragraphs past experimental and/or clinical findings leading to the formulation of this study. Include any relevant past or

current research by the Principal Investigator. For drug and device studies summarize the previous results (i.e., Phase I/II or III studies).

**During the last decade, it has become possible to image individual photoreceptors in the human retina. This capability has allowed researchers to study the normal and diseased retina at the cellular level for the first time. My collaborators and I were the first to show, in an animal model, that visual stimulation of single photoreceptors leads to detectable physiological responses in the brain. We would now like to examine if humans can perceive similar stimuli. This work will allow us to study the range of normal perception for these microstimuli. For example, we will learn how many photoreceptors must be stimulated in order for a spot of light to be seen, and what the minimum light levels must be for a single photoreceptor to be perceptually activated. Once this normal perceptual range is understood, disease conditions can then be studied usefully with our techniques. Our work will also allow us to characterize the spectral class of each photoreceptor (that is, whether sensitive to red, green, or blue light), which will be useful for understanding how perception is altered in subjects with color vision deficits.**

#### 15. Participants (Screening and Selection)

- a. How many participants are to be enrolled at UAB? **5-30**

If multi-center study, total number at all centers: \_\_\_\_\_

- b. Describe the characteristics of anticipated or planned participants.

Sex: **Either**

Race/Ethnicity: **Any**

Age: **19-65**

Health status: **Healthy and with visual acuity correctable to normal.**

*Note. If data from prior studies indicate differences between the genders or among racial/ethnic groups in the proposed research or if there are no data to support or to negate such differences, Phase 3 clinical trials will be required to include sufficient and appropriate entry of gender and racial/ethnic subgroups so that trends detected in the affected subgroups can be analyzed. If ethnic, racial, and gender estimates are not included in the protocol, a clear rationale must be provided for exclusion of this information. If prior evidence indicates that the results will not show gender or racial differences, researchers are not required to use gender or race/ethnicity as selection criteria for*

*study participants. They are, however, encouraged to include these groups. See Section II. Policy of the NIH POLICY AND GUIDELINES ON THE INCLUSION OF WOMEN AND MINORITIES AS SUBJECTS IN CLINICAL RESEARCH – Amended, October, 2001) for further details.*

- c. From what population(s) will the participants be derived?

**Residents from the Birmingham area.**

Describe your ability to obtain access to the proposed population that will allow recruitment of the necessary number of participants:

**Some subjects will be students in the Vision Sciences department; others will be recruited by word of mouth.**

Describe the inclusion/exclusion criteria:

**The conditions for inclusion will be: (1) visual acuity correctable to 20/60 or better, (2) clear cornea and lens media, (3) less than 8 diopters of myopia, (4) absence of obvious visual system pathology that can be seen during a standard fundus exam, and (5) ability to understand and sign the informed consent form and be willing to comply with study-related instructions.**

**The conditions for exclusion will be: (1) pseudophakia (artificial lens implant), aphakia (absence of the lens), cataract of any grade, corneal opacification, or lack of optical clarity, (2) nystagmus (involuntary, rapid, oscillating movement of the eyes), (3) greater than 8 diopters myopia, (4) sensitivity to tropicamide, cyclopentolate, or phenylephrine, and (5) subjects with prior history of any refractive surgery.**

- d. If participants will comprise more than one group or stratification, describe each group (e.g., treatment/intervention, placebo, controls, sham treatment) **and** provide the number of participants anticipated in each group.

**Subjects will not be grouped or stratified. As the study uses a survey approach, there are no control groups.**

- e. Indicate which, if any, of the special populations listed below will be involved in the protocol. Include the Special Populations Review Form (SPRF) if indicated.

Pregnant Women: Attach [SPRF—Pregnant Women, Fetuses, Neonates/Nonviable Neonates](#)

Fetuses: Attach [SPRF—Pregnant Women, Fetuses, Neonates/Nonviable Neonates](#)

- Neonates/Nonviable Neonates: [SPRF—Pregnant Women, Fetuses, Neonates/Nonviable Neonates](#)
- Prisoners: Attach [SPRF—Prisoners](#)
- Minors (<19 years old): Attach [SPRF—Minors](#)
- Employees or students at institution where research conducted
- Persons who are temporarily decisionally impaired
- Persons who are permanently decisionally impaired (e.g., mentally retarded)
- Non-English Speakers

**For each box checked**, describe why the group is included **and** the additional protections provided to protect the rights and welfare of these participants who are vulnerable to coercion: **Students will be included because they will be most aware of and interested in the outcome of the study. All participants will sign a consent form indicating their understanding that they are free to withdraw from the study at any time without any negative consequences. The consent form details how refusing to or withdrawing from participation will not affect their relationship with UAB in any way.**

**Some subjects may be graduate students or post-doctoral fellows recruited by the graduate student (Ms. Bruce) helping to conduct the study; in these cases, potential coercion should be minimal. However, subjects will often be members of the PI's laboratory, and they will participate because they are interested in answering the scientific questions. As often happens in psychophysical research, the subjects and the experimenters are the same group of people. Nonetheless, every effort will be made (beyond those mentioned above), to ensure that their participation stems only from their interest in the science rather than in retaining their employment. Because the experiments are relatively demanding, only suitably motivated trainees will be recruited to work in the PI's laboratory.**

- f. List any persons other than those directly involved in the study who will be at risk. If none, enter "None": **None**
- g. Describe the process (e.g., recruitment, chart review) that will be used to seek potential participants (e.g., individuals, records, specimens). Research recruitment by non-treating physicians/staff may require completion of Partial Waiver of Authorization for Recruitment/Screening. (See <http://main.uab.edu/show.asp?durki=61981>.)

**Recruitment will be by word of mouth. Students will learn of the research through Vision Science and Neurobiology Department brochures, the undergraduate Neuroscience program, the PI's laboratory website, or through other students already participating in the research.**

- h.** If you will use recruitment materials (e.g., advertisements, flyers, letters) to reach potential participants, attach a copy of each item. If not, identify the source (e.g., databases) from which you will recruit participants.

**Recruitment materials will not be used. Students interested in participating in the research will be interviewed by the PI, and they will be provided with copies of prior publications that demonstrate the type of research to be conducted.**

- i.** Describe the procedures for screening potential participants.

**The subject will be given a copy of the consent form to read but not sign. Within a few days, if the subject decides to participate in the study, the staff member conducting the study will verbally review the consent form to ensure that the subject understands the nature of the study and the purpose of consent. The subject will then be allowed to voluntarily sign the consent form. The subject will then be tested for normal color vision (Hardy-Rand-Rittler plates, Ishihara plates, and/or the Farnsworth D-15 or D-100 test). Subjects with abnormal color vision may be used as controls for those with normal color vision; however, we will not be explicitly recruiting such subjects.**

**Because pupil dilation agents must be used during the experiments, subjects will be screened beforehand for risk of acute angle-closure glaucoma that may occur in a small percentage of subjects as a result of these drugs. subjects who are susceptible to this problem can be identified by an ophthalmic exam prior to administration of the drug. Before beginning any retinal imaging, each subject will be given an ophthalmic exam to ensure they are not susceptible to acute glaucoma. To assess the risk of complications from the dilation agents, we will use the Van Herick test. The clinician compares the width of the cornea to the width of the shadow of the anterior chamber at the limbus. If the width of the shadow of the chamber angle is less than one quarter of the corneal thickness, then the subject is deemed to be at risk and will be excluded from participating further. If the results of the Van Herick test show that the subject may be at risk for glaucoma, it will be recommended to them that they seek an examination by an ophthalmologist for further assessment.**

## **16. Protocol Procedures, Methods, and Duration of the Study—in nontechnical language**

- a.** Describe the study methodology that will affect the participants—particularly in regard to any inconvenience, danger, or discomfort.

Following consent, subjects will first receive a one-time ophthalmic exam by a clinician (Dr. John Laurent) in the School of Optometry. Visual acuity and refractive error will be measured, and risk of acute angle-closure glaucoma will be assessed as described above in Question 15i. If the subject is not excluded from the study based on the examination outcome and the exclusion criteria listed in Section 15c, the subject will then be tested for normal color vision (Hardy-Rand-Rittler plates, Ishihara plates, and/or the Farnsworth D-15 or D-100 test). All of these procedures are standard in optometric practice, and will be conducted prior to any psychophysical testing, which may be done later on the same day, or on subsequent days.

On the day of psychophysical testing, the subject will have one eye's pupil dilated with cyclopentolate hydrochloride (1%), or a combination of phenylephrine (2.5%) and tropicamide (1%). This is required to optimize retinal imaging and to restrict accommodation (focusing ability) of the subject's eye. Once dilation has occurred (about 20 minutes), the subject will be positioned in front of an adaptive-optics scanning laser ophthalmoscope (AOSLO). Depending on the stability demands of the experiment, the subject's head will be held within a head/chin rest, or, if more stability is required, a bite-bar will be used to minimize head motion.

The AOSLO images the retina and is capable of delivering stimuli to retinal locations selected by the experimenter. AOSLO imaging is non-invasive, and uses light levels at least 10 times below the safety limit established by the American National Standard for the Safe use of Lasers (ANSI Z136.1-2007). The subject has no direct contact with the instrument.

A single psychophysical session is expected to last about 2 hours, although this varies because the experiment is self-paced. At the beginning of the session, a multi-wavelength image of the retina is taken with the AOSLO in order to measure transverse chromatic aberration (TCA) at the retinal location where stimuli will be delivered. TCA is the lateral offset on the retina that light of different wavelengths will be displaced due to the eye's optics (e.g. red light will be diffracted laterally more than green light). This step is required to correctly target selected photoreceptors with light of different wavelengths. Once TCA is measured, the subject dark-adapts for a minimum of 15 minutes, as the light used in this step is perceptually bright.

After dark-adaptation, the subject will be engaged in detecting the presence or absence of a briefly flashed small spot of light while a portion of the retina is being imaged with the AOSLO. Typically, this will require the subject to fixate on an externally presented fixation target (always on), while the subject signals for a test flash to be delivered. The subject then reports their percept (seen or not seen) by pressing a button on a keyboard. A computer program controls the sequence of intensities that are delivered through the AOSLO during the trials. The subject can voluntarily perform as many trials as they wish; typically this is about 400-500 trials

for a practiced, motivated subject. The subject will perform the task until a threshold criterion is reached (for one set of ~25 trials). This threshold measurement is then repeated 3 or 4 times for one condition, and usually two conditions will be compared. This leads to about 200-300 trials per session. The subject can sit out of the head rest or bite bar at any time and for any reason (e.g. to rest, or to voluntarily end the session). The experimenter monitors the subject's performance, and can terminate the session if performance degrades (e.g. subject appears to not be performing the task). At the end of each session, TCA is measured once more, to assess accuracy of stimulus delivery.

We note that the light levels are calibrated prior to any testing to be well below safety levels (as described in Question 18), and this light level is what is passing through the optical train to the eye. The custom software used to control this light is only capable of making delivered light less intense, as it controls an optical switch which can only dim the light. Thus, failure of any of the software that controls light delivery is incapable of exposing a participant to more than permissible light levels.

The number of sessions that a subject will participate in will be determined by the amount of data required to measure an effect, and to show consistency upon repetition. To achieve this, the minimum number of sessions is 4 (including at least 1 practice session). More typically, the number of sessions needed for a single study will be about 20. Ordinarily, sessions will be conducted only once per day, but the number of days between sessions may vary. Thus, the total time commitment for a single study is 1-3 months. Because subjects will most often be students (as well as the PI himself), this time commitment is simply part of their research work

- b. What is the probable length of time required for the entire study (i.e., recruitment through data analysis to study closure)?

2 years

- c. What is the total amount of time each participant will be involved?

2 hours for ophthalmic exam and color testing (done once, typically on a separate day), and 2 hours for each psychophysical session. Each psychophysical session generally yields one data point (e.g. intensity threshold at one locus). Thus, multiple sessions are required to complete any specific study, and it is not possible to predict how many sessions in total are needed as it depends on subject performance and the nature of the study (e.g. retinal topography survey, longitudinal effects, etc.).

d. If different phases are involved, what is the duration of each phase in which the participants will be involved? If no phases are involved, enter "not applicable."

**Not applicable.**

e. List the procedures, the length of time each will take, and the frequency of repetition, and indicate whether each is done solely for research or would already be performed for treatment or diagnostic purposes (routine care) for the population. *Insert additional table rows as needed.*

Procedure	Length of Time Required of Participants	Frequency of Repetition	Research (Res) – OR- Routine Care
<b><u>Informed consent</u></b>	<b><u>30 minutes</u></b>	<b><u>1</u></b>	<input checked="" type="checkbox"/> Res <input type="checkbox"/>
<b><u>Ophthalmic exam</u></b>	<b><u>1 hour</u></b>	<b><u>1</u></b>	Routine
<b><u>Color testing</u></b>	<b><u>1 hour</u></b>	<b><u>1</u></b>	X Res
<b><u>Retinal imaging and psychophysical testing</u></b>	<b><u>2 hours/session</u></b>	<b><u>As needed, usually on separate days from eye exam and color testing</u></b>	X Res X Res

f. Will an interview script or questionnaire be used? Yes No

**If Yes**, attach a copy.

g. Will participants incur any costs as a result of their participation?

Yes No

**If Yes**, describe the reason for and amount of each foreseeable cost.

\_\_\_\_\_



h. Will participants be compensated? Yes No

**If Yes**, complete i-v:

i. Type: (e.g., cash, check, gift card, merchandise): \_\_\_\_\_

ii. Amount or Value: \_\_\_\_\_

iii. Method (e.g., mail, at visit): \_\_\_\_\_

iv. Timing of Payments: (e.g., every visit, each month): \_\_\_\_\_

v. Maximum Amount of Payments per Participant: \_\_\_\_\_

### 17. Describe the potential benefits of the research.

These experiments will lay the foundation for single photoreceptor methodologies that will benefit ophthalmologists and physiologists studying normal and diseased photoreceptor function, as well as those interested in the neural basis of color processing in the cerebral cortex. It will be useful for probing, at a cellular level, the physiological and perceptual changes associated with cone dystrophies and colorblindness. It will also be useful for testing the effectiveness of gene therapies being developed for retinal ciliopathies.

### 18. Risks

a. List the known risks—physical, psychological, social, economic, and/or legal—that participants may encounter as a result of procedures required in this protocol. Do not list risks resulting from standard-of-care procedures. *Note. Risks included in this protocol document should be included in the written consent document.*

Pupil dilation is done with drugs routinely used in a clinical fundus exam; thus risks associated with cycloplegia are no more than those present during a visit to an optometrist's clinic. There is mild irritation when the eyedrops are first introduced. There may be some discomfort when bright light is shone in the eye during the moment when the TCA measurement is made, because the measurement is conducted in a darkened room and the sudden appearance of a small bright light can seem uncomfortable to some subjects. A small proportion of the population can develop an allergic conjunctivitis in response to topically applied eye drops. This is a benign condition that is self-limited upon discontinuing the drops, and will either spontaneously resolve in 1 to 3 days without treatment or can be treated with mild anti-inflammatory medications, if needed. An optometrist at the School of Optometry would supervise the care of an allergic condition, should it occur.

Pupil dilation may lead to some discomfort once the subject is exposed to normal daylight. The subject will be asked to bring their sunglasses to wear after testing; if they do not have sunglasses; a temporary/disposable pair will be provided.

There may be fatigue and/or anxiety for subjects because of the requirement of sitting still in front of the instrument for extended periods of time, or from participating in a task where performance can be interpreted as “good” or “bad” by the subject.

Risk of excessive light exposure is eliminated by ensuring that the light beam present at the cornea is always at least 10 times below the minimum acceptable exposure level established by the American National Standard for the Safe use of Lasers (ANSI Z136.1-2007).

The collected data are coded from the beginning to ensure anonymity. The code linking the data to the subject is kept in a bound notebook in a locked drawer in the PI’s office. There is a very small chance that if unauthorized personnel obtain access to this notebook, there may be a loss of confidentiality for the subject.

- b. Estimate the frequency, severity, and reversibility of each risk listed.

Cycloplegia-induced conjunctivitis: very unlikely, not severe, and fully reversible especially with anti-inflammatory treatment (if indicated).

Fatigue/anxiety: uncommon, not severe, and reversible when session is completed.

Excessive light exposure: physical containment of light makes this essentially impossible during normal operation.

Loss of confidentiality is extremely unlikely, and would only occur via unauthorized access.

- c. Is this a therapeutic study or intervention? Yes No

**If Yes**, complete the following items:

- i. Describe the standard of care in the setting where the research will be conducted: \_\_\_\_\_
- ii. Describe any other alternative treatments or interventions: \_\_\_\_\_
- iii. Describe any withholding of, delay in, or washout period for standard of care or alternative treatment that participants may be currently using: \_\_\_\_\_

- d. Do you foresee that participants might need additional medical or psychological resources as a result of the research procedures/interventions? Yes No

**If Yes**, describe the provisions that have been made to make these resources available.

**If additional medical attention is warranted after the initial eye exam or after any retinal imaging session, we will recommend that the participant seek medical evaluation by their primary care physician or ophthalmologist.**

- e. Do the benefits or knowledge to be gained outweigh the risks to participants? Yes No

**If No**, provide justification for performing the research: \_\_\_\_\_

## 19. Precautions/Minimization of Risks

- a. Describe precautions that will be taken to avoid risks and the means for monitoring to detect risks.

**Pre-screening of subjects by an optometrist will minimize risks associated with pupil dilation agents. If an enrolled subject complains of continued eye irritation or discomfort beyond a few minutes after dilation agents are administered, the session will be discontinued and the subject will be examined by the participating optometrist.**

**Pupil dilation may lead to some discomfort once the subject is exposed to normal daylight. The subject will be asked to bring their sunglasses to wear after testing; if they do not have sunglasses; a temporary/disposable pair will be provided.**

**Light levels are measured before every experimental session with a calibrated light power meter.**

**To reduce the likelihood of confidentiality loss, the notebook linking data codes to the respective subjects will be stored in different locations, moved on a random basis.**

**If study involves drugs or devices skip Items 19.b. and 19.c., go to Item 20, and complete the [Drug](#) or [Device](#) Review Sheet, as applicable.**

- b. If hazards to an individual participant occur, describe (i) the criteria that will be used to decide whether that participant should be removed from the study; (ii) the procedure for removing such participants when necessary to protect their rights and welfare; and (iii) any special

procedures, precautions, or follow-up that will be used to ensure the safety of other currently enrolled participants.

**Individual hazards are limited to a reaction to the dilation agents. If the subject reports eye irritation or discomfort beyond the first few minutes after drug administration, the subject will not proceed to the psychophysical testing stages, and will be examined by the participating optometrist for treatment.**

- c. If hazards occur that might make the risks of participation outweigh the benefits for all participants, describe (i) the criteria that will be used to stop or end the entire study and (ii) any special procedures, precautions, or follow-up that will be used to ensure the safety of currently enrolled participants.

**If we find that most participants cannot perform the psychophysical tasks, we will interview the subjects over their inability to perform as expected and modify the experimental design to ameliorate the apparent difficulties.**

## 20. Informed Consent

- a. Do you plan to obtain informed consent for this protocol?

Yes No

**If Yes**, complete the items below.

**If No**, complete and include the [Waiver of Informed Consent](#) or [Waiver of Authorization and Informed Consent](#), as applicable.

- b. Do you plan to document informed consent for this protocol?

Yes No

**If Yes**, complete the items below.

**If No**, complete the items below **and** include the [Waiver of Informed Consent Documentation](#).

- c. How will consent be obtained? **Subjects will be given a copy of the consent form to read at least one day before participating in the study. The experimenter will review the consent form with the subject, answer any questions the subject may have, and then ask if they are interested in participating. This process will be conducted in private.**

- d. Who will conduct the consent interview? **Dr. Sincich, in conjunction with any trainee.**

- e. Who are the persons who will provide consent or permission? **The subjects.**
- f. What steps will be taken to minimize the possibility of coercion or undue influence? **Use of the consent form. In the case that the subject is a UAB student, they will be assured that their participation and performance in the study will have no effect on any of their coursework or their educational progress.**
- g. What language will the prospective participant or the legally authorized representative understand? **English**
- h. What language will be used to obtain consent? **English**
- i. If any potential participants will be, or will have been, in a stressful, painful, or drugged condition before or during the consent process, describe the precautions proposed to overcome the effect of the condition on the consent process. If not, enter "no such effect."  
**No such effect.**
- j. If any project-specific instruments will be used in the consenting process, such as flip charts or videos, describe the instrument(s) here, and provide a copy of each. If not, enter "not used."  
**Not used.**
- k. How long will participants have between the time they are told about the study and the time they must decide whether to enroll? If not 24 hours or more, describe the proposed time interval and why the 24-hour minimum is neither feasible nor practical. **No time limit, participation is voluntary.**

## 21. Procedures to Protect Privacy

Describe the provisions included in the research to protect the privacy interests of participants (e.g., others will not overhear your conversation with potential participants, individuals will not be publicly identified or embarrassed).

**Subjects are examined and tested privately. Personnel involved with subjects are explicitly informed to not discuss subject data with others not involved in the study.**

## 22. Procedures to Maintain Confidentiality

- a. Describe the manner and method for storing research data and maintaining confidentiality. If data will be stored electronically anywhere other than a server maintained centrally by UAB, identify the departmental and all computer systems used to store protocol-related data, and describe how access to that data will be limited to those with a need to know.

**Digital research data will consist of retinal image movies and coded responses from the subjects; both data sets are completely coded to ensure anonymity. Data are stored on secure computers in a room which is only accessible electronically by lab personnel. The list that relates subjects to their codes is kept in non-digital form, and stored in the PI's office in a locked drawer.**

- b. Will any information derived from this study be given to any person, including the subject, or any group, including coordinating centers and sponsors? Yes No

**If Yes**, complete i-iii.

- i. To whom will the information be given? \_\_\_\_\_
- ii. What is the nature of the information? \_\_\_\_\_
- iii. How will the information be identified, coded, etc.? \_\_\_\_\_


### **23. Additional Information**

In the space below, provide any additional information that you believe may help the IRB review the proposed research, or enter "None."

**None.**

MEMORANDUM

**TO:** Lawrence C. Sincich, PhD  
Principal Investigator

**FROM:** Cari Oliver, CIP  
On behalf of IRB 01 

**DATE:** January 22, 2016

**RE:** F121221001  
Perception of Visual Microstimuli

The IRB 01 met on **January 20, 2016** and **approved** the protocol referenced above. The approval form and IRB-stamped consent form are attached. **This approval will expire and no longer be valid on January 20, 2016.**

**Please note the following as related to this review:**

- The IRB noted approval of this protocol expired on **January 14, 2016**. The IRB recommends submitting renewal materials 4-6 weeks before the protocol expiration date to avoid a lapse in approval. Allowing IRB approval to lapse constitutes non-compliance. Any further instance of non-compliance may be considered serious and/or continuing non-compliance, which must be reported in accordance with POL024, UAB Policy on Reporting to Institutional Officials and Regulatory Agencies.

CO/jdc

470 Administration Building  
701 20th Street South  
205.934.3789  
Fax 205.934.1301  
irb@uab.edu

The University of  
Alabama at Birmingham  
Mailing Address:  
AB 470  
1720 2ND AVE S  
BIRMINGHAM AL 35294-0104

**Protection of Human Subjects  
Assurance Identification/IRB Certification/Declaration of Exemption  
(Common Rule)**

Policy: Research activities involving human subjects may not be conducted or supported by the Departments and Agencies adopting the Common Rule (56FR28003, June 18, 1991) unless the activities are exempt from or approved in accordance with the Common Rule. See section 101(b) of the Common Rule for exemptions. Institutions submitting applications or proposals for support must submit certification of appropriate Institutional Review Board (IRB) review and approval to the Department or Agency in accordance with the Common Rule. Institutions must have an assurance of compliance that applies to the research to be conducted and should submit certification of IRB review and approval with each application or proposal unless otherwise advised by the Department or Agency.

1. Request Type <input checked="" type="checkbox"/> ORIGINAL <input type="checkbox"/> CONTINUATION <input type="checkbox"/> EXEMPTION	2. Type of Mechanism <input checked="" type="checkbox"/> GRANT <input type="checkbox"/> CONTRACT <input type="checkbox"/> FELLOWSHIP <input type="checkbox"/> COOPERATIVE AGREEMENT <input type="checkbox"/> OTHER: _____	3. Name of Federal Department or Agency and, if known, Application or Proposal Identification No.
4. Title of Application or Activity Perception of Visual Microstimuli		5. Name of Principal Investigator, Program Director, Fellow, or Other SINCICH, LAWRENCE C.

6. Assurance Status of this Project (Respond to one of the following)

- This Assurance, on file with Department of Health and Human Services, covers this activity:  
Assurance Identification No. FWA00005960, the expiration date 01/24/2017 IRB Registration No. IRB00000196
- This Assurance, on file with (agency/dept) \_\_\_\_\_, covers this activity.  
Assurance No. \_\_\_\_\_, the expiration date \_\_\_\_\_ IRB Registration/Identification No. \_\_\_\_\_ (if applicable)
- No assurance has been filed for this institution. This institution declares that it will provide an Assurance and Certification of IRB review and approval upon request.
- Exemption Status: Human subjects are involved, but this activity qualifies for exemption under Section 101(b), paragraph \_\_\_\_\_.

7. Certification of IRB Review (Respond to one of the following IF you have an Assurance on file)

- This activity has been reviewed and approved by the IRB in accordance with the Common Rule and any other governing regulations.  
by:  Full IRB Review on (date of IRB meeting) 1/20/2016 or  Expedited Review on (date) \_\_\_\_\_  
 If less than one year approval, provide expiration date \_\_\_\_\_
- This activity contains multiple projects, some of which have not been reviewed. The IRB has granted approval on condition that all projects covered by the Common Rule will be reviewed and approved before they are initiated and that appropriate further certification will be submitted.

8. Comments Protocol subject to Annual continuing review.	Title F121221001
	Perception of Visual Microstimuli

IRB Approval Issued: 1/22/16 IRB Approval No Longer Valid On: 1/20/17

9. The official signing below certifies that the information provided above is correct and that, as required, future reviews will be performed until study closure and certification will be provided.	10. Name and Address of Institution University of Alabama at Birmingham 701 20th Street South Birmingham, AL 35294	
11. Phone No. (with area code) (205) 934-3789		
12. Fax No. (with area code) (205) 934-1301		
13. Email: irb@uab.edu		
14. Name of Official Ferdinand Urthaler, M.D.	15. Title Chairman, IRB	
16. Signature <i>Ferdinand Urthaler MD/cw</i>	17. Date <u>1/22/16</u>	Sponsored by HHS

According to the Paperwork Reduction Act of 1995, no persons are required to respond to a collection of information unless it displays a valid OMB control number. The valid OMB control number for this information collection is 0990-0263. The time required to complete this information collection is estimated to average 30 minutes per response. If you have comments concerning the accuracy of the time estimate(s) or suggestions for improving this form, please write to: U.S. Department of Health & Human Services, OS/OIG/PRA, 200 Independence Ave., S.W., Suite 336-E, Washington D.C. 20201, Attention: PRA Reports Clearance Officer.



APPENDIX B

UNIVERSITY OF ALABAMA AT BIRMINGHAM INFORMED CONSENT  
DOCUMENT FOR HUMAN SUBJECTS

## Consent Form

---

**Title of research:** Perception of Visual Microstimuli  
**IRB Protocol:** F121221001  
**Investigator:** Lawrence Sincich, Ph.D.  
**Sponsor:** National Eye Institute

---

### Purpose of the Research

Our research is aimed at studying how visual perception works at the cellular level. The cells in your eye that are sensitive to light are called photoreceptors, and they are located in the tissue lining the back of your eye called the retina. It is now possible to see these cells using a special retinal microscope like the one used in our laboratory. By shining tiny spots of light onto individual photoreceptors, we hope to learn how the signals they produce normally lead to visual perception. With your participation in this kind of research, we may eventually improve our understanding of how retinal diseases affect the function of these photoreceptors. To perform the research we will be using FDA approved eye-drops. We expect to enroll 15 subjects for a single study.

### Explanation of Procedures

Our study will enroll adult participants with normal vision who will participate in tests involving briefly flashed spots of light. If you decide to volunteer for the study, you will be asked to perform the following procedures:

**1. Eye exam and color vision testing:** Prior to participating in our study, you will be examined by a UAB optometrist who will determine (a) if your eyes appear normal, (b) what your visual acuity and refractive errors are, and (c) if you appear to be at risk for side-effects of the drugs used to dilate your pupils. If the examining optometrist concludes that you can be enrolled in the study, you will perform a standard color vision test to determine if your color vision is normal. The color tests are simple and may vary; they involve either verbally describing what is seen in colored figures, or arranging color chips in a particular order. The eye exam and color testing will last less than 2 hours, and will be conducted one time only and may be done on a separate day from the perceptual testing described below.

**2. Pupil dilation:** Before any perceptual testing session, we will dilate the pupil in one eye with commonly used eye-drops.

**3. Retinal imaging:** While your pupil is dilated, we will image your retina with a research instrument known as a scanning laser ophthalmoscope. You will be asked to sit in front of the ophthalmoscope with your head placed in a chin rest. If additional stability of your head is required, we may ask you to use a personally fitted bite-bar to minimize head motion.

This ophthalmoscope uses light to create a movie of a small region on your retina. In some instances, this light will momentarily appear bright and may produce an after-image similar to the after-image from a camera flash; these afterimages will fade away after a few minutes. The light source used will not harm your eye. The researchers are careful to keep the light level at least 10 times below the accepted safety standard for light exposure (developed by the American National Standards Institute for ophthalmic instruments).

**4. Perceptual testing:** For these investigational tests, you will be instructed on how to respond to briefly flashed spots of light by pressing keys on a standard computer keyboard. Testing will be conducted in dimly lit room. The test will consist of a series of trials that you control at your own pace. While your retina is being imaged, you will be told when you can begin initiating trials. For each trial, you will press one key to have the stimulus flashed, and then respond whether or not you saw the stimulus by pressing assigned keys. You will also have the option to press a third key to have the trial repeated. You can pause or rest between any trial, or terminate the session voluntarily at any time for any reason.

The number of trials executed will be determined by you. Most participants are comfortable performing several hundred trials per session once they have become practiced at the task. The total time for one psychophysical testing session will be about 2 hours. The total number of sessions is unpredictable because it will vary with the experiment's requirements and the performance of the participant. However, a minimum of 4 sessions will be required to obtain meaningful data (this includes 1 practice session to become familiar with the testing conditions). For a single study, we expect about 20 sessions will be required. Only one session will be conducted per day, and the number of days between sessions can vary. We emphasize here that a participant can freely discontinue testing at any time without any consequences.

#### **Incidental Findings**

We are imaging only for the research purposes described above. The imaging is not a clinical technique intended for diagnostic or therapeutic purposes. Under no circumstance will the research personnel interpret the images as normal or abnormal. They are unable to make any medical comments about your retinal images, nor will the images be looked at or read for any healthcare treatment or diagnostic purpose. If you want your images to be reviewed by a physician so that the physician can look for medical issues, you can request a copy. We will provide an electronic copy at no charge.

### **Risks and Discomforts**

The imaging done with the ophthalmoscope is non-contact and non-invasive. The light exposure is strictly controlled and is at least 2 times less than the maximum permitted exposure allowed by the American National Standard for the Safe use of Lasers (ANSI Z136.1-2014). Consequently, participation in this study does not involve any serious risk due to light exposure.

However, participation in this study may involve some discomforts, which are similar to those encountered in any comprehensive eye examination. These discomforts may be associated with dilation of your eye, bright lights shown into your eye temporarily, and fatigue or anxiety at having to sit still for each of the tests and study procedures.

Pupil dilation may result in blurred near vision or sensitivity to bright light for a few hours after administration of the eye drops. We recommend that you bring sunglasses to wear after any testing; if you do not have sunglasses, we will provide a pair of disposable ones. The dilating drugs may cause some transient irritation to your eye; and there may be risks associated with allergic reactions to these drugs.

The collected data are coded from the beginning to ensure anonymity. The code linking the data to the subject is kept in a bound notebook in a locked drawer in the Dr. Sincich's office. There is a very small chance that if unauthorized personnel obtain access to this notebook, there may be a loss of confidentiality for the subject.

### **Benefits**

You may not benefit directly from taking part in this study. Your participation will help us to understand how photoreceptors normally work, and will provide insight into how to study photoreceptors that are affected by retinal diseases.

### **Alternatives**

Our study is not considered medical treatment. Your only alternative is to not participate.

### **Confidentiality**

Information obtained about you for this study will be kept confidential to the extent allowed by law. However, research information that identifies you may be shared with the UAB Institutional Review Board (IRB) and others who are responsible for ensuring compliance with laws and regulations related to research, including the Office for Human Research Protections (OHRP) and the UAB Department of Vision Sciences. The results of the study may be published for scientific purposes. These results could include your test performance and/or images of the inside of your eye; however, your identity will not be associated with these results.

### **Voluntary Participation and Withdrawal**

Whether you participate in this study is your choice. There will be no penalty of any kind if you decide not to be in the study. If you decide not to be in the study, you will not lose any benefits you are otherwise owed. You are free to withdraw from the study at any time. Your choice to leave the study will not affect your relationship with the University of Alabama at Birmingham (UAB).

If you are a UAB student or employee, taking part in this research is not a part of your UAB class work or duties. You can refuse to enroll, or withdraw after enrolling at any time before the study is over, with no effect on your class standing, grades, or job at UAB. You will not be offered or receive any special consideration if you take part in this research.

You may be removed from the study without your consent if the sponsor ends the study, if the study personnel decide it is not in the best interest of your health, or if the acquired data are considered compromised by the investigators.

**Costs of and Payment for Participation**

There will be no costs to you for taking part in this study, nor will you be paid for participating.

**Payment for Research-Related Injuries**

The National Eye Institute, UAB, and the Department of Vision Sciences do not provide for any payment in the unlikely event that you are harmed as a result of taking part in this study. If such harm occurs, treatment will be provided. However, this treatment will not be provided free of charge.

**Questions**

If you have any questions, concerns, or complaints about the research or a research-related injury including available treatments, please contact Dr. Lawrence Sincich. He will be available to answer any of your questions. Dr. Sincich's office phone is 205-975-3446.

If you have questions about your rights as a research participant, or concerns or complaints about the research, you may contact the Office of the Institutional Review Board for Human Use (OIRB) at (205) 934-3789 or 1-855-860-3789. Regular hours for the OIRB are 8:00 a.m. to 5:00 p.m. CT, Monday through Friday. You may also call this number in the event the research staff cannot be reached or if you wish to talk to someone not associated with laboratory personnel.

**Legal Rights**

You are not waiving any of your legal rights by signing this informed consent document.

**Signatures**

Your signature below indicates that you agree to participate in the study outlined above. You will receive a copy of this signed document.

_____ Signature of Participant	_____ Date
_____ Signature of Principal Investigator (or other person obtaining consent)	_____ Date
_____ Signature of Witness	_____ Date

**University of Alabama at Birmingham**  
**AUTHORIZATION FOR USE/DISCLOSURE OF**  
**PROTECTED HEALTH INFORMATION (PHI) FOR RESEARCH**

**Participant Name:** \_\_\_\_\_  
**Research Protocol:** Perception of Visual Microstimuli

**UAB IRB Protocol Number:** F121221001  
**Principal Investigator:** Lawrence Sincich, PhD  
**Sponsor:** National Eye Institute

**What is the purpose of this form?** You are being asked to sign this form so that UAB may use and release your protected health information for research. Participation in research is voluntary. If you choose to participate in the research, you must sign this form so that your protected health information may be used for the research.

**Why do the researchers want my protected health information?** The researchers want to use your protected health information as part of the research protocol listed above and as described to you in the informed consent.

**What protected health information do the researchers want to use?** All medical information, including but not limited to information and/or records of any diagnosis or treatment of disease or condition, which may include sexually transmitted diseases (e.g., HIV, etc.) or communicable diseases, drug/alcohol dependency, etc.; all personal identifiers, including but not limited to your name, social security number, medical record number, date of birth, dates of service, etc.; any past, present, and future history, examinations, laboratory results, imaging studies and reports and treatments of whatever kind, including but not limited to drug/alcohol treatment, psychiatric/psychological treatment; financial/billing information, including but not limited to copies of your medical bills, and any other information related to or collected for use in the research protocol, regardless of whether the information was collected for research or non-research (e.g., treatment) purposes.

**Who will disclose, use and/or receive my protected health information?** All individuals/entities listed in the informed consent documents, including but not limited to, the physicians, nurses and staff and others performing services related to the research (whether at UAB or elsewhere); other operating units of UAB, HSF, UAB Highlands, Children's of Alabama, Eye Foundation Hospital, and the Jefferson County Department of Health, as necessary for their operations; the IRB and its staff; the sponsor of the research and its employees and agents, including any CRO; and any outside regulatory agencies, such as the Food and Drug Administration, providing oversight or performing other legal and/or regulatory functions for which access to participant information is required.

**How will my protected health information be protected once it is given to others?** Your protected health information that is given to the study sponsor will remain private to the extent possible, even though the study sponsor is not required to follow the federal privacy laws. However, once your information is given to other organizations that are not required to follow federal privacy laws, we cannot assure that the information will remain protected.

**How long will this Authorization last?** Your authorization for the uses and disclosures described in this Authorization does not have an expiration date.

**Can I cancel this Authorization?** You may cancel this Authorization at any time by notifying the Principal Investigator, in writing, referencing the research protocol and IRB Protocol Number. If you cancel this Authorization, the study doctor and staff will not use any new health information for research. However, researchers may continue to use the protected health information that was provided before you cancelled your authorization.

**Can I see my protected health information?** You have a right to request to see your protected health information. However, to ensure the scientific integrity of the research, you will not be able to review the research information until after the research protocol has been completed.

Signature of participant: \_\_\_\_\_

Date: \_\_\_\_\_

or participant's legally authorized representative: \_\_\_\_\_

Date: \_\_\_\_\_

Printed Name of participant's representative: \_\_\_\_\_

Relationship to the participant: \_\_\_\_\_